NUMERICAL MODELLING FOR THE RECOVERY OF PROTECTING PILLARS IN SOMA DISTRICT

A Thesis Submitted to the
Graduate School of Natural and Applied Science of
Dokuz Eylül University
In Partial Fulfillment of the Requirements for
The Degree of Doctor of Philosophy in Mining Engineering, Mining Engineering Program

by
Cemalettin Okay AKSOY

February, 2002
İZMİR

Ph.D. THESIS EXAMINATION RESULT FORM

We certify that we have read the thesis, entitled **"NUMERICAL MODELLING FOR THE RECOVERY OF PROTECTING PILLARS IN SOMA DISTRICT"** completed by **CEMALETTİN OKAY AKSOY**under supervision of Prof. Dr. Halil KÖSE and that in our opinion it is fully adequate, in scope and in quality, as a thesis for the degree of Doctor of Philosophy.

Prof.Dr. Halil KÖSE
Supervisor

Doç. Dr. Turgay ONARGAN

Jury Member
(Thesis Committee Member)

Doç. Dr. Yalçın KOCA

Jury Member
(Thesis Committee Member)

Prof. Dr. Vedat DİDARİ

Jury Member

Prof. Dr. A. Hakan ONUR

Jury Member

Approved by the
Graduate School of Natural and Applied Sciences

Prof.Dr.Cahit Helvacı
Director

ACKNOWLEDGMENTS

I would like to express my appreciation to Prof. Dr. Halil KÖSE for his kind supervision, valuable suggestion and discussions during the preparation of this thesis.

With respect and gratitude, I also acknowledge the valuable guidance and support extended by all members of my thesis research commitee: Assoc. Prf. Dr. Turgay ONARGAN and Assoc. Prof. Dr. Yalçın KOCA.

I would like to express gratitude to Prof. Dr A. Hakan ONUR, for his encouragement and support during this study, and especially to Prof. Dr. Üner İPEKOĞLU and Assist. Prof. Dr. Hayati YENİCE for their support.

My special thanks to Dr. Chris MARK and Dr. Keith A. HEASLY for their immense help, valuable suggestion and interesting discussions throughout this thesis. I also thankful to Pitsburgh Research Center, NIOSH for allowing to the investigation about my research.

I want to thank my friends Kerim KÜÇÜK (MSc.) and Kemal ÖZFIRAT (MSc.) for their associate throughout this study.

My last but not the least greatful appreciations go to some very special people in my life. Especially, I present my most greatful thanks to my wife, Berna AKSOY for her unlimited patience, love and encouragement. I also greatfully appreciate the sacrifices and unlimited love from my parents.

Cemalettin Okay AKSOY
Master of Science

ABSTRACT

The need for more production has become necessary in recent years as a result of increase in lignite demand in TURKEY. Therefore, it is important to increase productivity in longwall mining method to provide as much utilization as possible from this source. Safety pillars, which have been left for the stability of main drift and shaft, should therefore be recovered after the operational life of the mine.

In this research work entitled "Numerical Modelling for the Recovery of Protecting Pillars in Soma District", an underground mine based in Soma-Manisa, belonging to Hüstaş A. Ş. of Turkey was studied. Stability of main drift and shaft safety pillars due to stresses and deformations occurring during the production have been investigated by means of a numerical analysis method, namely LAMODEL, operating by boundary element technique. Stability of shaft due to stresses and deformations has similarly been investigated by using one of the numerical analyses methods known as finite element technique which operates with ANSYS computer software.

ÖZET

Türkiyede artan linyit talebi ile birlikte, daha fazla üretim yapma ihtiyacı gündeme gelmiştir. Bu nedenle, uzunayak metodu ile yapılan madencilikte üretim ve verimliliği artırmak ve bu kaynaktan mümkün olduğunca fazla yararlanmak gerekmektedir. Bu amaçla, daha önce ana giriş desandresi ve kuyu gibi yapılar için bırakılan emniyet topuklarının, madenin ömrü bittikten sonra kazanılması gerekmektedir. "Soma Bölgesinde Emniyet Topuklarının Geri Kazanılması İçin Nümerik Modelleme" isimli bu çalışmada, Manisa-Soma'da bulunan Hüstaş A. Ş.'ye ait yeraltı kömür ocağında ana giriş desandresi ve kuyu emniyet topuklarının kazanılması sırasında oluşan gerilme ve deformasyonlar ile topukların duraylılığı numerik analiz yöntemlerinden boundary element tekniği ile çalışan LAMODEL isimli bilgisayar programı ile incelenmiştir. Ayrıca, kuyu emniyet topuğunun kazanılması sonucunda oluşan gerilmeler ve deformasyonlar sonucunda kuyunun duraylılığı numeric analiz yöntemlerinden biri olan finite element tekniği ile çalışan ANSYS isimli bilgisayar programı ile incelenmiştir.

CONTENTS

Page

Chapter One
INTRODUCTION

Chapter Two
PILLAR DESIGN AND CONCEPTS

Chapter Three
SUBSIDENCE EFFECTS

Chapter Four
BOUNDARY ELEMENT MODELLING
FOR SAFETY PILLARS STABILITY
A CASE STUDY: HÜSTAŞ MINE

Chapter Five
FINITE ELEMENT MODELLING FOR HÜSTAŞ MINE SHAFT 1

Chapter Six
CONCLUSIONS

LIST OF FIGURES

LIST OF TABLES

Page

Chapter One
INTRODUCTION

1.1 Introduction

In coal mines, a portion of the coal is left in pillars to support the great weight of the overburden and to provide stability to the immediate roof and floor of the openings for ingress and egress. In a room-and-pillar section, the pillars are designed primarily to support the roof and to provide long-term stability to the overburden. In longwall mining, the roof and overburden is allowed to cave in a controlled manner behind the active longwall face. The caving of the strata produces concentrated stresses around the perimeter of the caving zone known as abutment stresses. Because of this variable stress field, a variety of pillar types with different designs philosophies commensurate with their particular application have evolved. In the gateroads of the longwall, the "abutment" pillar is designed to support the abutment loads and maintain stability in the gate entries. Also, "yield" pillar are used in the gateroads in some situations. These yield pillars are designed essentially to support the immediate roof and maintain stability of the entries while yielding and transferring most of the abutment load to adjacent pillars. Associated with longwall mining, and room-and-pillar mining, there are also "barrier" or "safety" pillars, which are designed sufficient, large enough to isolate critical areas of the mine from abutment stresses or other unfavorable conditions. Two particularly important barrier pillars are those left to protect the main drifts and the main shafts from dangerous stresses and/or displacements generated by the adjacent mining. The main drifts and the shafts are generally the main access for men and materials to the mine, and the main conduit for coal transport from the mine; therefore, protection of the main drifts and shafts is crucial through the mine life.

It will give an additional benefit to extract the safety pillars, those are used to provide stability for main drifts and shafts as far as economy and production is concerned. For this reason, it is important to mine these safety pillars. For this purpose above mentioned, the stresses and deformations due to mining operations on safety pillars, their effects and results are the subject of this study.

1.2 Description of Study Area

The depth of the lignite, which called Km-2, at Hustas mine averages about 200 meters and the seam ranges in thickness from 15 to 25 m with an average extractable thickness of about 18 meters. A manual double-slice longwall mining method is used for the main production at the mine. In this method, the face area is maintained about 2 m high using hydraulic steel props and wooden posts. The coal is extracted from the face using drill and blast and the additional lignite thickness above the supports is recovered as it caves behind the face. Faces average about 120 m length and production averages about 1,000,000 tons per year.

The main production sections of the lignite reserve were finished in early 2000. Before abandoning the mine, the company plans to extract the final lignite pillars, which were originally left as protection for both the main drift and Shaft 1. The main drift was opened in the clayey marlstone formation above the lignite and has been used as the primary transport entry for the lignite from the production panels during the previous years. The main drift is about 30-35 m above the lignite and dips at 12^0. The main drift starts at the 330 m. level northwest of the mine and ends at the 141.19 m. level at the southeast end of the mine. Its cross-section area is 12 m^2 and it has supported rigid steel (I profile). The pillar left to protect the main drift contains approximately 2,000,000 tons of lignite (see Figure 1.2). The shaft starts on the surface at the 368 m level and finishes in the seam at the 220 m level. It is located on the northwest side of mine and was primarily used for transportation of the workers and staff. The lining of the shaft is concrete with a thickness of 50 cm. Concrete type is C50 and structure of shaft boundary contains double dack wire mesh for tensile stress. The barrier pillar left around the bottom of the shaft for protection contains about 500,000 tons of lignite. The company plans to extract the main drift safety pillar (from south-east to north-west) in the next 2.5 – 3 years. During this period, main drift will not be supported and will be allowed to collapse. Next, the shaft pillar under Shaft 1 will be extracted from the southeast to the northwest. During the extraction of the Shaft 1 safety pillar, the shaft will still be used for primary access to the reserve.

1.3 Location of Study Area

The Hüstaş Mine Company, which was founded in the mid 1980s, is one of the leading lignite mining companies in Turkey. The actual Hüstaş Mine is located southwest of Ankara, 140 km. from İzmir and has been in production since early 1988. Between 1988 and 2000, the lignite was extracted from various production areas of the mine. Figure 1.1 shows the location of the Hüstaş mine, Figure1.2 shows the chronology of the main production sections and the location of the main drift, shaft and associated protection pillars and Figure 1.3 shows double slice mining method.

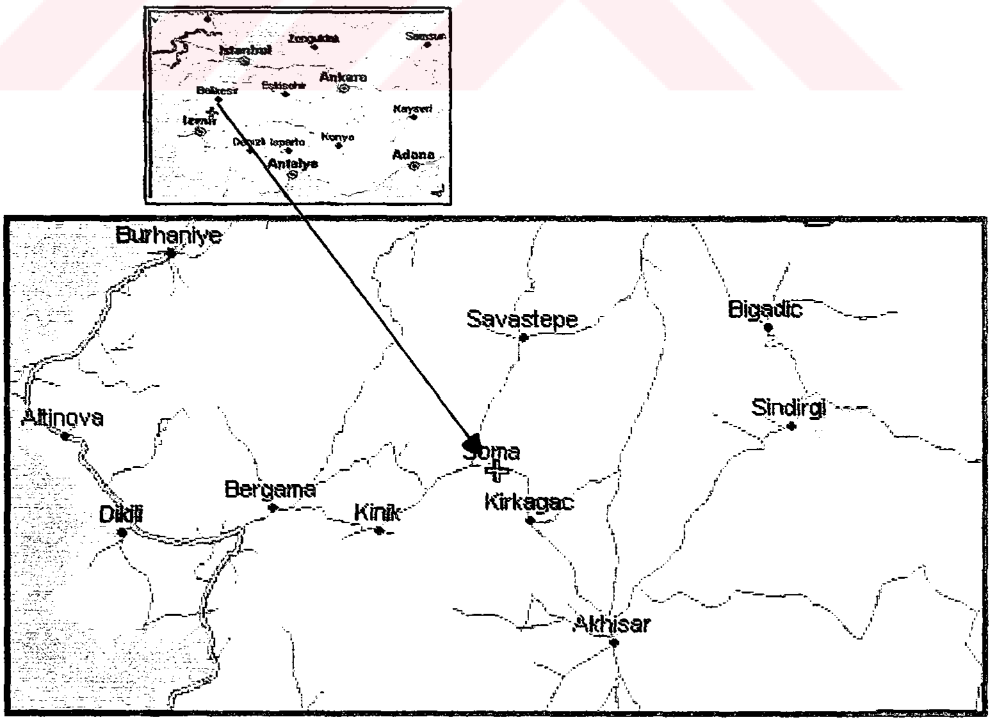

Scale: 1/ 1 000 000

Figure 1.1 Location map of the Soma, Turkey

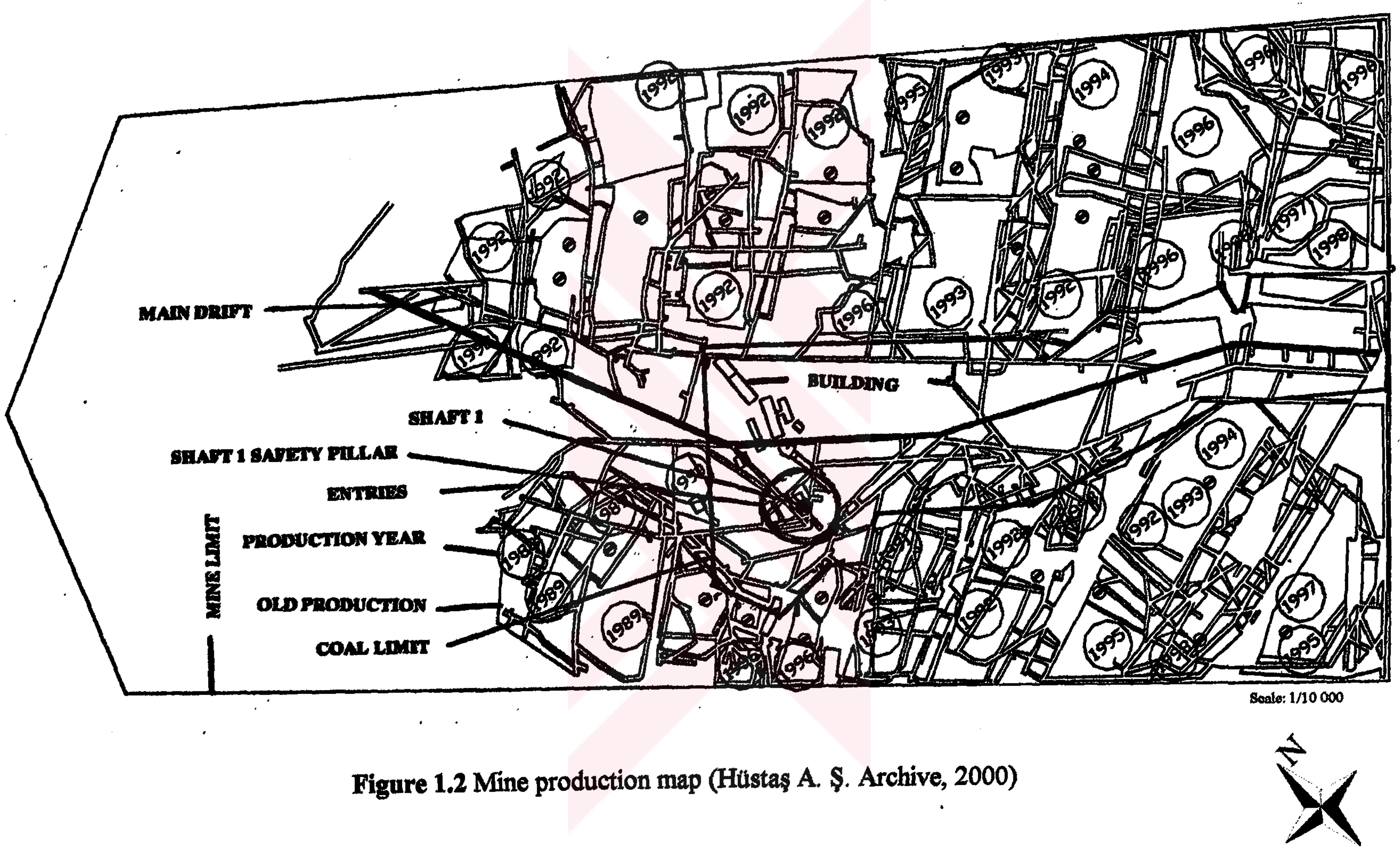

Figure 1.2 Mine production map (Hüstaş A. Ş. Archive, 2000)

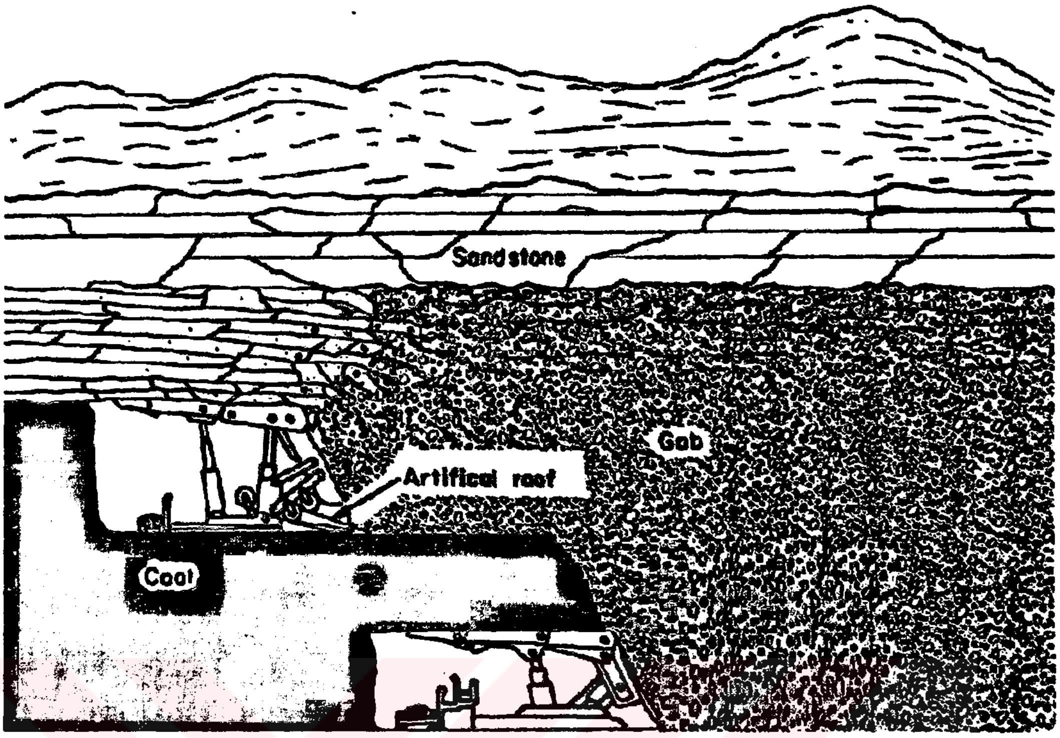

Figure 1.3 Double slice mining method

1.4 General Geology of Study Area

1.4.1 General Geology Of Soma District

The lignite deposits of southwestern Turkey are contained within a series of northeast-southwest trending in Tertiary basins. The Soma basin contains two thick Miocene lignite seams designated as the KM2 and KM3. The Miocene deposits rest unconformable on Mesozoic basement rocks. Pliocene deposits rest conformably on the Miocene and contain two poorly developed lignite seams designated as the KP1 and KP2. Pleistocene and more recent cover is found throughout the area. It is thought that the Miocene and Pliocene sediments were deposited in ancient lakes (limnic deposits) in intermontane basins, which are thought to have been formed during a phase of the Alpine Orogeny. The sediments in the Soma basin reflect the overall infilling of the lake. The Soma basin sediments dip towards southwest, striking northwest-southeast. Throughout the basin the average dips are approximately 20°, but dips are steeper around the northeastern basin edge where the lignite and sediments outcrop or subcrop against the Mesozoic basement. Dips increase in the deeper parts of the basin to about 35°. The basin has been dislocated by a series of northeast-southwest trending normal faults with some slip component which has caused off-sets ranging up to 300 m. Downthrows vary from a few meters to over 100 m. Some faults have a surface expression, which may be reflected in the drainage pattern. Not all faults have surface expressions as evidenced by faults intersected in the underground workings at Soma Merkez. The Soma region has been mined since 1913, first for local domestic and industrial consumption and later as a feed for the Soma A power station. TKI took over lignite production in 1979. The only seam, which can be recovered by underground mining, is the KM2 seam. It occurs in the Miocene series overlain by marlstone. Variations in the vertical thickness of the lignite unit (including partings) occur within a range from about 15 m to about 30 m. The average true thickness of mineable lignite is about 18 m.

1.4.2 Stratigraphy

Deposits from the Mesozoic, Tertiary (Miocene and Pliocene) and Quaternary are present within the concession (mining) area. The stratigraphy of the Soma Eynez is summarized in a general stratigraphic column as shown in Figure 1.4. From the base upward the stratigraphic column contains:

1) The Mesozoic basement (TM). This deposit consists of immature, dark grey, coarse-grained greywacke and massive, light to medium grey limestone with calcite filled fractures. The top of the basement is thought to be an old erosion surface, and what has been interpreted as landslide material has been observed in selected boreholes;

2) The Miocene sediments unconformable overlie the Mesozoic basement. The Miocene Group has been divided into three formations, which from the basement upward are the M!, M2 and M3 Formations. The M1 formation is predominantly immature sandstone and conglomerate and there is a gradational upward fining of the sediments to the lignite horizon. Increasing amounts of sandy clay, clayey silt and

carbonaceous clay appear towards the top of the M1 until this grades into the KM2 lignite seam. The M1 formation has been measured from 0-40 m thick although it is suspected that it may be thicker in places. The M1-M2 contact is gradational and is usually placed at the base of the KM2 lignite seam. The M2 Formation is mostly massive marl with tight calcite filled fractures. There are occasional clay stringers. The KM2 lignite zone occurs below the sharp basal contact of the marl, and because of its thickness and extent, it has the most economic potential in the Soma Işıklar basin. The upper contact with the M3 Formation is gradational and usually placed where the lithology changes to predominately freshwater limestone. The M2 Formation ranges from 0 to 160 m thick. The M3 Formation consists of freshwater limestone and contains the KM3 lignite seam that occurs at varying levels within the M3. The KM3 consists of lignite beds separated by non-lignitic sediments, normally marls and sandy/silty clays and some limestone. The lignite tends to be concentrated at the base of the KM3 seam with thinner units occurring up to 24 meters above the base. The M3 ranges from 90 to over 250 meters thick.

3) The Pliocene Group has been divided into two formations that are in ascending order, the lower P1 and the upper P2 Formation. The P1 Formation is massive marl with the KP1 lignite seam occurring as a thin lenticular horizon, which is not considered to have significant economic potential. The P1 Formation ranges in thickness from 0 to 170 m. The base of the P2 Formation is placed at the bottom of the KP2 lignite seam when it is present. The P2 consists of massive marl and limestone. The P2 Formation ranges up to 300 m thick in the Işıklar concession area. The KP2 lignite seam, a member of the P2, is thin and lenticular and not considered economic.

4) There is a surface cover of alluvial material and dumps of waste material generated from past and current mining operations. In some areas the historic waste dumps are up to 125 m thick.

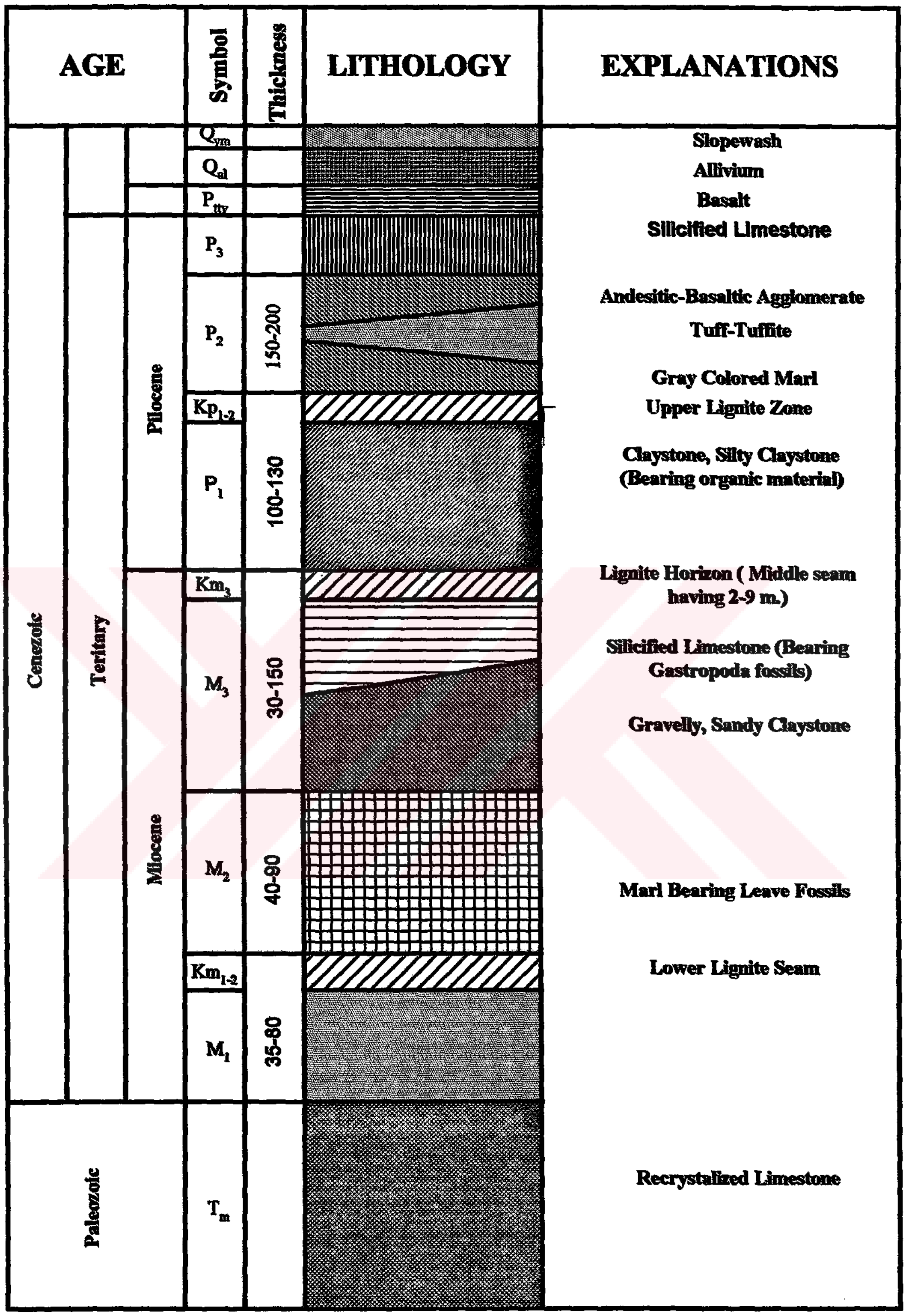

Figure 1.4 Generalized stratigraphic section of Soma-Eynez Coal Basin (Onargan, et al., 2000)

Chapter Two
PILLAR DESIGN AND CONCEPTS

2.1 Introduction

The researchers have been studying the coal pillars for almost 100 years and the first pillar strength formula were derived early in the twentieth century. The laboratory testing of coal samples of different sizes was the basis of those derived equations. From then a number of pillar design formula have been developed by the mining engineers and/or researchers in the geomechanics field worldwide by using different approaches. A numerous research papers were published in the journals and conference proceedings worldwide. The literature review for this study has been carried out in two steps, the first being the reviews of the papers on the general pillar design theories and the second on the papers specifically on the long term stability of the coal pillars.

2.2 Pillar Design Theories

A careful survey of the literatures published on the general pillar design theories aids to broadly categorize the approaches used by different researchers for their pillar design theories in the following categories (Mark & Iannacchione, 1992), namely,

i. Empirical approach,
ii. Mechanics-based approach,
iii. Numerical modeling approach.

2.2.1 Empirical approach

The empirical approach is based on either extensive laboratory testing of coal samples or the statistical analysis of previous experiences of the behavior of coal pillars. The *measurement based* formula generally incorporate information from large scale laboratory testings by taking into account the shape and size effect on the pillar strength. The followings are the most commonly known formula based on the above said approach (Mark & Iannacchione, 1992):

1. Obert-Duvall's formula:

$$S_p = S_l\,[\,0.78 + 0.22\frac{w}{h}\,] \tag{2.1}$$

2. Holland-Gaddy's formula:

$$S_p = S_l\,[\,\frac{w}{h}\,]^{0,5} \tag{2.2}$$

3. Bieniawski's formula:

$$S_P = S_1\,[\,0,64 + 0,36\frac{w}{h}\,] \tag{2.3}$$

Where, S_p = pillar strength, psi

S_1 = in-situ coal strength, psi

w = pillar width or least edge dimension, ft

h = pillar height, ft.

In all of the above mentioned formula, the pillar strength, S_p, is dependent on the pillar geometry in terms of the width to height ratio.

The following formula were developed on the basis of the *statistical analysis* of the previous experiences of the pillar behavior or in other words the back analysis of the information gathered from the field:

1. *Salamon-Munro's formula:*

$$S_p = S_1 \left[\frac{w^{0,5}}{h^{0,66}}\right] \tag{2.4}$$

2. *Sheorey's formula:*

$$S_p = S_1 + 0.28\,H\left[\frac{w}{h} - 1\right] \tag{2.5}$$

Where, H = Seam depth or overburden depth, ft.

Though these methods are widely accepted and used by the designers/operators for coal pillar design each of these methods has its own shortcomings. These drawbacks can be summarized as below:

a. The pillar strength calculations can not be extrapolated beyond the data range they were developed from,

b. The pillar stress is assumed to be uniform throughout the pillar section,

c. The pillar is considered as a single structural element not a part of the system consists of roof, pillar and floor,

d. The pillar strength calculated is the average pillar strength defined by the pillar's ultimate load bearing capacity divided by the pillar's cross-sectional area,

e. The pillar failure is assumed to be instant not gradual.

In reality, it is found that the pillar stress in highly non-uniform i.e., it varies considerably between the pillar rib and the pillar core. The tests conducted by (Wagner, 1974) illustrate this stress variation in the pillar and it is shown in the Figure 2.1. The stress profile at various stages of pillar failure strongly suggests that the pillar failure process is gradual, progressive in place of instant. It also indicates that a yield zones form as the rib side of the pillar starts yielding long before the pillar attains the maximum load.

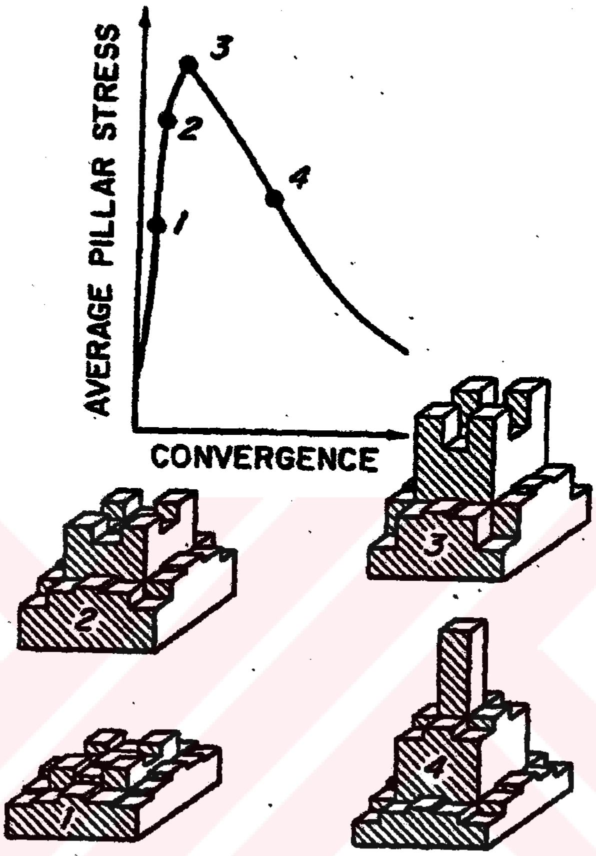

Figure 2.1 Pillar stress profile measured in small coal pillars ((Mark & Iannacchione, 1992))

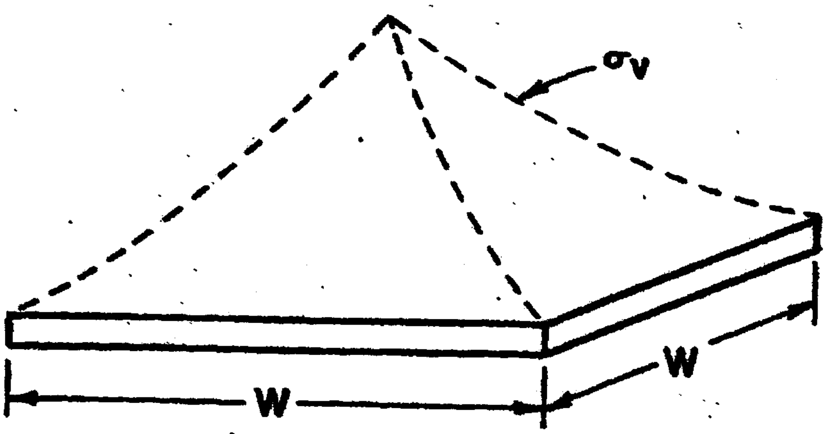

Figure 2.2 Determination of pillar load bearing capacity as the integral of the pillar stress distribution (Mark, 1992)

2.2.2 Mechanics-based approach

This approach of pillar design considers an outer yield zone and a confined core. It was assumed that this outer yield zone provides a confinement to the solid inner core and there exists a stress gradient in the yield zone until it reaches the yield-solid interface. The following methods have used this approach:

1. *Wilson's approach:*

It assumes that coal follows a linear Mohr-Coulombs failure criterion (Wilson, 1973) and the stress gradient in the yielded zone is given as:

$$\sigma_v = p' k \left[\frac{x + \frac{h}{2}}{\frac{h}{2}} \right]^{k-1} \qquad (2.6)$$

Where, σ_v = vertical stress in yield zone, psi

k =tri-axial stress factor = $(1+\sin\varphi)/(1-\sin\varphi)$

φ= the internal angle of friction,

x = distance from rib line, ft.

p' = the unconfined compressive strength of the failed coal at the pillar edge, psi.

The ultimate pillar resistance, R can be calculated by integrating equation 2 .6 over the area of the pillar (Figure 2.2) and the pillar strength is given by the expression as follows:

$$Pillar\ strength = \frac{Ultimate\ Pillar\ Resistance}{Pillar\ Cross-Sectinal\ Area} \qquad (2.7)$$

Wilson had used p' = 14 psi and φ = 30 - 37° and assumed an exponential increase in stress level from the rib side till the end of the yield zone.

2. Salamon's squat pillar formula:

$$S_p = S_1 \left[\frac{Ro^b}{V^a} \right] \left[\frac{b}{e} \left[\left(\frac{R}{Ro} \right)^e - 1 \right] + 1 \right] \qquad (2.8)$$

Where, R = width to height ratio,

R_O = critical w/h ratio = 5,

V = pillar volume,

e = rate of strength increase = 2.5,

b = 0.5933,

a = 0.0667

This method predicts an indefinite exponential stress increase within the yield zone.

3. Barron's approach:

In his approach, Barron also assumes the stress increase in yield zone but it is not indefinite as in Salamon's squat pillar formula, which is unrealistic (Barron, 1984). In Barron's formulation the stress increase in yield zone is limited by the following ways:

i. Nonlinear Mohr envelope is assumed to describe the strength of failed coal,

ii. Gradual decrease of friction angle due to failure in coal,

iii. At high stress, the failure mechanism is pseudo ductile in nature where the frictional strength exceeds the fracture strength.

2.2.3 Numerical modeling approach

In recent past, the numerical modeling technique in pillar design has started to gain the momentum over the empirical or closed form pillar design approaches (Mark & Iannacchione, 1992). The following advantages and recent improvement in computing facility have established the numerical technique over the other pillar design approaches:

i. Can model the pillar as a part of the system incorporating roof and floor,

ii. Can model the layers present in roof or floor,

iii. Can model the effect of the slippage at the interfaces or bedding planes or any other fracture planes in the model domain,

iv. Can model the strain softening behavior of the rock materials in the post-failure region,

v. Can use the exact stress-strain curve to model the rock behavior,

vi. Can utilize the material properties for each layer and the non-linear failure criteria to simulate the yielding,

vii. Can handle the variation in the material properties in the same rock layer at various locations,

viii. Can model any irregularities in geometrical shape,

ix. Generally, the output consists of stress distribution and the displacements at every location of the model,

x. Is very easy to visualize the condition of the structure as a whole.

So, from the design point of view, the numerical modeling technique has proven to be a very efficient tool and it generates results, which can be very realistic depending on the quality of the inputs and detailing of the model. The noteworthy works, which have used this technique in pillar design, are by (Peng, 1986 and Kirpakov, 1981). According to results of finite element analysis of Yeniköy coal field, maximum vertical stress is found 2,5 MPa for square pillar with the dimension of 6,8 m. wide and 4 m. room span (Erçelebi & Nasuf, 2000).

At present, various techniques in pillar design methods are available and the results obtained from them vary considerably even the same problem has been solved. This can be summarized in the Figure 2.3 as it illustrates the comparison of five empirical formula, three analytical and two numerical techniques.

From the discussions above, it is evident that all of these pillar design methods generate an answer for a particular instance given the required inputs and that remains constant no matter at what stage of the pillar life the strength calculation is done. This is because none of these methods has incorporated any time dependent criteria, which is found to be very obvious from the field observations.

In the late eighties and early nineties some research initiatives were noticed where pillar stability long after mining started making its way into pillar design research and as a result some research papers were published. For all of these research initiatives, the main driving force was to minimize the surface subsidence caused by the sudden failure of the pillars from a abandoned underground mine. So it became important to study the long-term stability of coal pillars in great detail.

In a paper (Madden & Hardman, 1992), the issues of long-term stability of coal pillars were investigated in South African coal mines as the need of surface structure construction on the old room-and-pillar mining areas was increasing as a result of expansion of civil infrastructure. Basically, in this paper, the authors made an attempt to estimate the long term stability of the coal pillars by analyzing the old collapsed pillar data, back calculating their safety factors and plotting these safety factors against the time between the development of the pillars and their collapse. The authors mainly focused on the stability study of the shallow mines as the failure of the pillars would affect the surface more severely compared to a mine at greater depth.

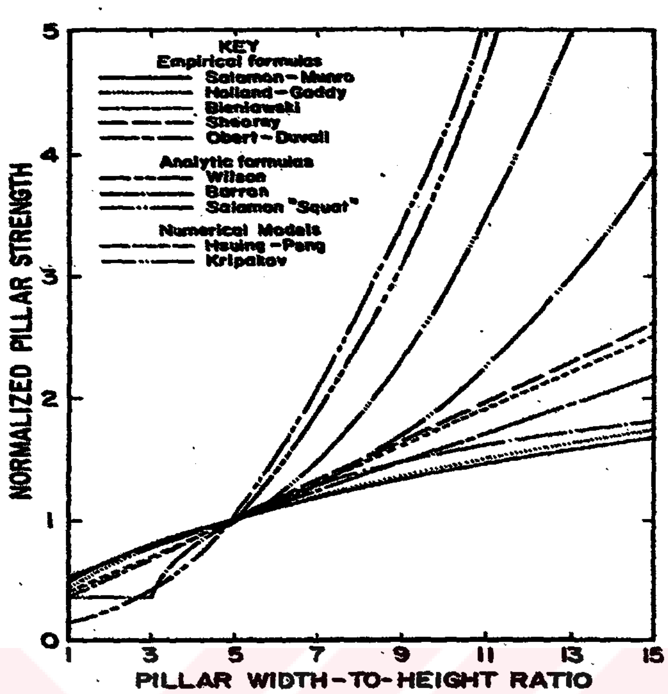

Figure 2.3 Comparison of pillar strength prediction from various formula (Mark, 1992)

2.3 Pillar Concepts

Pillar design is probably one of the oldest ground control problems in underground mining. Ever since coal mining began, tremendous efforts have been made to develop the more accurate and realistic design methods that can be used to design a safe pillar under various geological and mining conditions. Up to now, there are two pillar design concepts used in mining practice (Tsang & Peng, 1989): one is the traditional pillar design concept while the other which is relatively new is called the yield pillar design concept.

2.3.1 Two Pillar Design Concepts

The traditional pillar design, based on the ultimate strength theory, assumes that the stresses within a pillar are uniformly distributed and pillar will fail once the average stress reaches its strength. In order to design a safe pillar, both pillar load and strength are considered. The result from this concept is to design a stiff pillar that will support the whole overburden tributary to it such that it minimizes the interaction between entries and adjacent mining activities. In contrast, the yield pillar design concept takes the material's progressive failure into consideration. Since in reality the stresses inside a pillar and the surrounding materials are not uniformly distributed, failure is always initiated at the critically stressed regions, propagates and leads to final collapse. Based on this design concept, a pillar can be designed to yield properly during its service life period and transfer its load to adjacent stiff pillars or surrounding rocks, and still maintain a stable entry-pillar system. Therefore, under the same geological and mining conditions, the yield pillar design concept tends to design a smaller pillar than the traditional concept.

Conceptually, the traditional pillar design is quite simple and straightforward. A successful pillar design depends on the accuracy of calculation of pillar load and pillar strength. To achieve this goal, researchers have been focusing mainly on;

1) Determining pillar loading
2) Estimating pillar strength

On the other hand, the yield pillar design based on a more realistic assumption and more or less on try-and- error bases, has been practiced in underground coal mines for many years.

The yield pillar concept was first introduced by Holland in 1963 (Holland, 1963). Later, his work was reviewed by several other researchers (Adler & Sun, 1968; Britton, 1986). However, the application of yield pillars has not been widely accepted in the coal industry and no related research has ever been attempted. Reluctance of adopting yield pillars may be attributed partly to a lack of understanding on the fundamental aspect of yield pillars and partly to suspicion whether or not the yield pillars can be used in such complex geological conditions as that found in the coal mines.

Although yield pillars are not completely accepted by the coal industry, they are widely used in potash, salt, and trona mines. Several techniques utilizing the yield pillar concept have been introduced by Serata (Serata, 1976 and 1982) to control stress distribution around the openings and reportedly have achieved great success in potash, salt, and trona mines.

A recent application of yield pillar in coal mines at great depth has been successfully carried out at four of the mines operated by Jim Walter Resources (Carr, et al., 1985; Gauna, et al., 1985). The longwall development entries created by employing the original abutment pillar design in these mines were subjected to severe floor heave such that the entries were completely closed in some extreme cases. Under this situation, yield-abutment-yield pillar design has been tried. The original severe floor heave in the entries due to inadequate size of abutment pillars was reduced significantly. In addition to the improvement of the entry stability, a yield-abutment-yield pillar design offered an increase in recovery and production efficiency. (Barton, 1989) conducted a field survey in three longwall entry-pillar systems in Kentucky and indicated that the yield pillar system combined with heavy artificial support may be a viable ground control alternative for deep-cover multi-entry longwall system. The yield pillar experiments had also been carried out by others (Dahl, 1972; DeMarco, 1988; Haramy, 1989). The results have shown that yield pillar design have improved the stability of the entry-pillar system and increased coal recovery.

2.4 Conclusions

As described earlier, although researchers have developed a number of pillar design methods each of them has its own merits and shortcomings. Overall, the following characteristics can be observed;

- Without exception, all conventional pillar design methods consider the pillar stability only.

- To determine pillar loadings, the conventional methods for longwall pillar design assume that a pillar is subjected to vertical pressure only and that the vertical stresses within a pillar are uniformly distributed.

- All the pillar design methods attempt to design a stiff pillar, even though the progressive failure of pillar has been recognized by most researchers as more realistic in describing the failure mechanisms of underground structures.

- No methods have considered the deterioration of material properties as the time elapses.

- Although yield pillars have been practically used in underground coal mines, there is no uniform design method to design a yield pillar. Most practical application of the yield pillars remains at the stage of trial and error.

- However, years of mining practice have shown clearly that a stable pillar does not necessarily promise a stable entry system. Further, researchers have proven that both vertical and lateral pressures exist in underground coal mines. The magnitude of the lateral stress may vary from zero to a value greater than the vertical stress. Additionally, the stresses within a pillar are not uniformly distributed. Based on this information that previous researchers have discovered, the conventional pillar design method eventually will have some limitations on its applications. It can not deal with some ground control problems, such as coal bumps, floor heave, cutter roof, etc. The problems will become more severe when the mining activity goes deeper.

Chapter Three
SUBSIDENCE EFFECTS

3.1 Introduction

The removal of material from the earth's crust by underground mining creates an obvious potential for ground movement and consequential deformation of the surface. The circumstances under which this may arise vary widely, the main parameters being:

i. The geometry of the mineral deposit: This can range from thin stratified flat seams to steeply dipping irregular veins or lenses, and massive ore bodies large in al1 three dimensions.

ii. The method of mining: There may be partial or total extraction, with or without artificial support, and caving of the roof or hanging wall may be undesired or deliberately induced.

iii. The nature of the mineral deposit and the overlying strata: There is wide variety in the physical characteristics, hydrology, geology, depth of cover and other factors pertinent to ground behavior.

Despite significant advances in the science of rock mechanics in the last two decades, analysis and prediction of stress and strain in large rock masses remains formidably complex because of such factors as anisotropy, lack of homogeneity, and the presence of geological discontinuities. These problems have so far prevented the development of a unified phenomenological theory capable of predicting satisfactorily ground movement and surface subsidence in the wide range of mining situations described above.

The environmental importance of subsidence is related to three main factors:

i. The surface land area affected;

ii. The nature of the land uses within the affected areas;

iii. The type and magnitude of ground movement.

A large majority of the investigations into surface subsidence so far undertaken have concentrated upon areally extensive mining in countries of high population density. Underground extraction of seam deposits, such as coal, normally requires that large areas are undermined if significant tonnages are to be produced. Particularly in Western Europe, this type of mining has for many years co-existed with important surface land uses. There has thus been strong pressure to devise techniques to predict and minimize surface subsidence damage, especially since collapse of the roof and overlying strata behind the working faces is normally an integral part of the longwall mining systems most often adopted. Other types of mining have seldom presented the same urgency to understand and control the subsidence mechanism. Many mining methods commonly used in steeply dipping and irregular deposits require that the structural integrity of the hanging wall is preserved, as far as possible, by the use of natural or artificial support. For those methods, which rely upon caving often hanging wall, it is often assumed that major surface disruption is inevitable and that the affected surface zone must be cleared of installations and effectively left derelict. There have been very few attempts to predict or measure subsidence for these types of mining method (Riplay, E et al., 1996)

3.2 Predicting Surface Deformation

Mining one or more seams most commonly produces a relatively continuous surface deformation, which can be measured in terms of vertical and horizontal displacements. Various calculation techniques are used to predict these displacements, founded on extensive investigation in European coalfields. These are principally based on the complete extraction of stratified deposits in situations where the depth and area of excavation are large in relation to the seam thickness. Most techniques currently in widespread use rely upon an empirical approach, although there are continuing research efforts to base prediction upon theoretical or phenomenological considerations.

3.2.1 Empirical Methods

It is observed that surface deformation over a single extraction area in a flat seam has the following characteristics:

i. A subsidence trough is formed by the vertical displacements of surface points and this normally extends beyond the limits of the mined area.

ii. Horizontal displacements occur with magnitudes and directions approximately proportional to the slope of the subsidence profiles.

iii. If the extraction is geometrically regular in shape, the distribution of vertical and horizontal displacements is approximately symmetrical about the center.

Two concepts are fundamental to most empirical calculation techniques. The first is that vertical displacement has a maximum possible value (Smax) for a particular excavation and this full subsidence is determined from:

$$S_{max} = a\,m \qquad (3.1)$$

Where, *m* is the seam thickness and a is the "subsidence factor", which varies with local conditions.

The second concept is that full subsidence only develops if a sufficient area of the seam, relative to the depth of mining, is extracted. The 'critical area' is defined as the extraction area, which produces full subsidence at one surface point only. Areas that produce no full subsidence are termed sub-critical, and those, which produce full subsidence at more than one point, are super-critical.

Figure 3.1 shows the typical profile of a subsidence trough with the vertical and horizontal displacements of surface points. The angle of draw (or limit angle) is the angle of inclination, measured from a vertical axis, from the edge of the mine workings to the point of zero subsidence. It is a function of seam dip and local geology and in Britain is commonly in the range 25°-35^0. In practice an arbitrary small value of vertical displacement is often taken as the limit of subsidence.

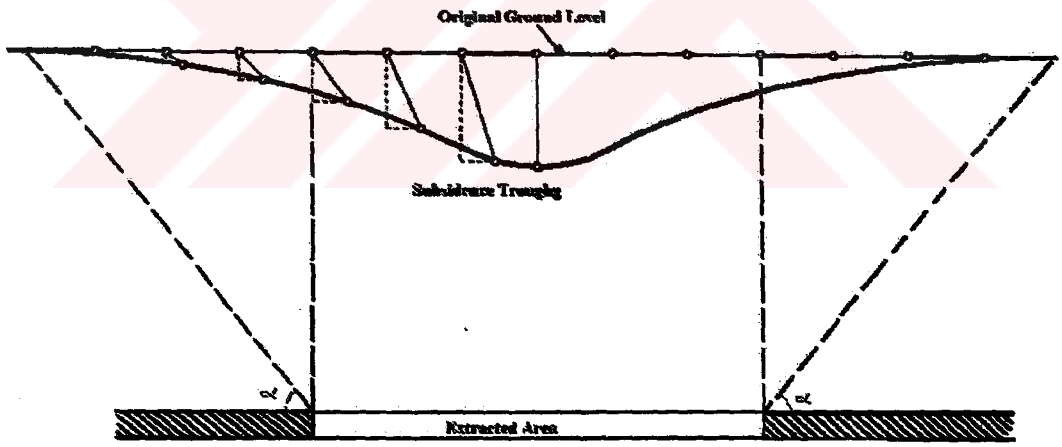

Figure 3.1 Profile of typical subsidence trough, α = limit angle (Riplay, E et al., 1996)

Figure 3.2 shows typical distributions of strain, horizontal and vertical displacements for critical, super-critical and sub-critical extraction areas. Maximum tensile strain normally occurs approximately vertically over the edges of the extracted panel and horizontal displacement is zero where full subsidence has developed.

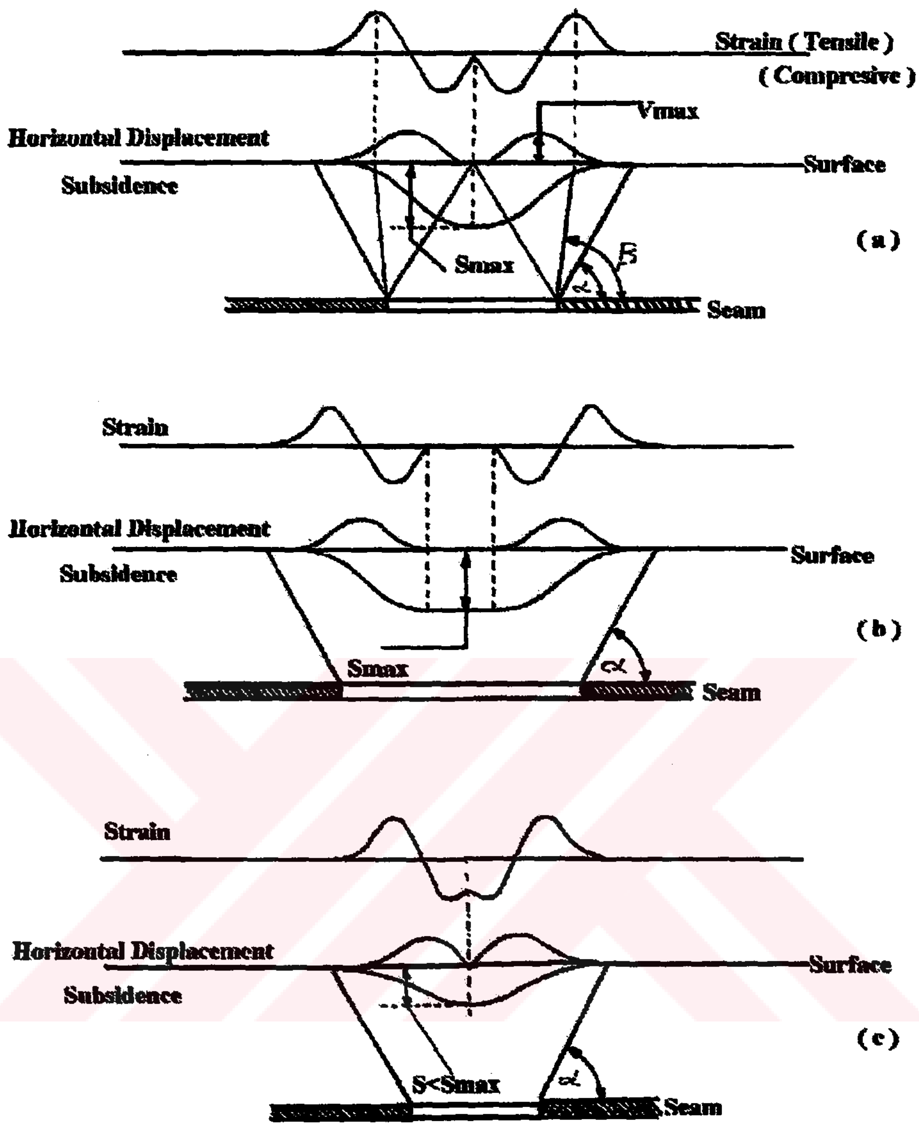

Figure 3.2 Critical (a), Super-critical (b), and sub-critical (c) mining depth (Riplay, E et al., 1996)

An empirical relationship in common use is that the maximum subsidence over a sub-critical area depends upon the size of that area in relation to its depth. Provided the length of the extracted area is at least 1,4 times the width, it is found in practice that the two-dimensional case can be considered adequate. In this case the relationship states that, for sub-critical widths, extraction areas having the same width-to-depth ratio produce the same maximum subsidence, other parameters being equal. Figure 3.3 shows a typical graph used for prediction by the National Coal Board (NCB, 1975) 2 based on the above principle. The graph assumes that there are no zones of special support and that the average panel width is used where panel sides are not parallel. An accuracy of ±10 % is claimed for this method in the majority of cases in British coalfields.

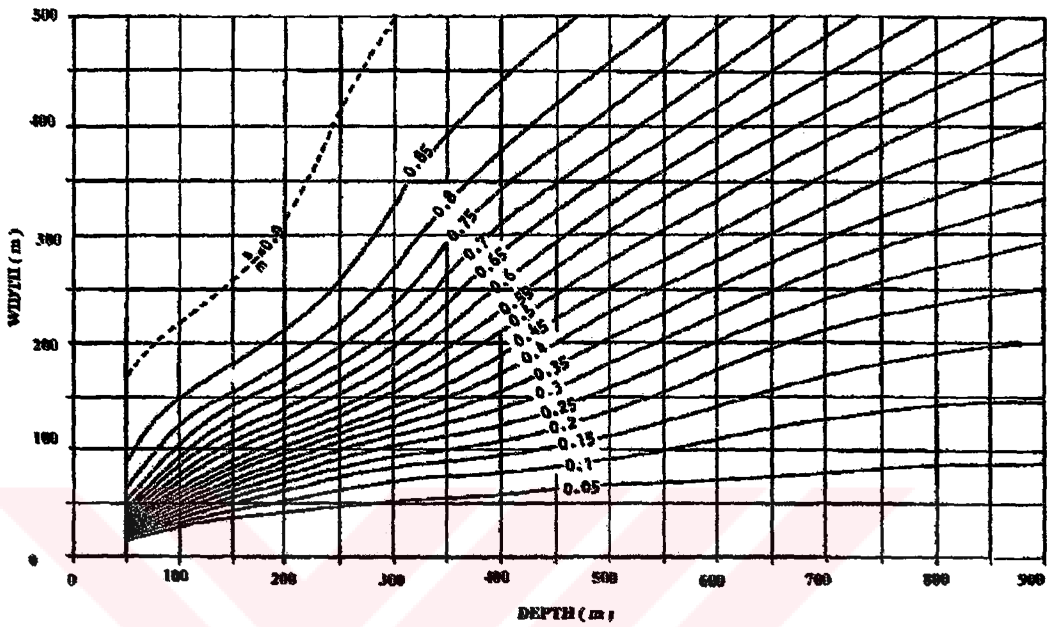

Figure 3.3 Relationship of subsidence to width and depth (NCB, 1975)

The greatest possible subsidence S_{max} is found to occur at width-to-depth ratios exceeding 1-2, where the subsidence factor a is approximately 0.9 for full caving. Solid stowing reduces a to about 0,4 - 0, 5.

Despite the fact that each subsidence process must obviously change the state of the affected rock mass, in practice the principle of super-position is often found to be accurate within acceptable limits.

The subsidence factor a used in equation 3.1 is determined by measuring the full subsidence over super-critical areas. Variations in *a* may be attributable to the type of packing (if any) used behind the working face, and additionally significant variations are found from one coalfield to another, indicating the influence of particular roof strata. Cites values of *a* determined in a number of major coal mining countries and these are summarized in Table 3.1 (Brauner, 1973) and the value of break angle and limit angle for different ground conditions are given in Table 3.2 from the different countries, respectively (Onargan et al., 2000)

Table 3.1 Typical value of subsidence factor, (a), (Brauner, 1973)

Location and Method of Packing	Subsidence Factor (a)
Britain: Roof caving or strip-packing	0,90
Solid stowing	0,45
Germany (Ruhr): Roof caving	0,90
Pneumatic stowing	0,45
Other solid stowing	0,50
France (Pas de Calais): Roof caving	0,85-0,90
Pneumatic stowing	0,45-0,55
Hydraulic stowing	0,25-0,35
Upper Silasia: Roof caving	0,70
Hydraulic stowing	0,12
U. S. S. R.: Roof caving	0,60-0,90
Pennsylvania	0,50-0,60

Table 3.2 The values of limit angle determined in coal mines for various group condition (Onargan, et al., 2000)

Draw Angle (Vertical Axis)	Ground Condition	Coal Site	Reference
45	Thick Alluvial Sediments	Limburg Coal Site Holland	Pöttgens, 1978
41	Thick Alluvial Sediments	Trend River Valley, England	Hazine, 1977
35	Rock Covered Shale and siltstone Sequence	Midlands Coal Site, England	Orchard, 1957
23-39	Rock Covered Shale and siltstone Sequence	Berton, U. S. A.	Nieto, 1979
25	Rock Covered Sedimentary Hard Sandstone	Seranton Wilkes Borne, U. S. A.	Howell, 1979

Calculation methods, which follow the principles discussed above generally, predict the final subsidence of horizontal formations and may be extended to other factors such as horizontal displacements and dipping strata. Two general methods are in use and involve functions termed *profile* or *influence* functions.

Profile functions express mathematically the distribution of displacements over two-dimensional critical extraction areas. For super-critical widths the central trough has a constant subsidence of S_{max} and for sub-critical widths the profile is determined from the critical case using empirical relationships. The method is normally restricted to rectangular extraction areas.

Influence functions apply the principle of super-position. The extraction area is considered as an infinite number of infinitesimal elements and likewise the subsidence trough is regarded as a composition of infinitesimal troughs produced by the extraction elements. The subsidence of any surface point is the sum of the individual subsidence's due to each extraction element. This method imposes no restrictions on the geometric shape of the excavation area.

3.2.2 Physical Model Studies

Quantitative simulation of subsidence by the use of physical models has seldom been undertaken because of the difficulties of devising three-dimensional models, which accurately reflect the mechanical behavior of actual rock masses. Most experiments have therefore concentrated upon qualitative investigations. Problems such as the justification of the principle of super-position or the effects of previous workings can be studied with the use of models.

In a paper (Onargan, et al., 2000), break angle has determined around 53^0 by physical model action results and also break angle has been found 56^0 from the subsidence cracks and extracted coal reserves border with then help of geological section derived from the 1/5000 scaled subsidence map for Hüstaş mine.

3.2.3 Theoretical Studies

Theoretical techniques consist essentially of replacing the rock mass with an idealized material, which deforms in accordance with the principles of continuum mechanics. Most of the traditional mathematical models of solids have been applied to the problems of subsidence. These include isotropic and anisotropy elasticity, viscoelastic and viscoplastic behavior.

Up to the present time this abstract model approach has had little practical significance. The great potential advantage of the method is that it can lead to a much deeper understanding of subsidence mechanisms than is achieved by empirical techniques. The current disadvantages are that application to actual problems requires simplifying assumptions, which seem to preclude realistic analytical solutions.

3.3 Subsidence Damage

Knowledge of damage occasioned by subsidence is mainly based on stratified deposits, although other types of mining have been the subject of some study (Crane, 1929).

In assessing subsidence damage there may be confusion with "pseudo-mining" damage, which can be similar in effect but is not caused by mining. Foundation settlement due to the weight of the building or plaster cracks caused by bad construction techniques are common examples of "pseudo-mining" damage. Changes in the level of the groundwater table, which may be caused by mine pumping, can cause soil shrinkage and settlement of buildings. In localities where damage due to mining subsidence might be expected, it can be difficult to determine unequivocally the cause of such damage.

3.4 Control of Subsidence Damage

The alleviation of subsidence damage may be undertaken either by precautionary measures on surface to protect installations or by modification of the mining method so as to minimize deformation of the surface (Voight, 1970, Brauner, 1973, NCB, 1975).

3.4.1 Structural Precautions

The location of new installations is an important control measure. It is advisable to avoid areas of natural geological discontinuity, such as the outcrop of a fault, because of the higher probability of discontinuous deformation. Likewise the hanging wall of a steeply dipping ore body, particularly if caved or unsupported, should be avoided.

3.4.2 Underground Precautions

Surface areas can be protected by leaving a safety pillar of mineral of sufficient dimensions or by controlled mining, which ensures that allowable deformations are not exceeded.

The size of safety pillars has often been determined by using a constant "angle of protection" often equated with the angle of draw (limit angle), as illustrated in Figure 3.4. This is now commonly regarded as unacceptable because most structures are only susceptible to differential movements and unnecessary sterilization of mineral may occur. This loss of mineral increases with depth of working. Furthermore, adequate protection may not be ensured, particularly in multi-seam mining, and other problems such as high stress concentrations underground can result. In workings where subsidence effects are predictable with reasonable accuracy, a better approach is to assess the allowable surface deformations and to undermine as far as possible without exceeding these deformations, subject to a reasonable safety factor. This method is particularly applicable to deep seams where a large loss of mineral may thus be avoided. In shallower workings, the loss of mineral is less severe and the potential surface deformations are more damaging and it may be economical to leave a relatively large safety pillar (Riplay, E et al., 1996).

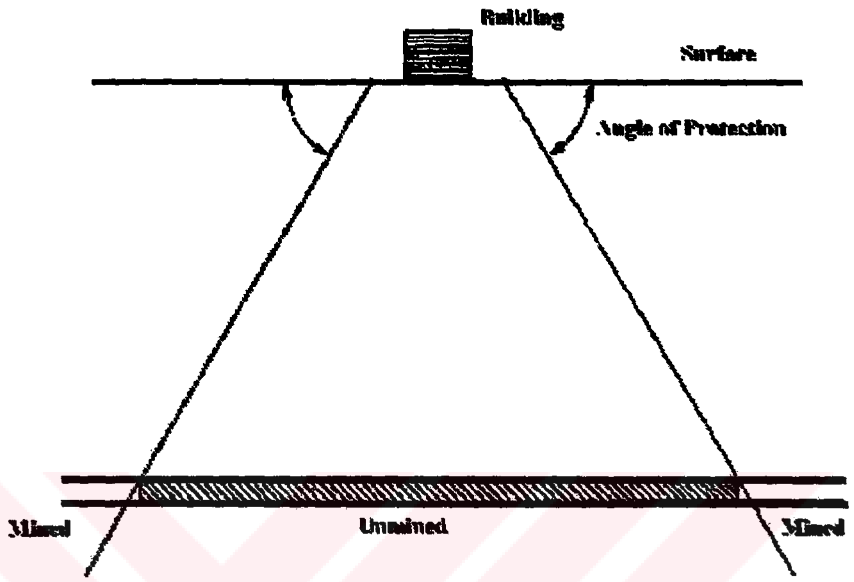

Figure 3.4 Safety pillar under constant angle (Riplay, E et al., 1996)

In seam mining it may be possible to avoid adverse configuration, which produce maximum differential movements. These are illustrated in Figure 3.5.

An alternative t leaving a completely unmined safety pillar is to mine only part of the deposit, leaving the remainder in-situ to reduce surface deformation. Mining system of this type are usually termed room and pillar or board and pillar. Cites data from European coalfields, which indicate a preference for relatively long narrow panels separated by permanent pillar, the width of both panels and pillars being of the order of 20-30 % of the depth of mining. With extraction ranging from 40-70 %, observed subsidences are 3-20 % of seam thickness (Brauner, 1973). Filling or stowing of the excavated area reduces the potential for subsidence damage.

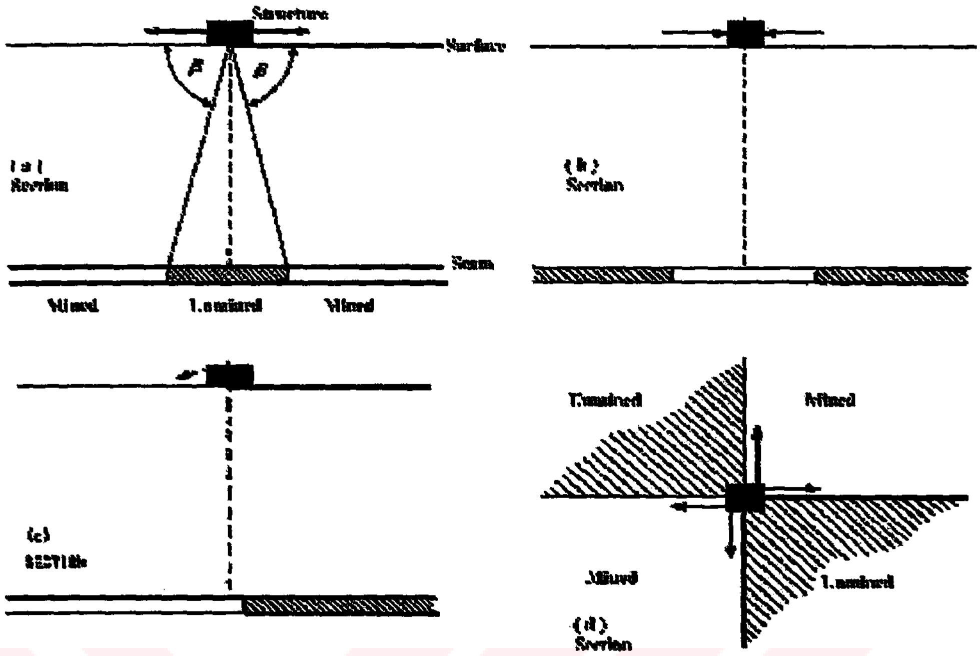

Figure 3.5 Unfavorable extraction layouts: β = angle of break and arrows show direction of strain. (a) the surface structure is placed under maximum extension, (b) under maximum compression, (c) gives maximum slope, (d) produce maximum distortion (Riplay, E et al., 1996)

In longwall mining of coal under British trunk roads, for example, three-shift, 7-days per week mining is employed during the critical period, thus avoiding the intermittent stresses arising from faces which stand for one shift in three and at weekends (Down, et al., 1977).

3.5 Subsidence Damage to the Shaft

When working takes place in the safety zone, the outer cylinder of the shaft wall, enclosed as it is by the rock mass, is exposed to the highly varied movements of the strata through which it passes. If the inner safety zone is worked, the lower part of the shaft is forced somewhat upwards into the mine excavation by the footwall beds, whereas the hanging wall or roof, to which the upper section of the shaft is bonded by mortar , concrete, or some general interlocking action, tends to drag it down with itself. In this process considerable compaction damage to the wall and internal structures of the shaft often results at the working horizon. Higher up, as workings pass round the shaft, it is axially stretched and lengthened by the strata as they become perpendicularly relaxed. If mining takes place at the outer boundary of the shaft safety-pillar, the part of the shaft nearest to the surface falls within the zone of vertical compression ahead of the face, a zone in which higher points in the rockmass subside more than lower ones. At the dividing line between the sandy surface layers, which slip down the shaft, and the solid rock beneath, which acts as a firm support for the shaft, a peak of axial compressive stress can build up in the shaft lining.

The horizontal components of strata movement have the effect of displacing the shaft outwards i.e., away from the center of the workings both in the floor and in the main roof, and inwards -towards the center- in the higher strata. The result is that the shaft structure, from the extraction level to the surface, leans towards the goaf and becomes bent. This inclined position of the shaft starts to develop ahead of the approaching face and is at its maximum just after the passage of the face, gradually reducing towards the center line where the shaft is once again vertical. In an inclined shaft a somewhat higher rate of wear is noticeable in the hoisting installations, but a rupture of the shaft is unusual given a regular pattern of strata displacement, since even a horizontal compressive stress of 2 mm/m implies that the walls of a 6 m diameter shaft well close in by only 12 mm. This degree of horizontal compression is largely taken up by the pressure arch in the rock mass encircling the shaft section and by the surrounding porous layer. If, however, the surrounding concrete has been tamped down and compacted, the rock pressure can produce a strain of 1 -2 mm/m of diameter in the shaft section itself (Skutta, 1979). Bending of the shaft axis is mostly slight, but possible bending stresses have to be taken into account in the construction of rigid linings. Horizontal shear movements in severely bent strata are always associated with fractures in shaft linings.

The method followed in Germany since the 1930s for calculating the amount of lengthening and shortening in mine shafts (Bals, 1939) starts from the assumption that each section of the shaft, all down its length, sinks to exactly the same extent as the subsiding rock mass around it. Axial deformation of the shaft is therefore equated with vertical deformation of the rock mass. Table 3.2 shows the effects of mining on the shaft.

Table 3.3 The effects of mining on the shaft, (Kratzsch, 1983)

Effects and Damage	Cause	Manner of Transmission	Critical Factors	To be Determined
Vertical compression and extension of shaft	Subsidence of rockmass of varying amplitude at depth	Frictional and adhesive shear stress	Vertical compression and extension of strata; shear force (wall area, effective length) deformation resistance (cross-section, linear changes, E modulus)	Transmission relationship of rockmass and shaft
Tilting, Bending	Horizontal strata displacement, varying at depth	Close fit between shaft section and rock face	Sitting of shaft in relation to workings	Extend of strata displacement
Shearing fracture	Intense bending of strata	Shear force parallel to stratification	Degree of bending resistance of bending planes to shear	Shaft path
Horizontal pressure	Compaction of a weak bed	Transverse expansion	Vertical compressive pressure, degree of yield in strata, compression	Degree of pressure on shaft

Although this simple method of calculation has served well for over three decades in the prediction of axial shaft stresses, the assumption that "shaft deformation equals strata deformation" is in fact valid only for the middle sections of the shaft. It does not hold good for the top and bottom sections, those nearest the surface and the workings. Measurements show that the shaft head frequently appears to "grow" out of the ground: which indicates that there is relative movement as between the upper shaft structure and the surface zone of strata. When the inner shaft safety pillar is mined, a shortening of the shaft structure has been observed both above and below the mining horizon where, according to calculations, only a lengthening or, as in the footwall, no effects at all should occur. Ahead of the face the structure has been shortened even below -i.e., outside -the limit of influence of the workings, whereas by calculation it should be unaffected. In one shaft, subsidence of 14 cm was measured as much as 300 m below extraction at the edge of the pillar (Skuta, 1979).

A shaft structure bound to the rock mass thus reacts to the influence of extraction differently from the rock mass itself.

The breaking strength of the shaft's close fit in the rock and its interlocking with it is of the order of τ_{Br} = 100 N/cm^2 = 1 MN/m^2 (Sitz, 1968). A break between the shaft wall and the rock face will accordingly occur almost as soon as the effects of extraction begin to be felt, i.e. when axial deformation of the shaft lining amounts to 0.05 mm/m in the case of concrete bonding, or to 0.1 mm/m with mortar bonding. Once a rupture plane has been formed in this way, the local force transmissible to the shaft wall drops to an adhesive shear or frictional stress of around 10 N/cm^2 in solid rock, and 3 N/cm^2 in loose ground.

For the frictional or tangential shear force F_t acting on the shaft as the rock strata slide down it, the following equation can be formulated (Kratzsch, 1983):

$$F_t = \tau Al \tag{3.3}$$

The transmitted shear force is met, by way of force of reaction, by the elastic deformation resistance D of the shaft lining:

$$D = \varepsilon ESl0^{-3} \tag{3.4}$$

The frictional force, which builds up and is transmitted to the shaft, thus increases linearly with shaft length. Correspondingly, the graph of shaft deformation will rise in a straight line until it reaches the magnitude of the strata deformation. Finally, after restatement, the required slope $\tan\alpha$ of this line of shaft deformation in mm/m per running meter of shaft length:

$$\frac{\varepsilon}{l} = \tan\alpha = \frac{\tau A 1000}{ES} \tag{3.5}$$

In this way a simple connection is found between the shear force and the degree of vertical extension or compression E in relation to shaft length. At the same time however (through this is not completely true), the coefficient of friction and the strata pressure normal to the shaft section 1 remain constant, while elastic, through not plastic, deformations after fracture of the lining cylinder are taken into account.

3.6 Extend of Vertical Expansion and Contraction in Strata and Shaft

Vertical strata deformation can be ascertained from the subsidence of points in the rock mass calculated with an integration grid, by dividing the difference in subsidence (in mm) by the vertical distance between points (in m). Special integration grids for the direct calculation of expansion and contraction have also been designed, but they offer no great saving in labor or time as compared with deriving strata deformation from subsidence values (Sauer, 1961, Kochmanski & Magdziorz, 1972).

What appears very promising for shaft investigation is the finite elements method, if the shaft-lining cylinder is regarded as a vertical column of infinitesimal elements with in the total mesh, to which is assigned a substitute elastic modulus for tubing, brickwork and concrete, related to the shaft section as a whole (Kose, 1978). The adhesive shear bond between the exterior wall and the rock face can be represented in model terms by a weak boundary layer. A gradual diminution of the elastic modulus in those elements of the boundary layer, which have reached a critical shear stress, enables the transition to kinetic friction to be modeled.

Calculate chiefly the situation at depth and maximum extend of vertical strata expansion or contradiction at the shaft and equate this value to axial shaft deformation (Knothe, 1969).

During working, dynamic contraction reaches only % 30 of its final value, whereas dynamic expansion is % 60 greater than final expansion (Pielok & Sroka, 1979).

3.7 An Analysis of Shaft Stresses Due to Mining

At the beginning of the mine planning exercise therefore, the section of the shaft to be protected and the permissible degree of deformation must be strictly decided. The degree of this determined by amplitude of subsidence in the workings and initially also by the added influence of deformation forces acting on the section of the shaft concerned. The type of deformation will depend on the sitting of the shaft in relation to the workings in horizontal terms.

Interim stress on the shaft can differ greatly from this final stage of strata deformation, depending on the conduct of the mining operation and the treatment of the shaft lining at the mining horizon (whether it is slit and provided with a timber crib, etc.). A working, which proceeds at critical extraction width 2R from the edge of the shaft pillar towards the shaft, and from one side only, has the effect at first of axially compressing the shaft head (Figure 3.6a). As the face advances, the zone of axial compression in the shaft lining extends to the mining horizon (curve 2). After the face has passed round the shaft, the middle and upper reaches of the shaft become extended (curve 3). The compression maximum which develops at the mining horizon, up to the area of extension-free shaft at the center of a critical area (curve 4), damages the shaft lining if it has not, as is more usual, been opened up to seam height and had a yielding timber crib inserted (Figure 3.6b). On this basis, a face carried inwards from one side stresses the shaft structure, first by compression and then by extension. Furthermore, the shaft becomes tilted in the meantime. With a face of less than 2R (critical width), a slight axial extension remind in the upper shaft lining after the shaft safety zone has been worked through, instead of curve 4.

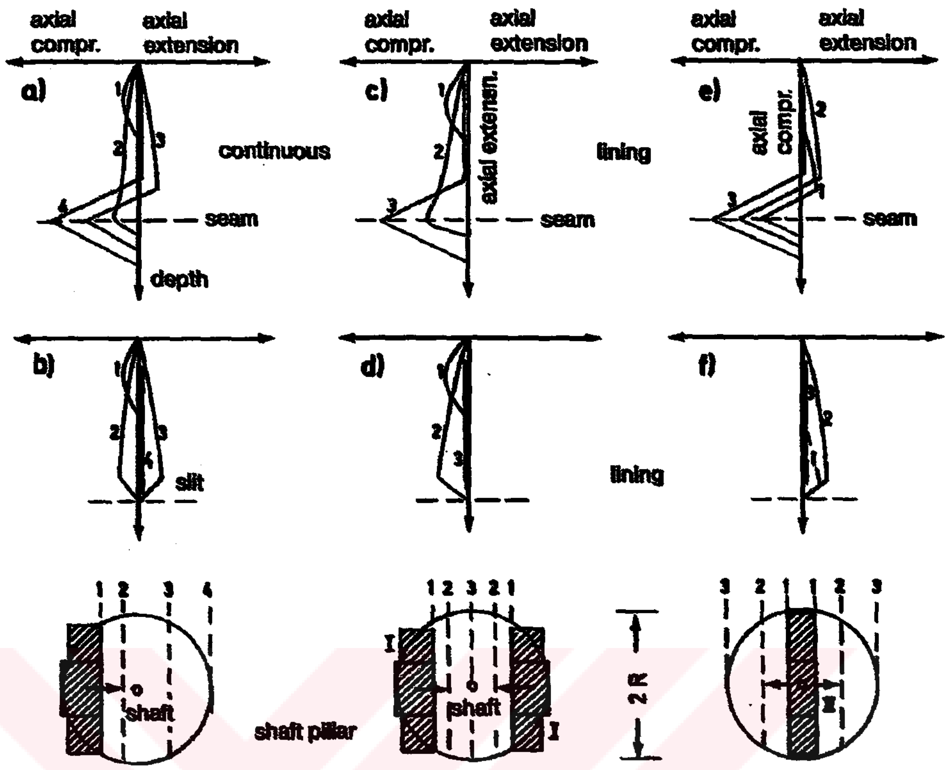

Figure 3.6 Stresses affecting a continuous shaft (top) and shaft which is "slit" at working horizon (center), with extraction proceeding from one side of shaft pillar, from both sides symmetrically, and from center of pillar symmetrically outwards (bottom) (Kratzsch, 1983)

The alternating stress on the shaft and its deviations from plumb can be avoided by working the shaft safety zone symmetrically and from the outer edge inwards. Compression of the upper section of the shaft, down to just below the limit of mining influence, is greater than shown at Figure 3.6a (curve 1) because of the doubled mining influence. At position 2 of the face, the lower section of the shaft is also axially compressed. After that the upper shaft structure becomes unstressed, but high compression remains above and below the workings (curve 3), unless the shaft lining has been slit (diagram d). Consequently, with symmetrical working from the edge of the pillar inwards, at no time does the dreaded stretching effect arise in the upper shaft structure, which consists of segments of tubbing to seal off the water-soaked sand beds of the overburden layer. With this mining procedure, stretching can be avoided throughout the length of a concrete shaft (which is vulnerable to tensile stress), provided it is slit at the mining horizon.

If the shaft pillar is mined symmetrically from the shaft outwards - and there are many good mining reasons for doing this, not least the early uncovering of the shaft walling at the mining horizon, which is at risk - then either the upper section of a continuous lining (diagram e) or the whole shaft structure above a slit (diagram f) remains free of axial compression. Working on both sides has the effect of acting first on the lower part of the shaft (curve 1), which is axially compressed and extended (diagram e) or only extended (diagram f). In position 2 of the face, the extending action is affecting the shaft lining right up to the pit-bank level. With a critical extraction area, a slit shaft shows no linear change on completion of mining. A continuous lining, on the other hand, shows (as in diagrams a and c) a dangerously high degree of axial compression at the working level. Since rupture cracks in the lining cannot be ruled out, this mining plan can only be followed in dry strata.

Shear fracture occurs at the shaft if the beds, which it intersects, are so severely bent by one-sided working (position 2 of the face in Figure 3.6b that the bending shear stress rising parabolically at the center of group of beds overcomes the adhesive shear stress, or limiting friction, at a bedding plane.

Two points, standing on opposite side of the slip plane, are then displaced by a shear travel. No shaft lining, however strong, can withstand the shear movement of two bed. In inclined to steep-lying measures, however, shear movements can occur without causing bending (Sljachackij, 1974).

In the initial phases of mining it is not possible to achieve a complete balancing-out of deformation at the shaft by causing axial extension and compression to coincide, both in time and in place. The compression resulting from working at the pillar edge develops at the shaft head (Figure 3.6d). Axial extension over a central working, on the other hand, starts in the bottom section of the shaft (Figure 3.6f). Simultaneous opening-up of symmetrical edge workings I and central working II therefore leads to compressing the shaft lining at the top and extending it at the bottom. It is only from position 2 onwards that the extending and compressing effects on the shaft structure cancel themselves out. All the overlying strata then subside equally at the shaft side and take the lining cylinder down, without linear change, by the amount of the roof settlement.

For a face advance, which spares the shaft, it is usually sufficient to mine only the inner shaft protective zone from the point of view of balancing out expansions and contractions, in time and place, as much as possible. The protective zone in a seam, which at 700 m depth measures around 1000 m in diameter, is divided into three or four sections with a face length down the dip of 250 or 200 m, as the case may be. The outer segments of the circle, which will have only a slight compressional effect on the shaft head when mined later, are ignored. Where the protective area is very large, a limited approach such as this is all the more necessary to keep the operation within a manageable size and, by concentrating on the sectors having the strongest influence, to minimize the time during which the shaft is endangered (Kratzsch, 1983).

The mining plans represented in Figure 3.7 envisage, in ground-plan, "a" perimeter workings I starting first, followed slightly later by central working II in both directions; in ground-plan "b", central working I in both directions from eccentrically offset faces, followed by perimeter working II; and in ground plan c, extracting the shaft pillar on a checkerboard pattern, called harmonically (Lehman, 1938, Balls, 1939), which leaves the shaft practically stress-free. In a water-bearing surface rock, the initial compression of the shaft head expected under mining plans "a" and "b" is a desirable handicap to offset its elongation that will come later. The expansion in the lower roof strata caused by central working represents no threat to the operational security of the shaft in dry rock and does less damage to the loading stations than compression.

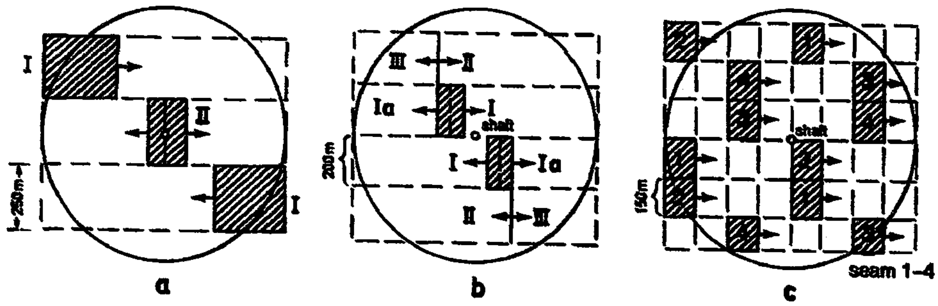

Figure 3.7 Examples of combined peripheral and central working of shaft's protective zone in one seam or in several seams (Kratzsch, 1983)

As regards the rate of face advance, rapid peripheral working will reduce dynamic contraction, and rapid central working will reduce dynamic expansion. Rapid caving causes rapid subsidence and, consequently, since the stiffness of the bitumen depends on the rate of movement, an increase in the axial force transmitted to the lining cylinder by the slip layer.

A mining plan such as this, entailing symmetrically combined peripheral and central working to cancel out stresses, and capable of being enlarged to take in several scams, often runs into serious difficulties in practice.

A further mining technique that can be mentioned for protecting the shaft lining is stowing the goaf. With stowing - which should be considered for at least the inner shaft-protection zone - subsidence of the roof beds is only half as great as with caving. Vertical contraction and expansion of the rock mass, and axial deformation of the shaft cylinder, both also decrease to a similar extent. In other words, stowing protects the shaft lining very effectively from linear changes, and this applies equally to "low-subsidence" chamber-and-pillar working.

Over the goaf, the lower strata become significantly more relaxed than the upper ones. When subsidence is rapid and bending is severe, the bonding between roof beds can become loosened up to a height of 200 m, causing the lower shaft structure to be pulled apart in the early stages of central working. It has been suggested that this expansion in the main roof be kept within bounds by a "core zone", formed either by leaving the shaft pillar unworked within a radius of 50 to 100 m of the shaft, or by stowing the same area with a very hard, unyielding material (Bals, 1956).

When the core zone itself, 1 in Figure 3.8, is extracted, axial tensional stresses (curve 1) are set up in the shaft lining which reduce the compressive effect (curve 2) of extraction starting at the edge of the protective zone (curve 3). In Polish coal mining, the core zone is stowed with flushed-in sand or with concrete, and this lessens strata subsidence down the length of the shaft cylinder. A staggered face is said to minimize the dynamic effects of extraction (Kowalczyk, et al., 1976).

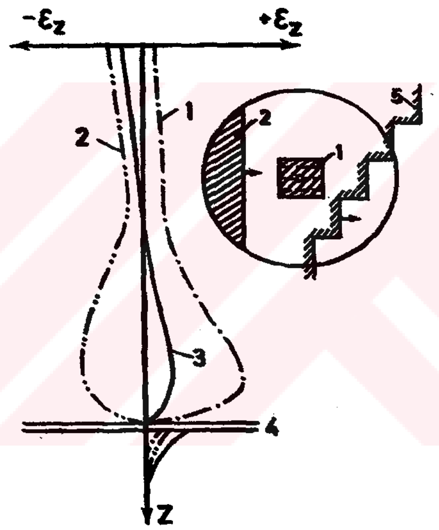

Figure 3.8 Extraction of shaft `s protective zone in Polish coal-mining practice 1-first of all, core zone is extracted and stowed; 2-extraction from pillar edge; 3-combined effects of 1 and 2; 4-seam; 5-staggered working face (stepped-face method) (Kowalczyk, et al., 1976)

3.8 Conclusions

Most of the available knowledge relates to trough subsidence over stratified deposits, particularly coal, worked by longwall methods. The prediction and control techniques in common use are based largely upon empirical investigation and measurement. The science of rock mechanics has enabled some progress on a phenomenological approach with an understanding the behavior of the rock mass overlying an excavation. However, this method still yields mainly qualitative rather than quantitative assessment of subsidence phenomena. Continuing research, both empirical and theoretical, will undoubtedly aid the mining engineer in the dual objectives of maximizing the percentage extraction of mineral whilst minimizing surface disruption.

Chapter Four

BOUNDARY ELEMENT MODELLING FOR SAFETY PILLARS STABILITY A CASE STUDY: HÜSTAŞ MINE

4.1 Introduction

The purpose of this study is to investigate the stress distribution on the main drift and the subsidences on Shaft 1 as their respective safety pillars are mined. This chapter is designed to determine the possibility of damage occurrence on both the Shaft 1 and the main drift safety pillars during the face advance while mining direction is from south to north and from east to west respectively. Properties of main drift and boundary of Shaft 1 has been given in Chapter One. For this purpose, various models for steps of the extraction of the safety pillars are developed and analyzed using the LAMODEL software. Additionally, in case of any damage occurrence, surface subsidence and seam convergence were analyzed to determine the specific parameters of rock such as limit angle and breaking angle. The radius of safety pillar for Shaft 1 is 75 m. and also the thickness of the pillar 18 m. The coal is extracted from south to north with two 160m. long faces for Shaft 1 safety pillar. Similarly; the main drift safety pillar is extracted from east to west with two faces of 120 m.

4.2 LAMODEL Program

This software is designed to analyze the displacements and stresses associated with the extraction of large tabular deposits such as coal, potash, trona and the other vein-type deposits. The displacement discontinuity variation of the boundary element technique is frequently the method of choice. In the displacement discontinuity approach, the mining horizon is treated mathematically as a discontinuity in the displacement of the surrounding media. Using this technique, only a planar area of the seam needs to be discretized, or gridded, in order to obtain the stress and displacement solution of the seam. Often, this limited analysis is sufficient, since in many applications only the distribution of the stress and convergence on the seam horizon are of interest. Also, by limiting the detailed analysis to only the seam, the displacement discontinuity method provides considerable computational savings over other numerical techniques, which discretize the entire body. It is a direct result of this computational efficiency that the displacement discontinuity method is able to handle large areas of tabular excavations as needed in many practical coal mining problems. If stress and/or displacements are required outside of the seam, the model can calculate these as required.

A displacement-discontinuity program incorporating a laminated media has recently been developed by NIOSH (National Institute of Occupational Safety and Health). This program is called LAMODEL. Traditional displacement-discontinuity programs use a homogeneous isotropic elastic formulation, which simulates the overburden as one solid material. In contrast, the LAMODEL program simulates the geologic overburden stratification as a stack of layer with frictionless interfaces. Specifically, each layer is homogeneous isotropic elastic and has the identical elastic modulus, Poisson's Ratio, and thickness. This homogeneous layering formulation does not require specifying the material properties for each individual layer and yet it still provides the realistic suppleness to the mining overburden that is not possible with the classic, homogenous, isotropic, elastic overburden model. This suppleness provides the more accurate strata response modeling local deformation, inter-seam interactions and/or surface subsidence.

The LAMODEL program calculates stresses and displacements at the seam level and at requested location in the overburden or at the surface. LAMODEL can use both linear and non-linear seam material properties, can calculate surface effects, can model single or multiple seams and can incorporate single or multiple mining steps. In order to most efficiently use LAMODEL for accurate stress prediction, the model is first calibrated to the site-specific geomechanics based on previously observed stress or displacement conditions at the mine. For this purpose, a previously mined area is generally stress mapped by quantifying the observed pillar and strata behavior using a numerical rating system, or the surface subsidence associated with a particular extraction area is measured. Then, the site-specific mechanical properties in the model are adjusted to provide to best correlation between the predicted stress/displacement and the observed underground stress rating or surface subsidence. Once calibrated, the model is then used to predict future stress and displacement problems ahead of the mining.

4.2.1 Initial Material Property Generation

One of the most difficult parts of using numerical models is determining the correct (most accurate) material properties for input. After developing numerous displacement-discontinuity models and then comparing their results with field measurements and observations, a fairly streamlined, systematic technique for developing initial material properties has been developed. Initially, the critical material properties (coal, gob and rock mass) are determined using a combination of laboratory research, empirical formulas and experience. Then, in the calibration process, these initial material properties are systemically adjusted in subsequent runs of the model until the calculated results correspond as closely as possible to field observations.

First, to address the problem of determining the input coal behavior, the basic coal strengths are derived from empirical pillar strength formulas, which are solidly based on observed pillar behavior. Specifically, the peak strength of a model coal element is directly determined based on an in situ coal strength and its distance from the edge of the pillar using the stress gradient implied by the Bieniawski pillar-strength formula (Heasly, 1998). For an initial estimate, in situ coal strength of 6.2 MPa (Mark & Barton, 1997) and an elastic modulus of 2 GPa is typically used.

This general procedure for generating the initial coal properties for elements in LAMODEL fulfills a number of practical requirements. It provides LAMODEL pillars with peak strengths, which closely follow the empirically proven Mark-Bieniawski pillar strength formula, and stress profiles which closely follow the Bieniawski stress profile,

$$S_p = S_1 \left[0,64 + 0,54 * \frac{w}{h} - 0,18 * \frac{w^2}{L*h} \right] \qquad (4.1)$$

Where, L is pillar length, w is pillar width and h is pillar height.

Next, to address the gob loading and compaction behavior, a combination of laboratory research and modeling experience is used. In the laboratory, (Pappas and Mark, 1993) found that an exponentially strain-hardening material with a tangent modulus that increases linearly with stress provided a reasonable representation of simulated gob material.

$$\sigma = \left[\frac{E_i * \sigma_u}{E_f - E_i}\right]\left[\left(e^{\frac{(E_f - E_i)}{n*\sigma_u}\varepsilon}\right) - 1\right] \qquad (4.2)$$

Where, E_i, initial tangent modulus at zero stress, E_f is the final modulus at ultimate stress (σ_u), n is the gob height factor.

The necessary input for this material is; initial modulus, final modulus, and final vertical stress. From experience, these three values are initially set at 6.2 MPa, 110 MPa and 27.6 MPa respectively (Heasly, 1998).

The third critical set of material inputs in LAMODEL is for the overburden and consists of a lamination thickness and an elastic modulus. In LAMODEL, the lamination thickness has a major influence on the stress and displacement distribution at the seam and throughout the overburden. Stress distributions (such as interseam stresses) or overburden displacements (such as subsidence) are of primary concern, then lamination thicknesses ranging from 3 to 15 m (10 to 50 ft) provide the best match to field observations (Karabin & Evento, 1994, Pappas & Mark, 1993). In this study, a lamination thickness of 4 m and an elastic modulus of 14 000 MPa were used for the overburden.

4.2.2 Model Calibration

In the model calibration process, the initial material properties are systematically adjusted in subsequent runs of the model until the results correspond as closely as possible to field observations and/or empirical formulas. For the coal properties, the in-situ coal strength is adjusted until the pillar stress/failure in the model matches the observed pillar behavior. For the gob properties, the final modulus value is typically adjusted up or down in LAMODEL in order to increase or decrease the gob stress until the model gob stress matches empirical abutment angle formulas (Mark and Chase, 1997) and/or field measurements and observations. For the overburden properties, the lamination thickness is typically adjusted up to provide wider abutment stresses, smaller interseam stresses and less surface subsidence or down to provide narrower abutment stresses, greater interseam stresses and more surface subsidence as dictated by the mine observations.

At this study, the model geometry was obtained from the production map of the Hustas Mine as shown in Figure 1.3. The material properties of the coal are defined by using equation of Bieniawski pillar strength and yielding material properties are used for yield zone. Elastic-plastic material properties were used for the yield zone whereas linear elastic material properties were used for the intact zone. To accurately simulate the gob zone, an exponential strain-hardening behavior was used. For calibration of the models used in this study, subsidence measurements from previous mining in Turkey were used (Kose & Onargan, 1993, Kuscu, 1985, Onargan et al., 2000). Based on these published works, the maximum subsidence over the 150 m wide extraction area in the Northern half of the mine was predicted to be 5–7 m. In the initial model of the mine with just the two safety pillars remaining, the lamination thickness and gob properties were adjusted to match this estimated value. The final material properties used in the models are shown in Table 4.1.

Table 4.1. Material properties, used in models

COAL ELEMENTS (FOR YIELD ZONE-ELASTIC-PLASTIC)		
ELEMENT	**PEAK STRESS (MPa)**	**PEAK STRAIN**
A	5.5	0.00228
B	6.9	0.00443
C	8.1	0.00443
D	9.9	0.00491
E	11.3	0.00516
F	12.9	0.00588
G	14.4	0.00660
H	15.9	0.00732
I	17.3	0.00804
J	18.9	0.00876
K	20.3	0.00948
L	21.9	0.01020
M	22.6	0.01092
N	24.0	0.01164
O	25.5	0.01236
P	27.0	0.01308
Q	28.5	0.01380
R	30.0	0.01442
S	31.5	0.01524
T	33.0	0.01597
COAL ELEMENTS (FOR INTACT ZONE - ELASTIC-LINEAR)		
ELEMENT	**ELASTIC MODULUS (MPa)**	**POISSON RATIO**
V	2 000	0.329
GOB ELEMENTS		
INITIAL MODULUS (MPa)	**FINAL MODULUS (MPa)**	**FINAL STRESS (MPa)**
6.0	153.2	29.7

4.2.3 Model Analyses

To define the stress, convergence, and subsidence and their effects, several different models were run. To define these parameters, models were analyzed step by step. All steps are given in Table 4.2 and in Figure 4.1 below.

Table 4.2 Mining steps with direction

SAFETY PILLAR OF MAIN DRIFT (EAST TO WEST)		
STEP	**DISTANCE FROM EDGE (GRID)**	**DISTANCE FROM EDGE (METRE)**
1	400	0
2	373	54
3	348	104
4	336	128
5	239	322
6	181	438
SAFETY PILLAR OF SHAFT 1 (SOUTH TO NORTH)		
STEP	**DISTANCE FROM EDGE (GRID)**	**DISTANCE FROM EDGE (METRE)**
1	36	0
2	44	16
3	54	36
4	66	60
5	82	92
6	100	128
7	113	154
8	155	230

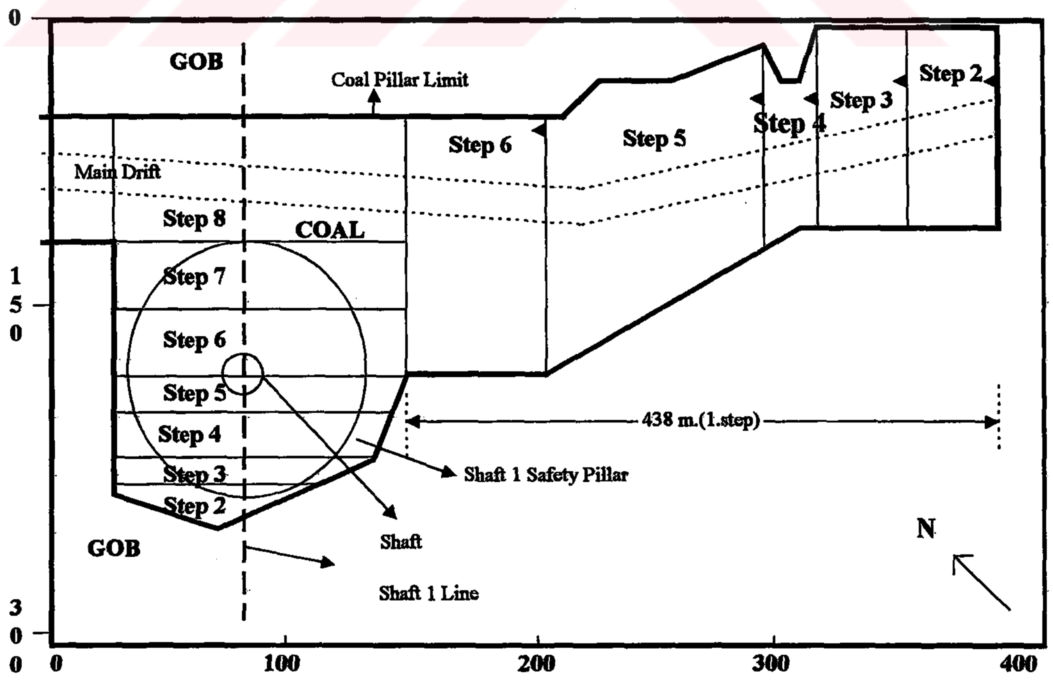

Figure 4.1 Mining steps for analyzing the safety pillar of main drift and shaft 1

After these steps have been defined, computer program has been run for each step and the stress and convergence contours are given Figure 4.2 to Figure 4.15 below.

The photos from field, graphs of vertical stress, gridded map for boundary element analyses and topographical map for subsidence analyses are given in appendix a, appendix b, appendix d and appendix e respectively. The unit of stress values is in Pascals, and convergence values and distances are given in meters.

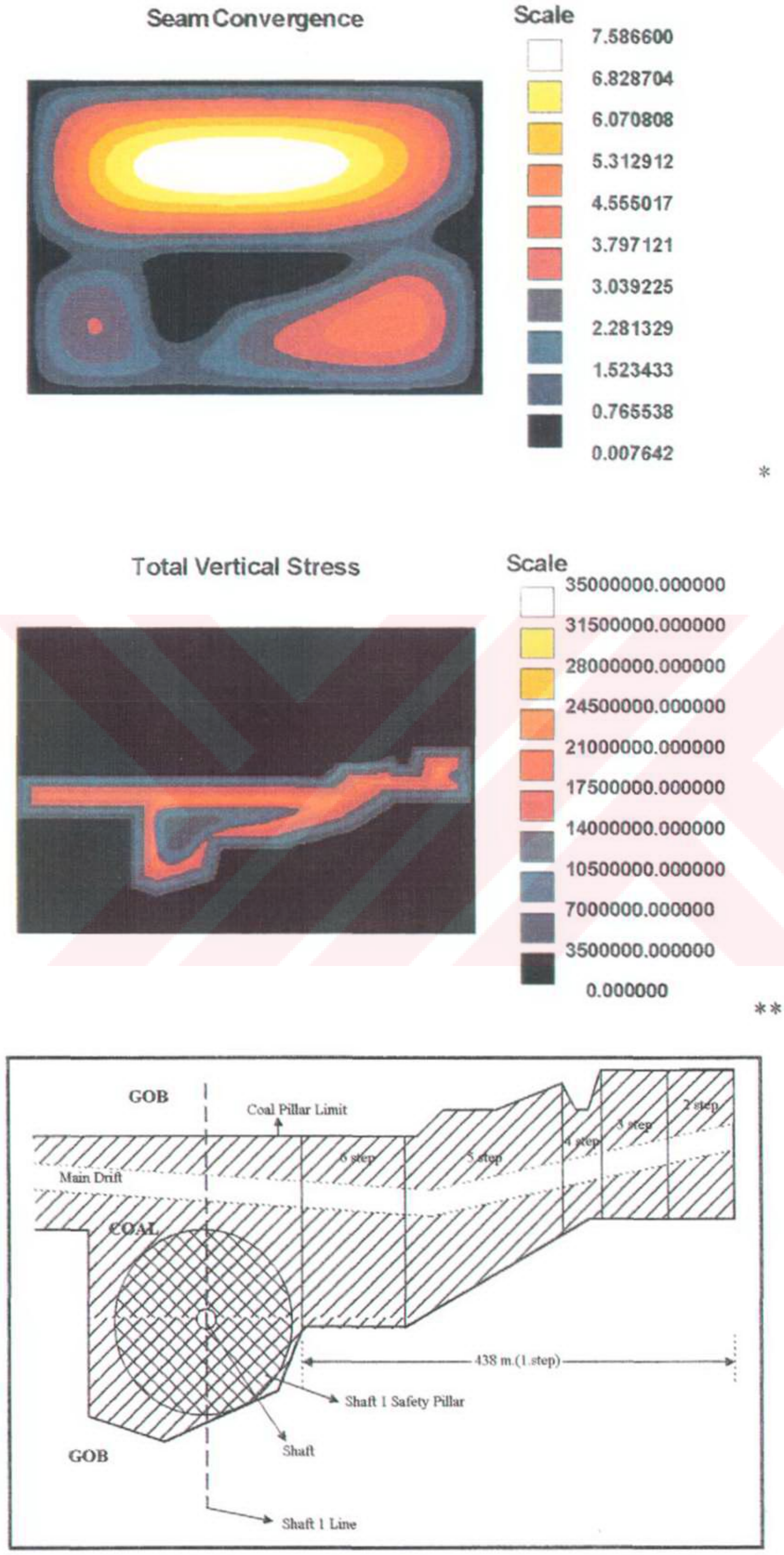

Figure 4.2 Seam convergence and vertical stress for through mining step 1 of the main drift safety pillar (*, in meters, ** in Pascals)

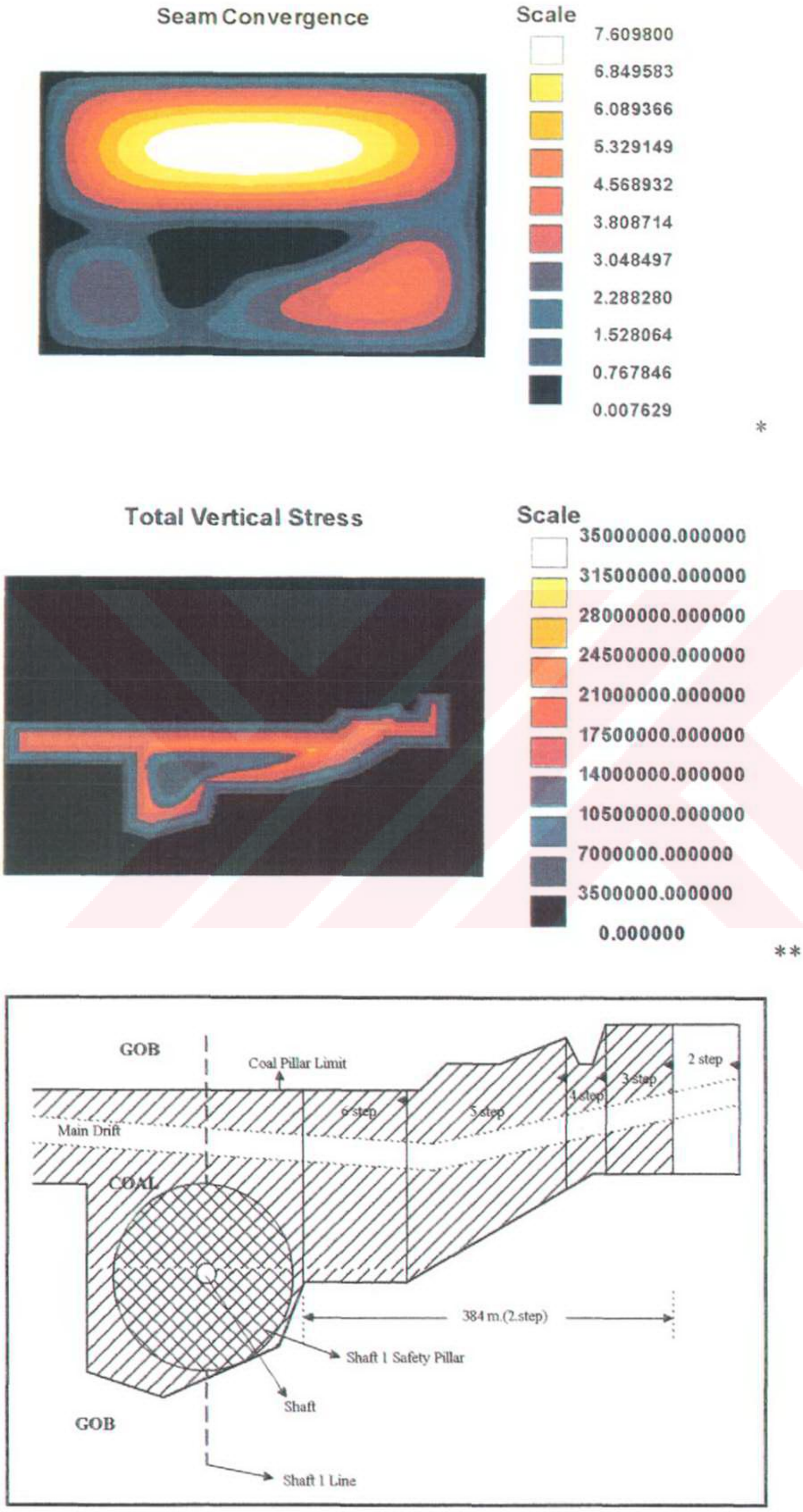

Figure 4.3 Seam convergence and vertical stress for through mining step 2 of the main drift safety pillar (*, in meters, ** in Pascals)

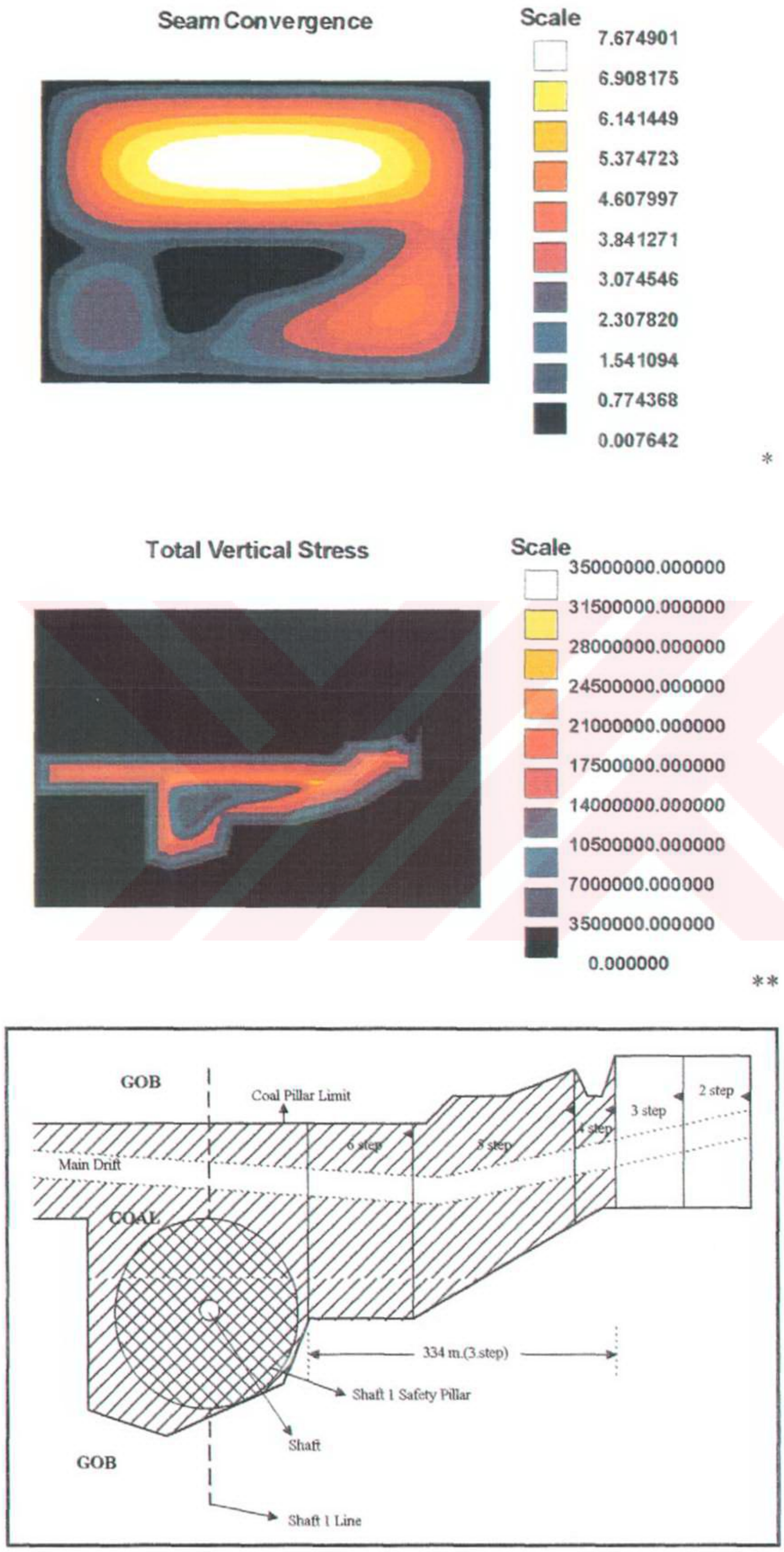

Figure 4.4 Seam convergence and vertical stress for through mining step 3 of the main drift safety pillar (*, in meters, ** in Pascals)

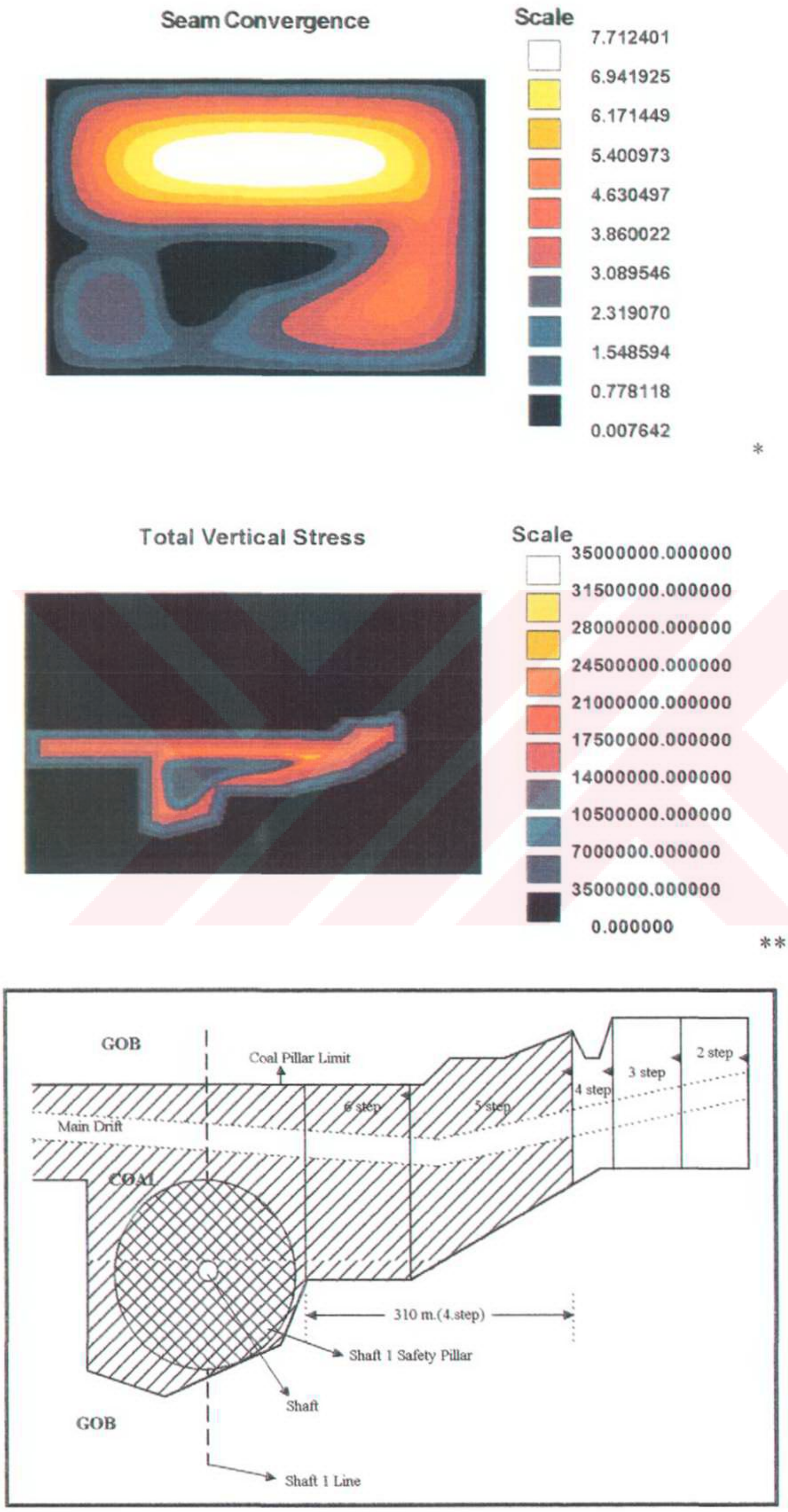

Figure 4.5 Seam convergence and vertical stress for through mining step 4 of the main drift safety pillar (*, in meters, ** in Pascals)

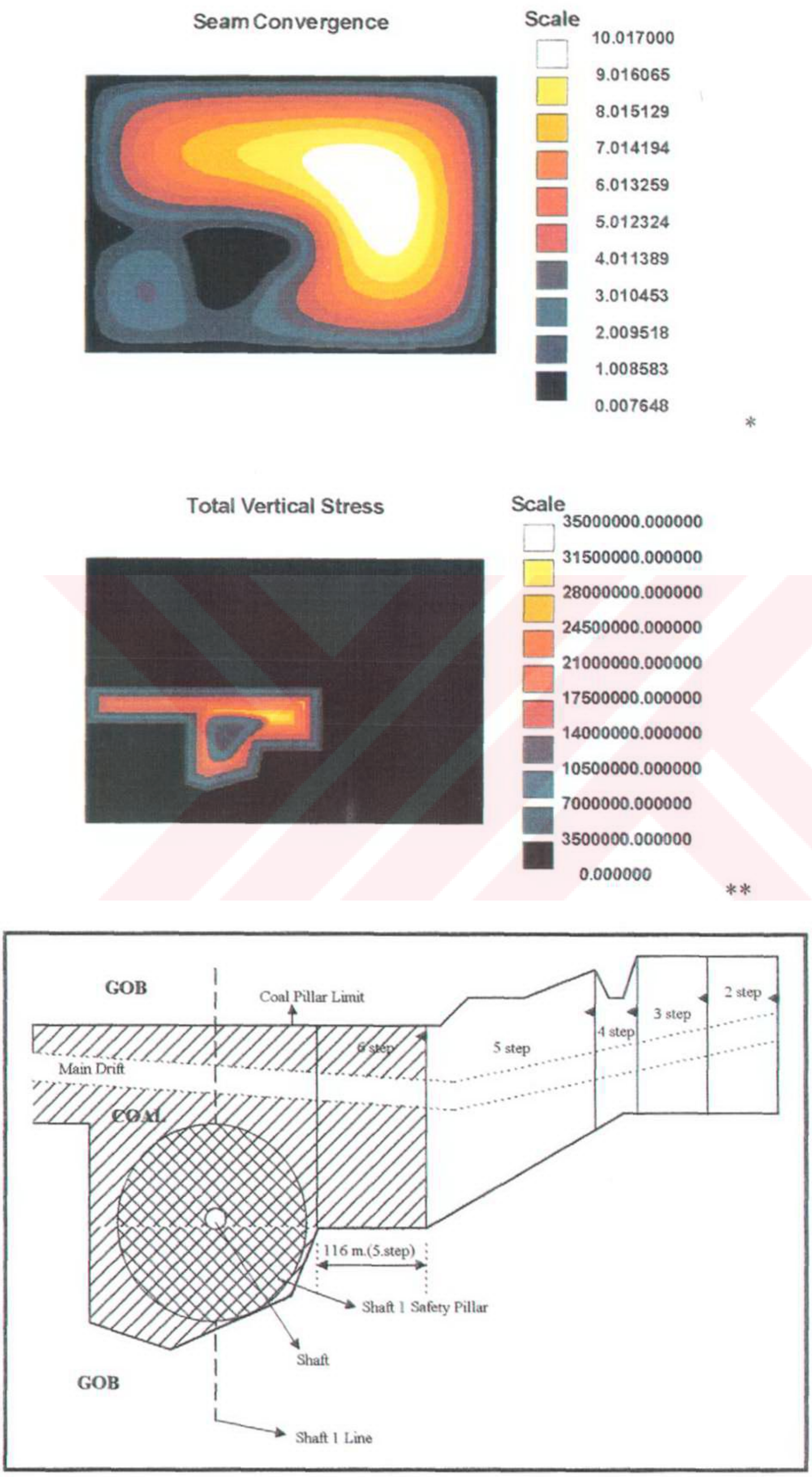

Figure 4.6 Seam convergence and vertical stress for through mining step 5 of the main drift safety pillar (*, in meters, ** in Pascals)

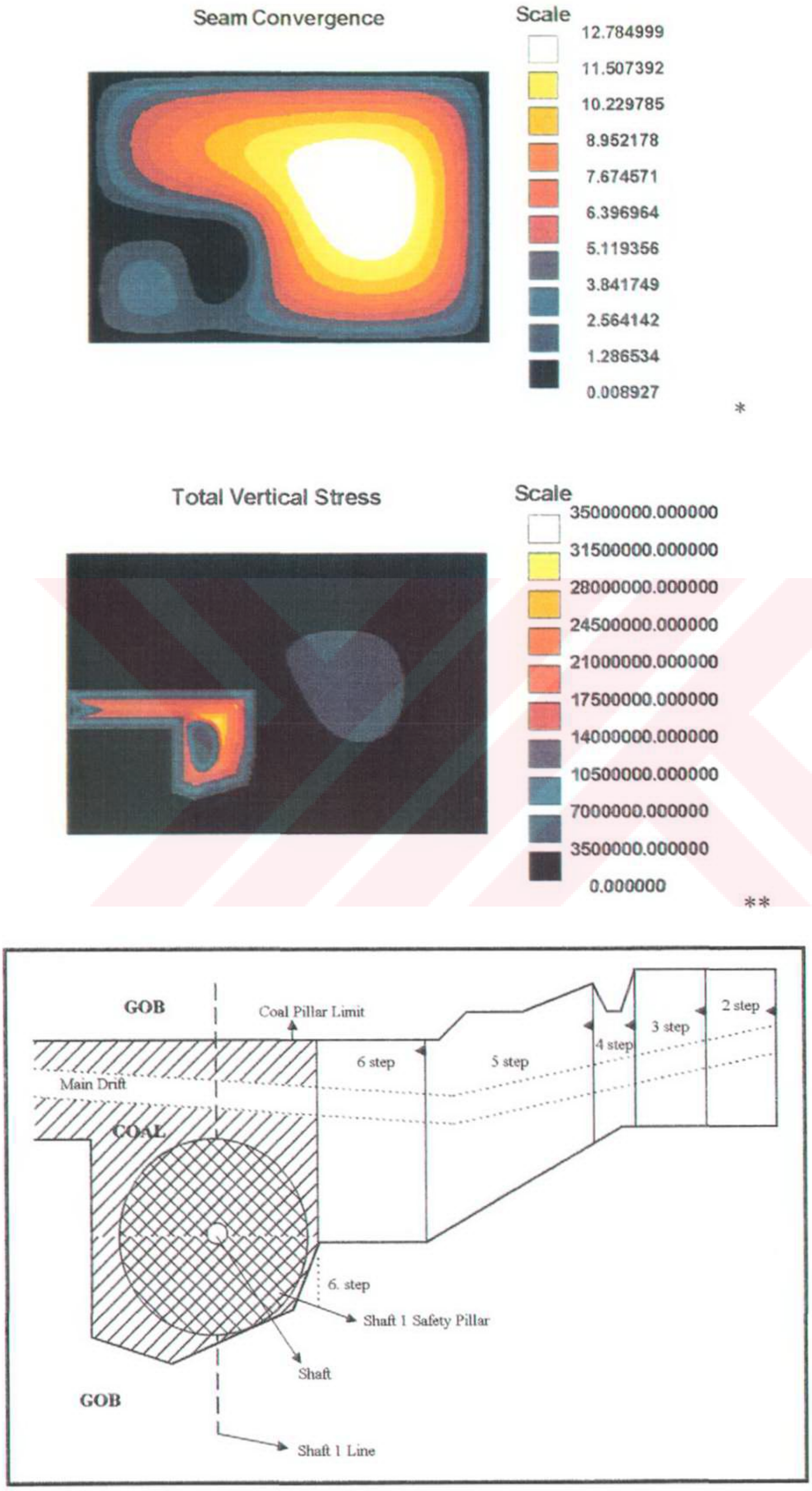

Figure 4.7 Seam convergence and vertical stress for through mining step 6 of the main drift safety pillar (*, in meters, ** in Pascals)

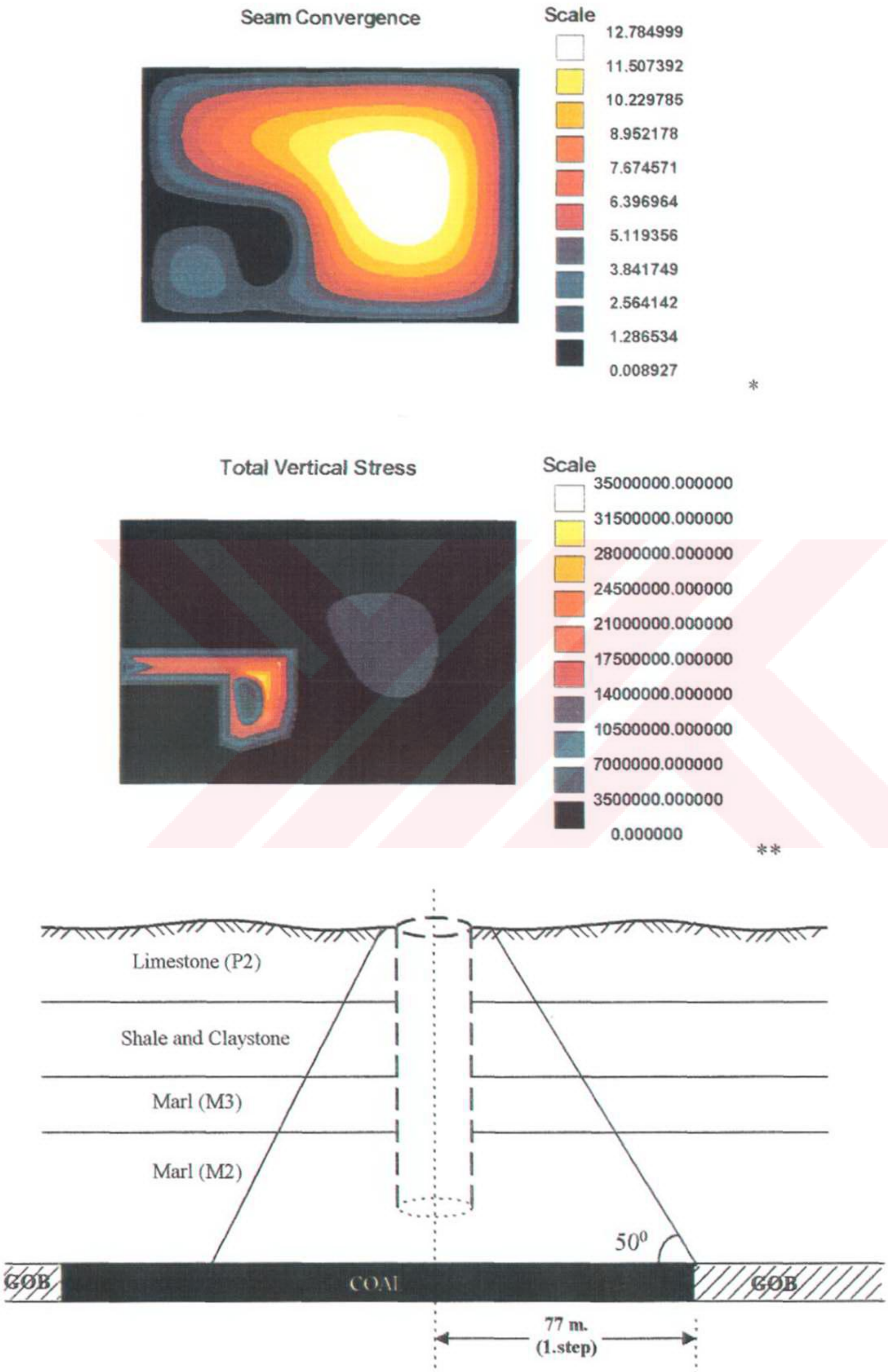

Figure 4.8 Seam convergence and vertical stress for through mining step 1 of the Shaft 1 safety pillar (*, in meters, ** in Pascals)

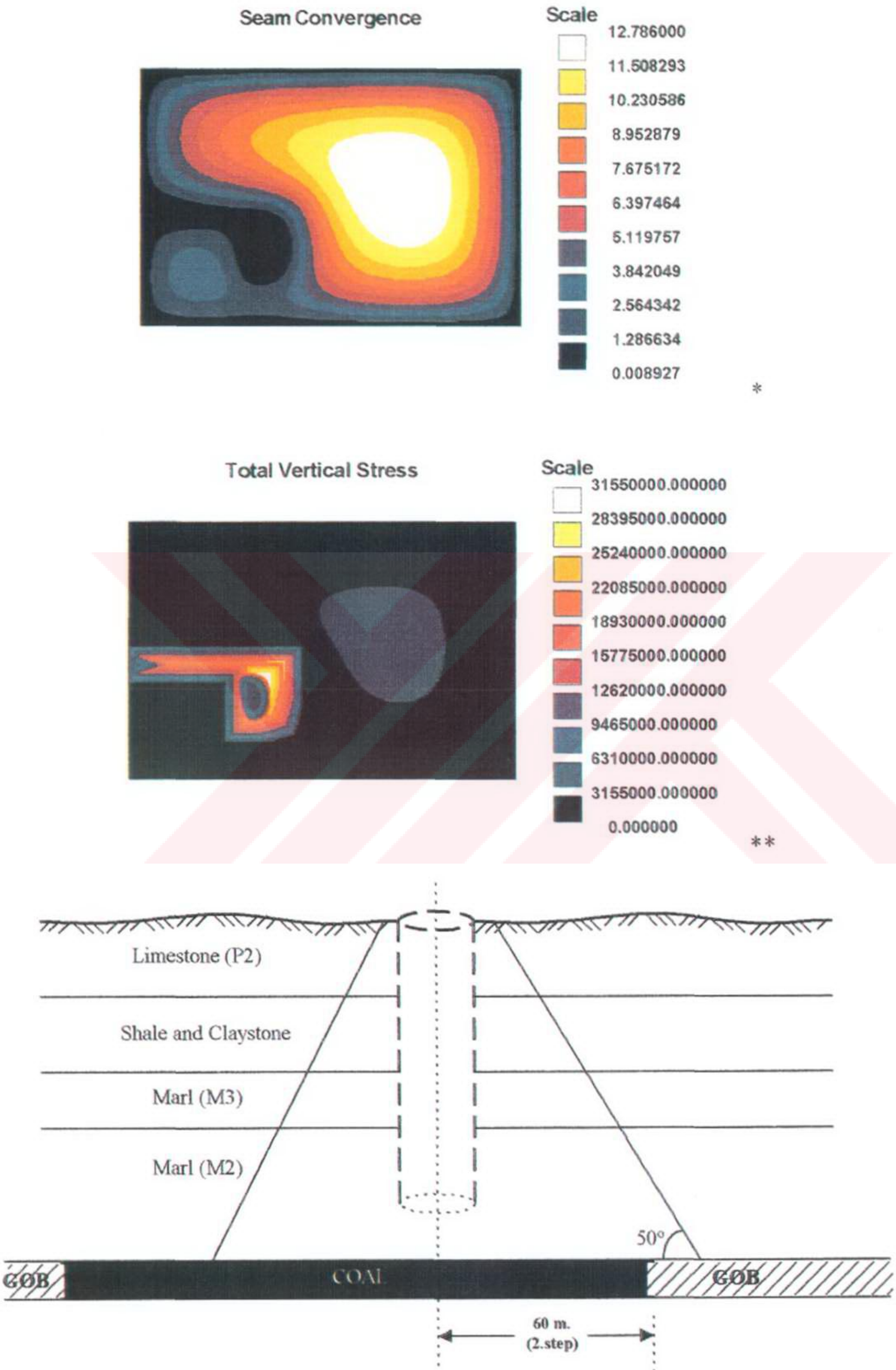

Figure 4.9 Seam convergence and vertical stress through mining step 2 of the Shaft 1 safety pillar (*, in meters, ** in Pascals)

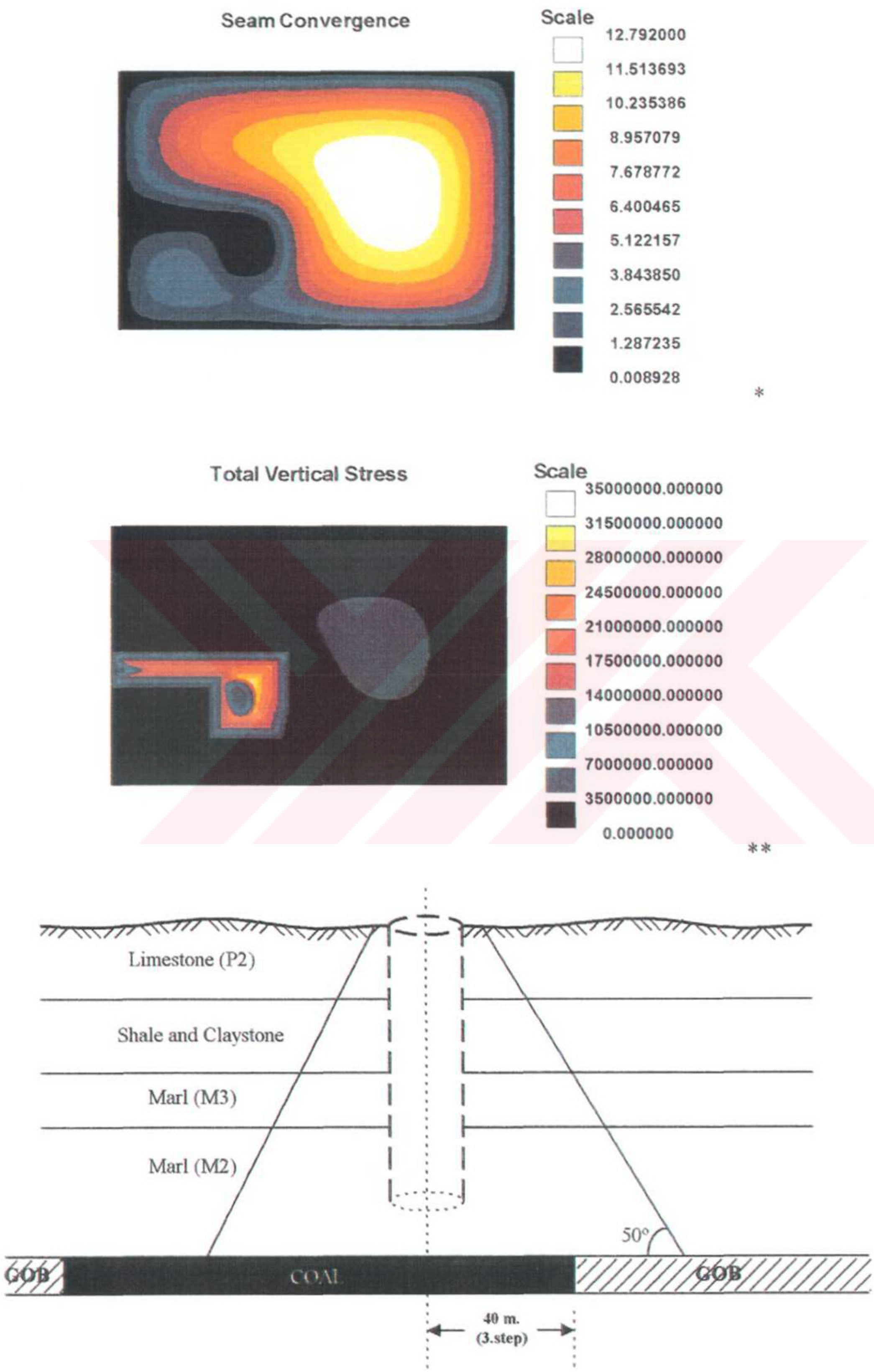

Figure 4.10 Seam convergence and vertical stress for through mining step 3 of the Shaft 1 safety pillar (*, in meters, ** in Pascals)

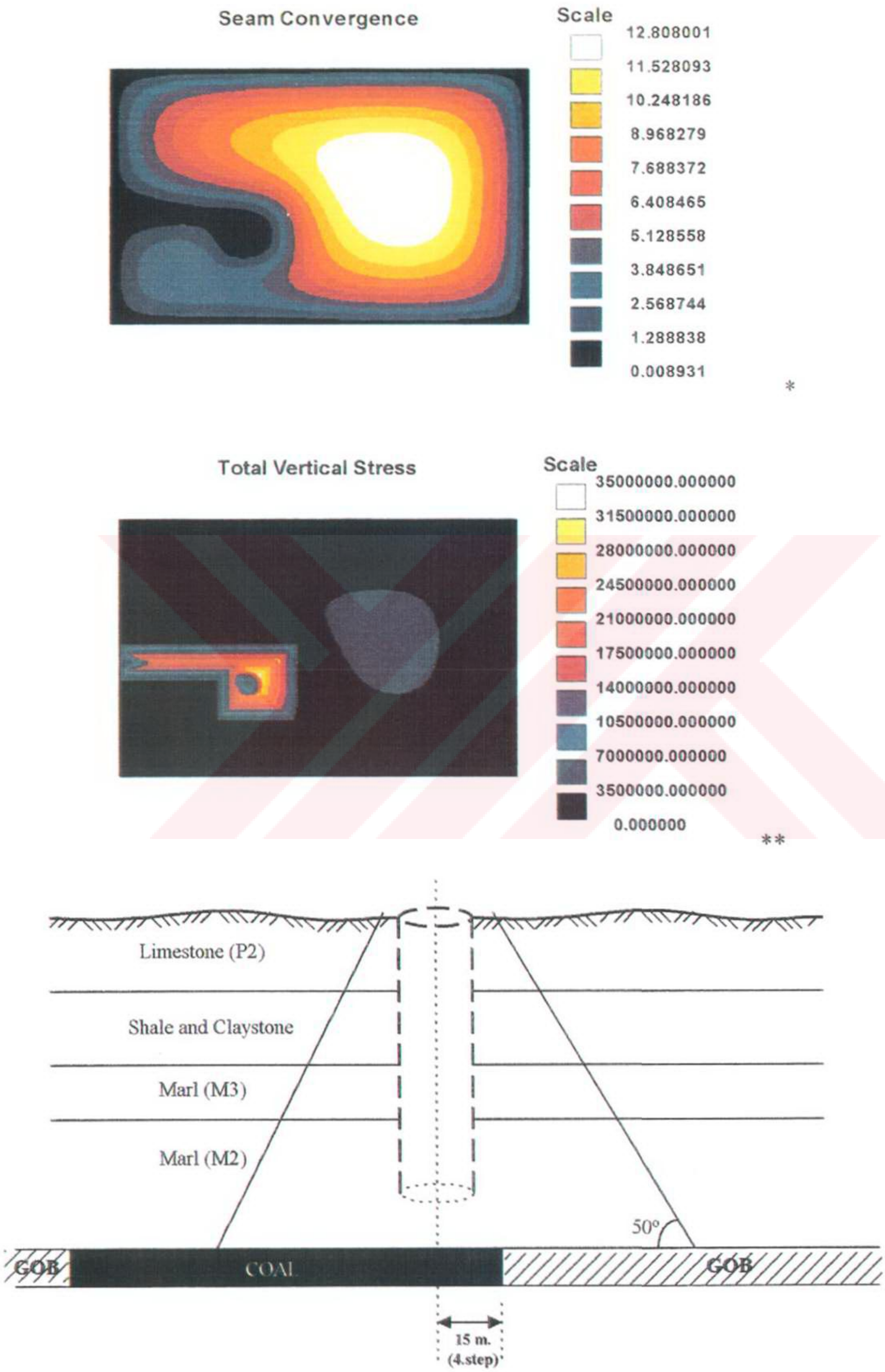

Figure 4.11 Seam convergence and vertical stress for through mining step 4 of the Shaft 1 safety pillar (*, in meters, ** in Pascals)

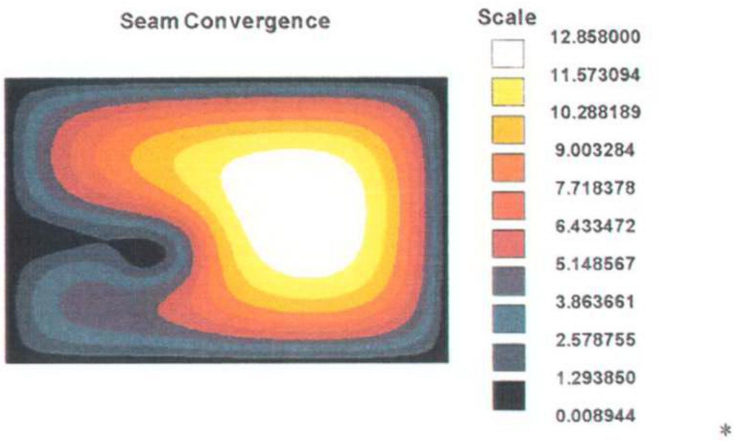

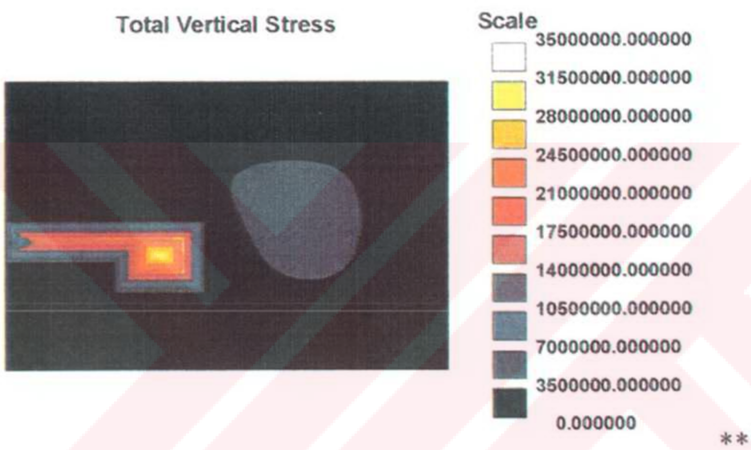

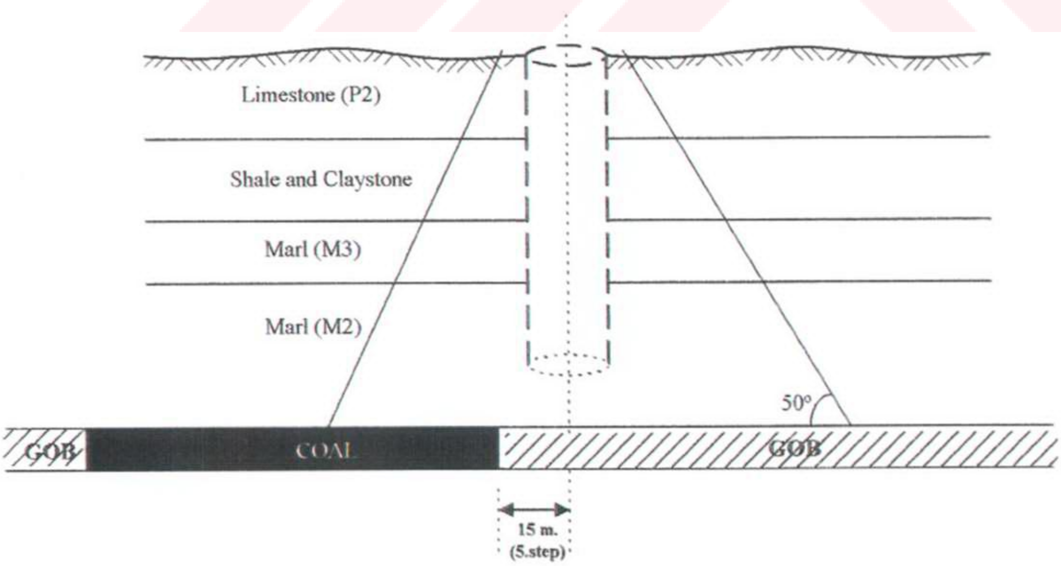

Figure 4.12 Seam convergence and vertical stress for through mining step 5 of the Shaft 1 safety pillar (*, in meters, ** in Pascals)

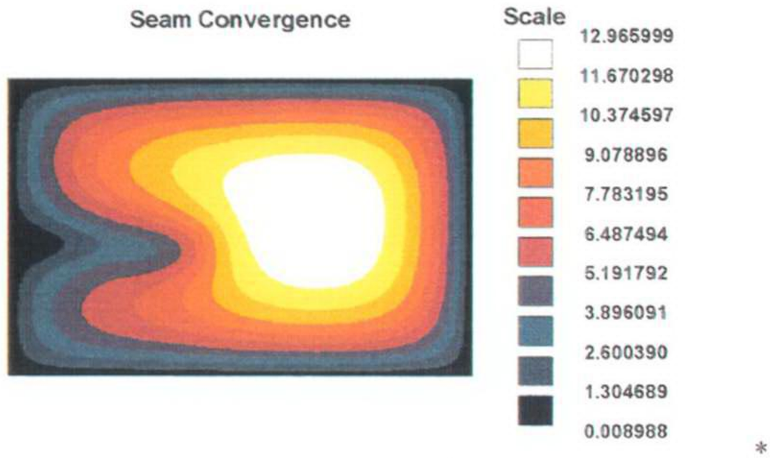

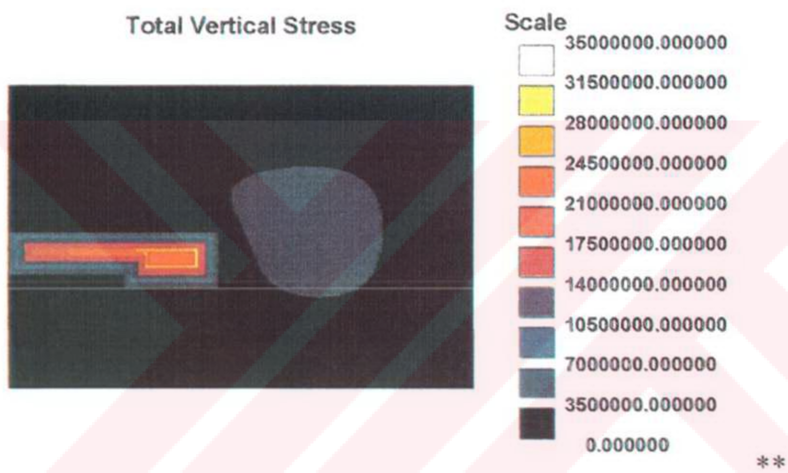

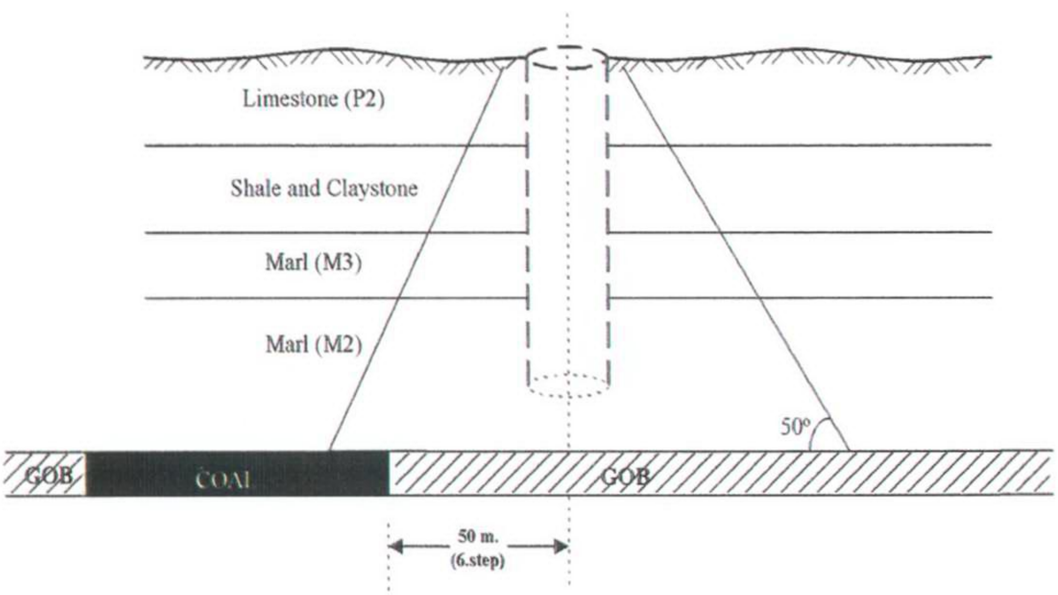

Figure 4.13 Seam convergence and vertical stress for through mining step 6 ofthe Shaft 1 safety pillar (*, in meter, ** in Pascal)

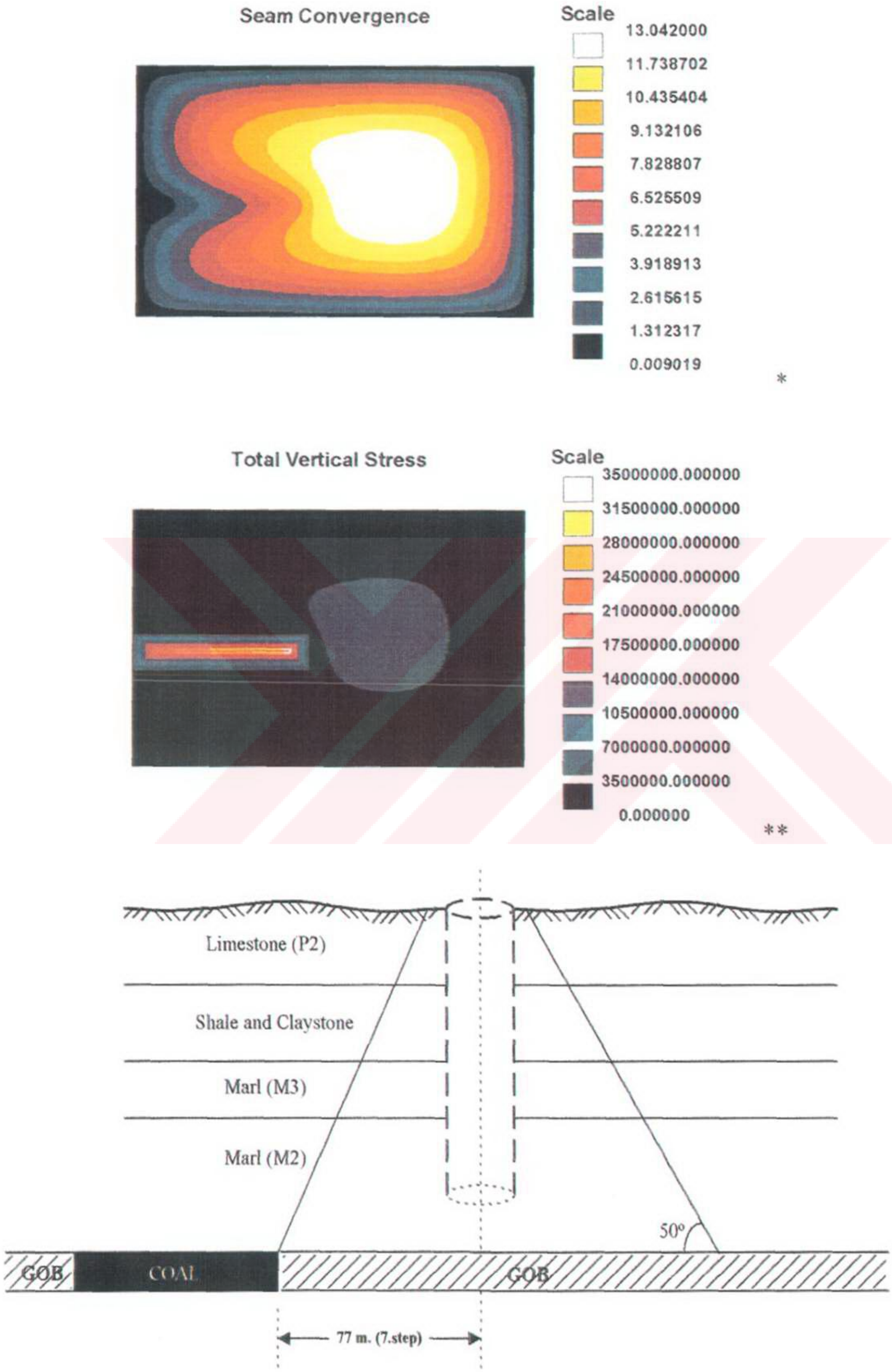

Figure 4.14 Seam convergence and vertical stress for through mining step 7 of the Shaft 1 safety pillar (*, in meters, ** in Pascals)

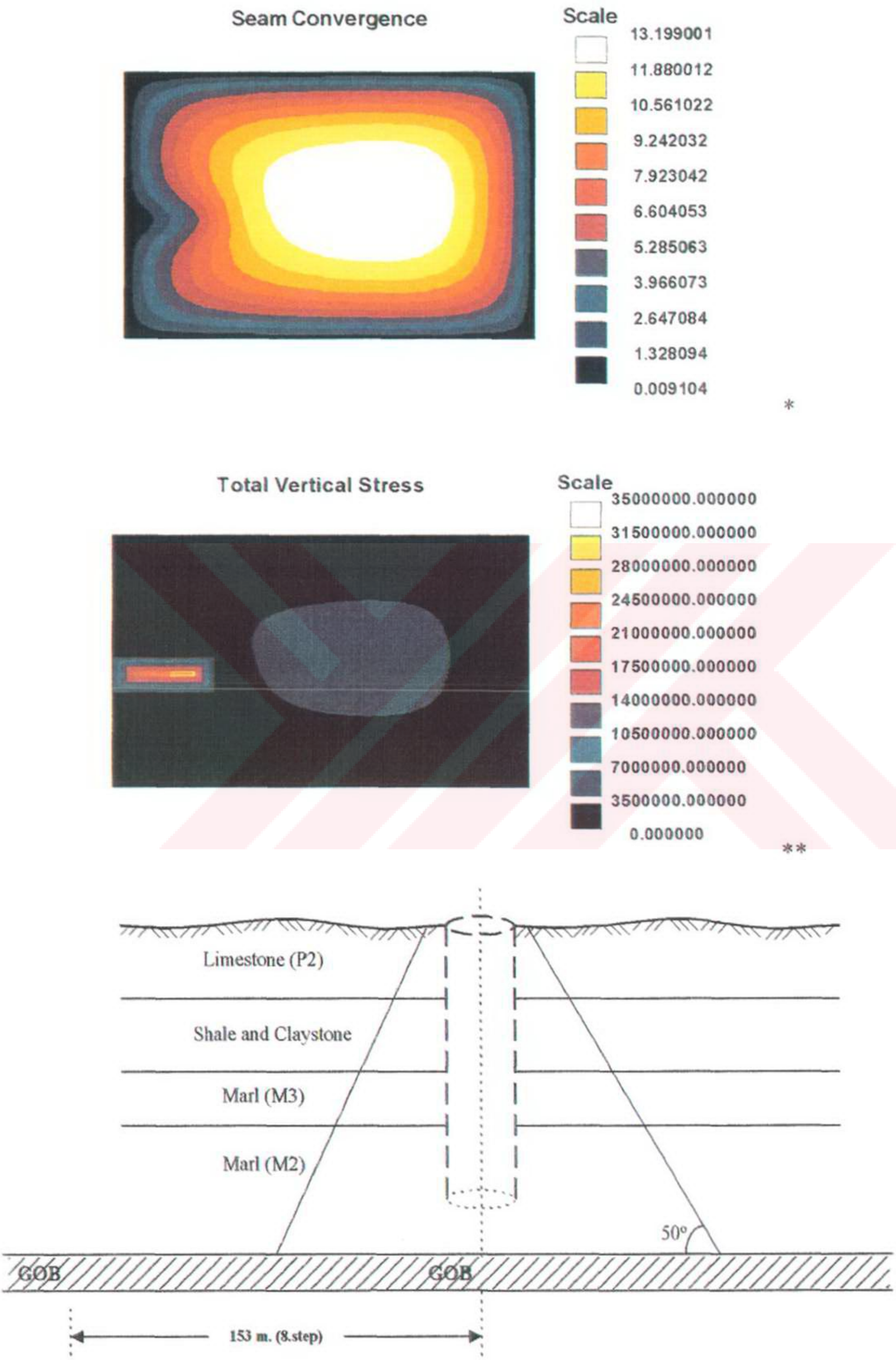

Figure 4.15 Seam convergence and vertical stress for through mining step 8 of the Shaft 1 safety pillar (*, in meters, ** in Pascals)

After all these analyses of the step sand under the light of literature review, surface subsidence and convergence of main drift and Shaft 1 were calculated together with the pillar strength. Analyses related to pillar strength are given in Table 4.3. The Main drift collapsed following the seam excavation from east to west. Since the main drift is in the influence zone of immediate roof, during face advance the main drift faced to huge stresses and convergences. So, the main drift is about to collapse 15-20 m. behind the extraction face. For the first two steps showing coal extraction in Shaft 1 safety pillar, no subsidence is encountered around Shaft 1. Subsidence starts with the 3rd step around Shaft1 surface. Figure 4.16 shows the subsidence on the Shaft 1 line step by step when Shaft 1 safety pillar is excavating.

Table 4.3 Calculated pillar strength for main drift and Shaft 1 safety pillar

	FORMULA	CALCULATED for MAIN DRIFT	CALCULATED for SHAFT 1
Obert-Duvall's	$S_p = S_l\,[\,0.78 + 0.22\frac{w}{h}\,]$	26,919 MPa	32,826 MPa
Holland-Gaddy's	$S_p = S_l\,[\,\frac{w}{h}\,]^{0,5}$	30,984 MPa	35,71 MPa
Bieniawski's	$S_P = S_1\,[\,0,64 + 0,36\frac{w}{h}\,]$	36,48 MPa	46,08 MPa
Salamon-Munro's	$S_p = S_l\,[\frac{w^{0,5}}{h^{0,66}}]$	19,495 MPa	22,522 MPa
Sheoray's	$S_p = S_l + 0.28\,H\,[\,\frac{w}{h} - 1]$	40,56 MPa	51,76 MPa

According to the analyses, peak stress is about 31-31,5 MPa on the Shaft 1 safety pillar and 28-28,5 MPa on the main drift safety pillar. Estimated pillar strength is 22,52-51,76 MPa for Shaft 1 safety pillar and 19,49-40,56 MPa for main drift safety pillar. The overall stresses occurred over the stope in the multi slice production method decrease % 30 compared to single slice method. So, it has san advantage to excavate the safety pillar with double slice method as far as the stresses over the coal seam are concerned (Köse & Çebi, 1988). So, it can be said that both pillar stay pillar stay stable. At the same time, the stresses occurred during the coal excavation reach its peak value 15 m. in front of the stope. Stresses over the gob reaches the gravity stresses 150 m. behind the face and keep it's level stable. Therefore, the results are similar with the theory of plastic overburden layer defended by Jacobi (Köse, 1985).

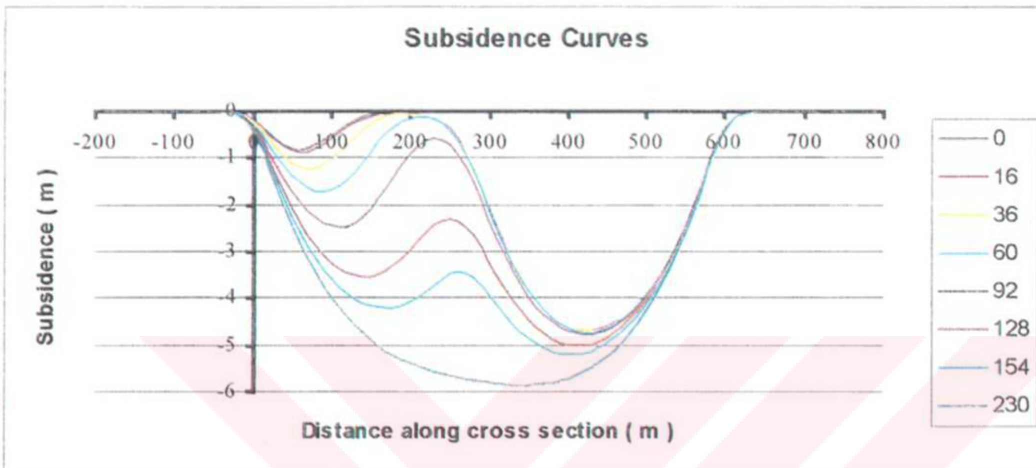

Figure 4.16 Subsidence curves on the Shaft 1 line from step 1 to step 8

Surface subsidence, around Shaft 1, has started after mining step 2. But subsidence value is too small to give any damage to boundary of Shaft 1. According to data obtained from the surface subsidence, the average limit angle of overburden is 50^0 and break angle of overburden is 56^0. These values have been confirmed with field observation. Cracks occurred on the surface has appeared 70 m. in front of the coal face from Shaft 1. After mining step 3, subsidence value, around Shaft 1, has increased and it is estimated that the subsidence effects would be able to give some damage to Shaft 1 boundary. This subject will be discussed in the next chapter. Previous effect of production has not observed because of sub-critical seam.

Seam convergence, which occurred during the excavating of shaft 1 safety pillar, is given in Figure 4.17. With face advance, seam convergence has increased and after the excavating all of the safety pillar of Shaft 1, seam convergence has reached maximum value, which is 11,998 m. As seen in Figure 4.17, seam convergence has started after mining step 4. This can be explained with yield zone. Yield zone has extended 12-15 m. inside face, because of coal thickness of 18 m.

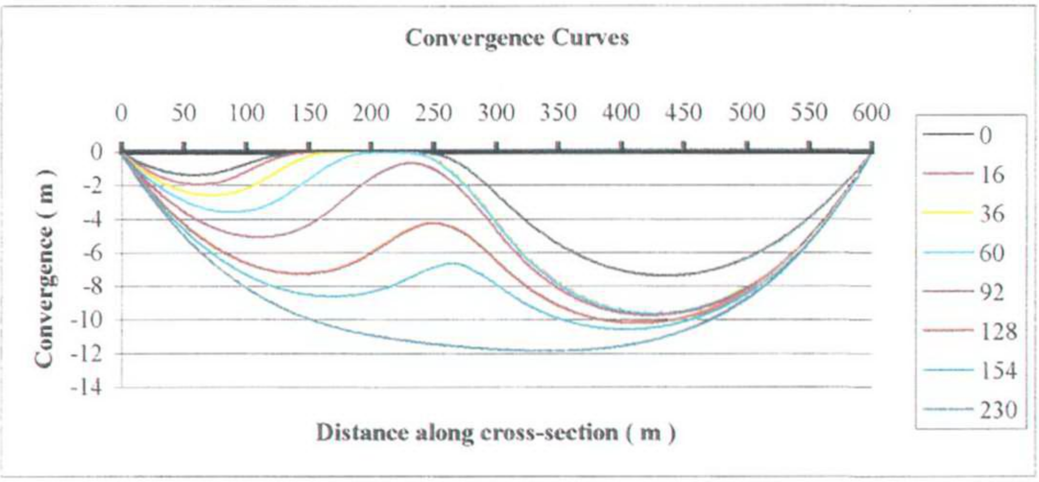

Figure 4.17 Convergence curves on the Shaft 1 line from step 1 to step 8

During these productions, horizontal strains occurred on the surface. But, this maximum horizontal strain cannot give any damage to Shaft 1 boundary. In next chapter, tangential and radial stress, which occurred on the Shaft 1 boundary, will be discussed. Figure 4.18 shows the strains occurred when the Shaft 1 safety pillar is excavated through different steps and the relation between subsidence and convergence are given in Figure 4.19. The results of the analyses, the relationship between seam convergence and surface subsidence is given in Figure 4.19. It has been observed that the upper part of the Shaft 1 has moved to southwest direction of the seam field when the excavations pass 40 m. from the Shaft 1, but any in-situ observation could not done because, the Shaft 1 boundary has disappeared.

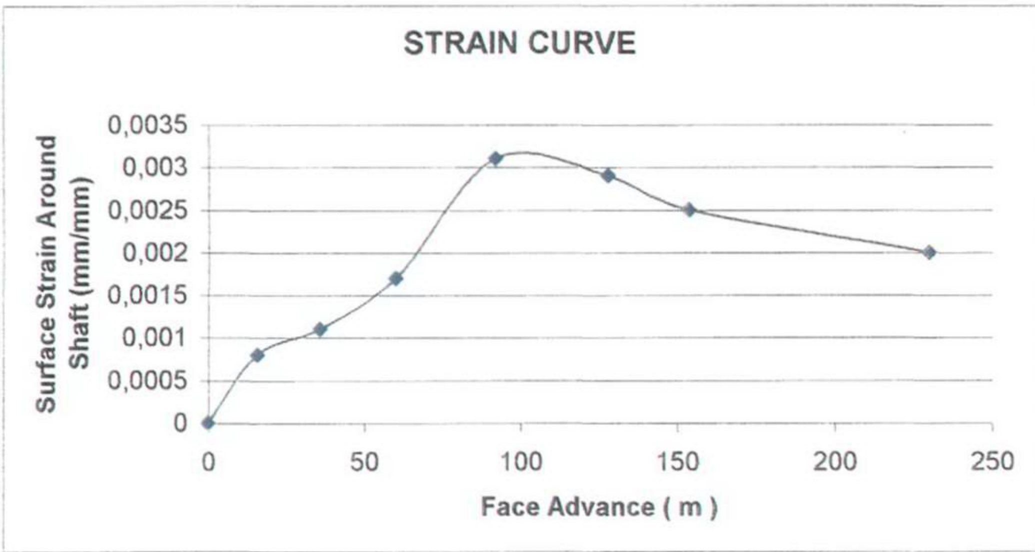

Figure 4.18 Surface horizontal strain curve around Shaft 1

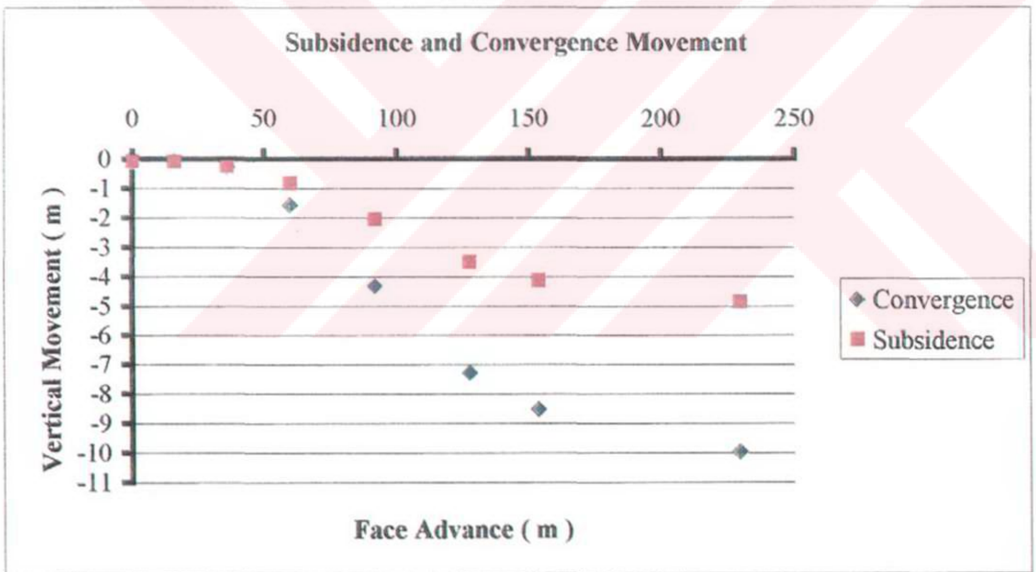

Figure 4.19 Subsidence and convergence movement around Shaft 1

Concerning the data obtained for subsidence and convergence, it has been found that seam convergence is two times greater than the surface subsidence. With face advance, seam convergence and surface subsidence increase together at Shaft 1 grid. Depending on the thickness of coal, it can be said that the amount of maximum convergence is about 73 % of coal thickness and maximum surface subsidence is about 33 % of coal thickness. Surface subsidence occurred around Shaft 1 has been confirmed by the field observations.

4.3 Conclusions

Under the light of knowledge and observation above, the results carried out from this study given below.

- LAMODEL, which uses D. D. A., is a usable computer software for thick coal seams. The stresses, convergences and subsidence data can be used for the prediction of the future mining steps and benefiting from these data, the direction of face advance can be controlled to provide problem free coal production.

- According to the calculations and analyses, main drift and Shaft 1 safety pillars behave as theoretical pillar behavior and they stay stable during the excavations.

- While the safety pillar under the main drift, is being mined, the main drift faced to huge stress and convergence. The stress extends the shear stress of surrounding rock of main drift. So, the main drift collapses about 15-20 m. behind the face depending on time and face advance rate. Because the main drift is in the immediate roof. On the other hand, it is deduced from analyses and field observation, analyses and previous studies that the break angle of location is about 56^0 and limit angle is 50^0.

- There is a linear relationship between surface subsidence and seam convergence. Convergence values are about two times higher than surface subsidence.

- During production steps, the stresses behave like in the longwall theory. The peak stress occurred about 10-15 m. in front of the face and it does not extend the covered stress on the gob.

- The maximum subsidence value, which occurred on grid line 240, is 5.95 m. and maximum convergence value is 13,190 m.

- On the shaft grid line, the surface subsidence was analyzed and it has been found that the surface subsided before the third step. If the shaft was driven under the coal seam, shaft boundary would face to compressive stress, this would result in subsidence of the upper part of the Shaft 1 and the top of the shaft boundary will subside with rock mass.

- On the shaft grid line, maximum subsidence is about 5.9 m (see Figure 4.16) maximum convergence is 11,998 m. and maximum horizontal strain occurred about 0.0031 mm/mm after the face pass to shaft lining at step 5 (see Figure 4.18). On the shaft point, maximum subsidence occurred is 4,896 m and maximum convergence occurred is 9,987 m

- While the shaft safety pillar is being mined, the maximum vertical stress is found about 31,5 MPA. This value is critical for 18 m. thick and 120 m. wide coal pillar. For the first four mining steps, vertical stress is about 25-28 MPa, when the face advances to the center of the safety pillar, the vertical stress increases to 31,5 MPa and then reduce about 28 MPa.

- On the last step, all the pillar were excavated, the seam convergence increases about 12 m, and vertical stress reduces 3 kg/cm^2, which do not exceed the covered load.

Chapter Five

FINITE ELEMENT MODELLING FOR HÜSTAŞ MINE SHAFT 1

5.1 Introduction

The fast improvement in technology renders the period of time shorter reserved for the assessment of a project at great scale. This situation has begun to emerge in the field of Mining Engineering as in other sectors. Several factors consulted in solving engineering problems are essentially as follows;

i. Analytical methods
ii. Empirical methods
iii. Observational-statistical methods
iv. Numerical Modelling methods

All those methods have their own advantages and disadvantages within their bodies. For better verification of the engineering problems and decreasing the amount of inevitable error, in engineering disciplines at least 2 different methods should be applied. At this study, Finite Element Technique and field observation have used and compared.

As known, an amount of coal is left under the shaft and main haulage for stability. This amount of coal depends on seam depth and site-specific parameters. Previous studies has investigated stress, which occurs on shaft boundary while safety pillar is winning, shaft go down under the coal seam. At this chapter, vertical stress and strain, which occurred on boundary of the Shaft 1, have been investigated step by step while safety pillar of Shaft 1 is winning by using finite element method. The position and location of Shaft 1 has given in Chapter One. Figure 5.1 shows cross-section and structure of the Shaft 1. As known, shafts are important entries for mining. Shafts use for transportation entries such as equipment, coal, and labour i.e. The purpose of this study, is to determine the shaft stability before abandoning the mine. For reach this goal, several finite element models have been analysed for stability of the Shaft 1.

5.2 Finite Element Analysis (ANSYS 5.6.2)

The first step in the finite element is to prepare a mesh of elements. The structure under consideration is divided to smaller zones, known as elements. The elements are assumed to be connected to each other at certain points (usually at the corners) called nodes. It is at the nodes that displacements are computed. Displacements are fundamental variables. Well-known finite element displacement formulation establishes a relationship between nodal forces and induced displacements (Zienkiewicz, 1971). At any point P in the element, displacements u^p are related to the nodal displacements u^e by,

$$u^p = Nu^e \qquad (5.1)$$

Where, N is a matrix of shape functions. From the displacement field within the element strain can be calculated.

$$\varepsilon^p = L\,u^p = L\,Nu^e = Bu^e \qquad (5.2)$$

From the strains, using stress-strain relationship, stresses are calculated. The total state of stress within an element is obtained from the induced strain, the elasticity matrix D, and the initial stresses

$$\sigma^p = De^p + \sigma_o^p \qquad (5.3)$$

In Finite Element modelling procedure, a latest version of ANSYS program called 5.6.2. has been utilized. The objective of the study includes the determination of the stresses during the excavation of Shaft 1 safety pillar.

5.3 Theoretical Definition

The ANSYS program used in the modelling of this project happens to be a beneficial software that could easily be adapted to other engineering branches individually or to multidiscipliner problems. This time, ANSYS has been effectively used in the solution of the problems regarding Rock Mechanics. The style of solution applied in modelling is the method of ***Structural*** and the type of elements are ***Solid 45***, for rock mass, and ***Solid 65***, for shaft boundary, which enable the user to do a 3-D modelling. Solid 45 and Solid 65 show the ability of failure under tensile and compressive strength and they can also be practised in sorts of material like fibreglass as well as geological investigation of the rock strata. The element, Solid 65, is defined associated with 8 node points, which are mobile in all 3 directions (X, Y, Z-axes). The non-linear material properties are likely to be better described in this type of element and solutions versus time can be achieved. This element comprises an ability of plastic deformation and creeping at the same time. The global shape of the elements explicitly explained above is given in Figure 5.1.

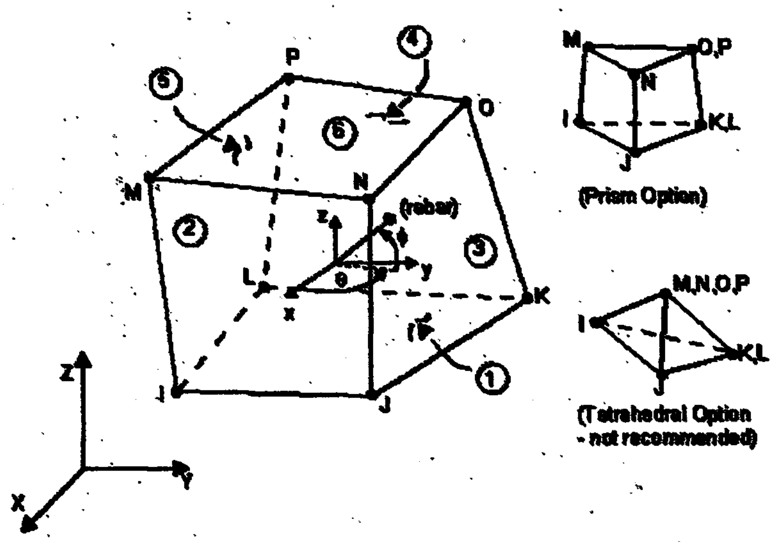

Figure 5.1 The demonstration of Solid 45 and Solid 65 elements (ANSYS, 1994)

The isotropic material property is decided and different properties are entered for every different kind of formation in the model that had been formed, but before the mentioning of material properties it sounds more useful to focus more attention on the solution theory.

ANSYS software exploits the method of Newton-Raphson in solving non-linear equations. In this method, the stress is divided into series of sub-stress aureoles fundamentally and the resulting graphical display of the full Newton-Raphson iterative solution is depicted in Figure 5.2.

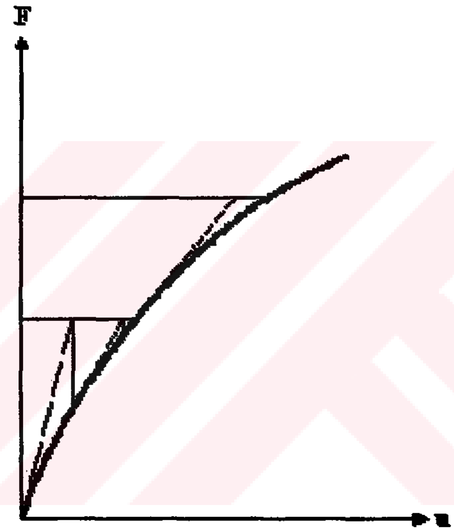

Figure 5.2 The solution by Newton-Raphson iteration (with 2 feedbacks), (ANSYS, 1994)

A non-linear analysis by this method is conducted in 3 phases;

i. The upper phase of the load steps defined within the specified period of time evaluates the time spent on loading. For the statically analysis of the load quantity, they are assumed to be applied rather in linear form.

ii. In every phase of loading, you can directly apply load to any desired phase.

iii. In every sub phase, the program uses various equations to make an approach solution.

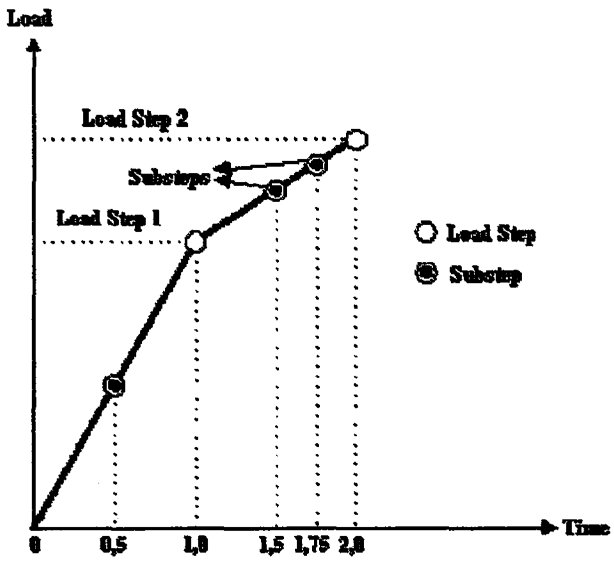

Figure 5.3 The graph of load phases and sub-phases versus time, (ANSYS, 1994)

As told before, ANSYS software fortunately bears solution techniques both applicable to the individual disciplines and sub-disciplines of the root disciplines. For instance, Solid 65 is able to reach solutions such as viscoelastic, creep, multielastic and etc. techniques. In this study, the solution is made by Drucker Prager method. Drucker Prager option offers solutions containing the Laws of Mohr-Coulomb for the granular substances (soil, rock and concrete). Merely 3 parameters are enough for the solution method. These parameters are;

i. Cohesion (> 0)
ii. Angle of internal friction (degree)
iii. Angle of expansion (degree)

The criteria of failure used mostly in soil and rock mechanics are the Mohr-Coulomb, Von Mises and Tresca criteria. The Von Mises and Tresca criteria have been derived from the studies on metals, therefore no practice of these 2 criteria is available in soil and rock mechanics any longer. On the contrary, Mohr-Coulomb criterion has been developed for rock and soil by making benefit of the compressive strength factor (Corp, 1975).

In general, Mohr-Coulomb theory is utilized rather more in the branch of routine stability problems, but it is not a continuous function for the 3-D breakage surfaces and not appropriate from the aspect of mathematics in solving plasticity problems. For this purpose, Drucker Prager option adaptable to the Mohr-Coulomb version has been put forward (Corp, et al., 1975).

This failure criterion is the extended and sophisticated form of Mohr-Coulomb and provides the intermediate stresses to be involved within the theory.

5.4 Data Used

First of all, the geometry of the region in which the modeling will be done by ANSYS software and later on, physical and mechanical properties of each formation are entered into the system. Amid those properties; the modulus of elasticity, Poisson's ratio, density, cohesion and angles of internal friction values of formations obtained after the laboratory tests and previous studies (Golder Associates, 1982), that have been considered to be entered as input to the program might be counted so as to best represent the site. Besides, it is also possible to feed input data of load change versus time and stress-deformation if the plastic characteristics of the formation are also demanded. The input parameters entered to the program are given in Table 5.1.

Table 5.1 In-put Parameters

Formation	Elasticity Modulus (E) (MPa)	Poisson's Ratio (v)	Density (d) (kg/m^3)	Cohesion (c) MPa	Angle of Intern. Friction (Φ) (^{0})
Limestone (P2)*	23 000	0,24	2 650	12	40
Shale and Claystone (P1)**	5 000	0,33	1 900	3,2	28
Marl (M3)**	14 000	0,27	2 100	23,2	35
Marl (M2)**	10 000	0,30	1 950	20,1	32
Coal (KM2)*	2 000	0,33	1 650	5,2	35
Conglomerate**	15 000	0,25	2 200	18,4	24
Shaft 1 Concrete**	21 000	0,18	2 380	25	70

(*) From Laboratory Test, (**) From Previous Study

In order to define the plasticity of the formations, the data of cohesion and angle of internal friction are prepared according to the results of the tests carried out at the Department of Mining Engineering in Dokuz Eylul University and previous studies (Golder Associates, 1982). The boundary circumstances of the model have pre-determined prior to the solution. For this reason, while the lateral sides of the model cannot move in X-axis Z-axis, the lower portions are restricted in a way not to move in any direction. The acceleration of gravity is taken naturally 9,81 m/s^2 in modeling operations.

5.5 Model Analyses

As told before, the purpose of this study is stress analysis on boundary of the Shaft 1 while the safety pillar of Shaft 1 is being recovered following the excavation of the safety pillar of main drift. For this reason, Shaft 1 safety pillar, (its radius is 75 m.) has been excavated step by step. Figure 5.4 shows structure and cross-section of Shaft 1 safety pillar and Table 5.2 shows mining steps points with direction. On the other hand, the latest mining step contains final result when the whole seam is excavated from seam. The results of the finite element analyses are given in appendix c.

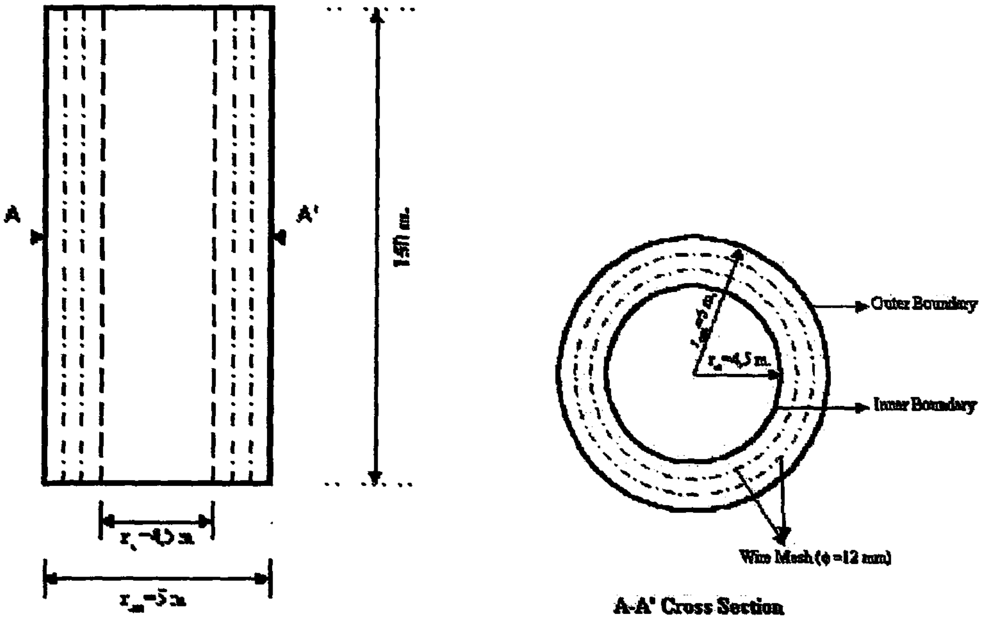

Figure 5.4 Structure and cross-section of the Shaft 1

At this study, Shaft 1 safety pillar is excavated in 9 mining step (given Table 5.2 and Figure 5.5). Utilizing the related equation (Çetmeli, 1974), compressive strength and tensile strength have been calculated as approximately 42 MPa and 12 MPa respectively, for the concrete shaft support studied in this project.

Table 5.2 Following mining steps for finite element analyses

MINING STEP	FACE ADVANCE (m) (From South to North)
1 Mining Step	Front 70 m. from Shaft 1
2 Mining Step	Front 50 m. from Shaft 1
3 Mining Step	Front 30 m. from Shaft 1
4 Mining Step	Center of the Shaft 1
5 Mining Step	Pass 30 m. Shaft 1
6 Mining Step	Pass 50 m. Shaft 1
7 Mining Step	Pass 70 m. Shaft 1
8 Mining Step	Pass 77 m. Shaft 1
9 Mining Step	All coal excavated

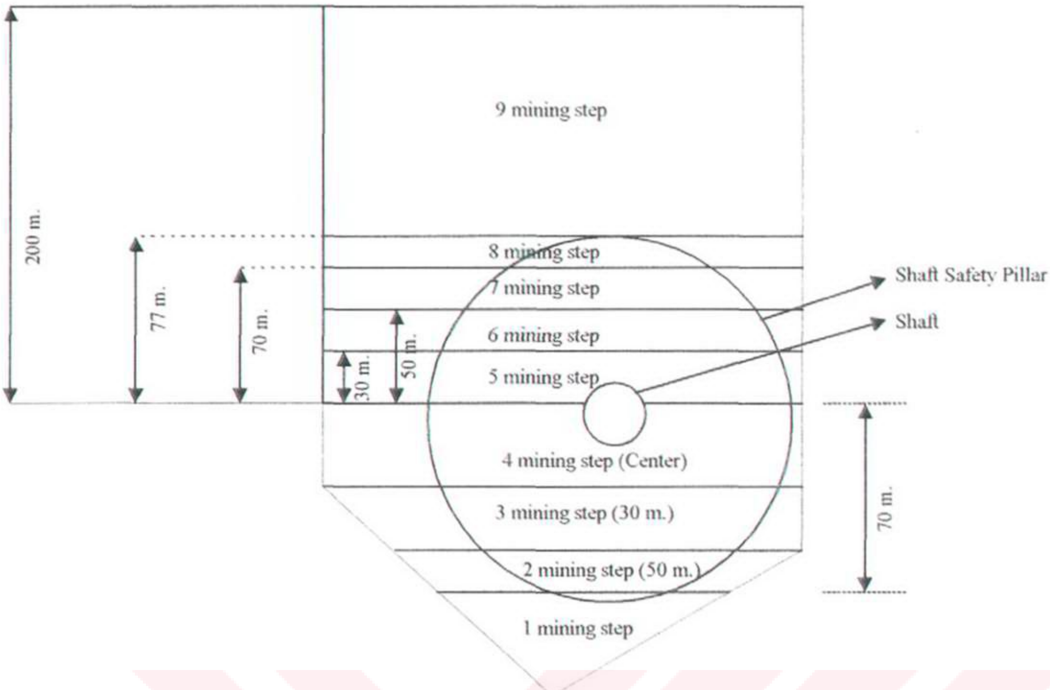

Figure 5.5 Mining steps for finite element analyses

Figure 5.6 shows the general model of finite element model with model parts.

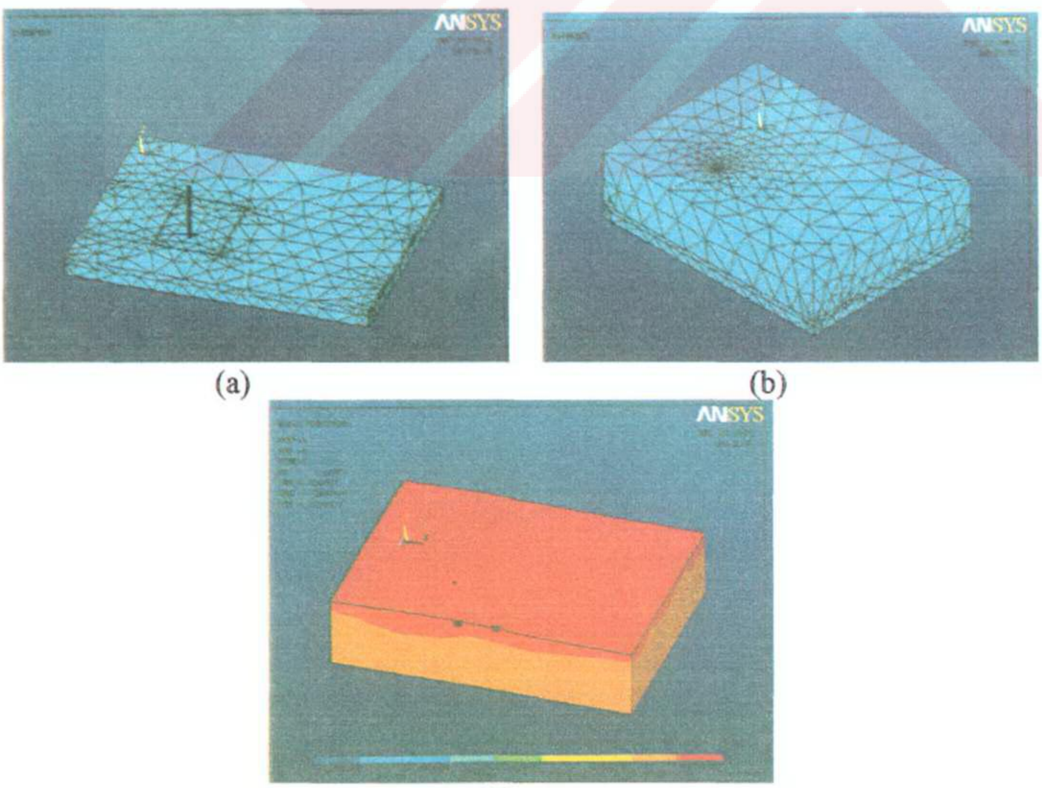

Figure 5.6 General model of F. E. M. (a) Shaft 1 in model, (b) complete model, (c) result of model

Results of these analyses are given in Figure 5.7 - 5.15 and results of all steps is given Figure 5.16 for stress and Figure 5.17 for strain.

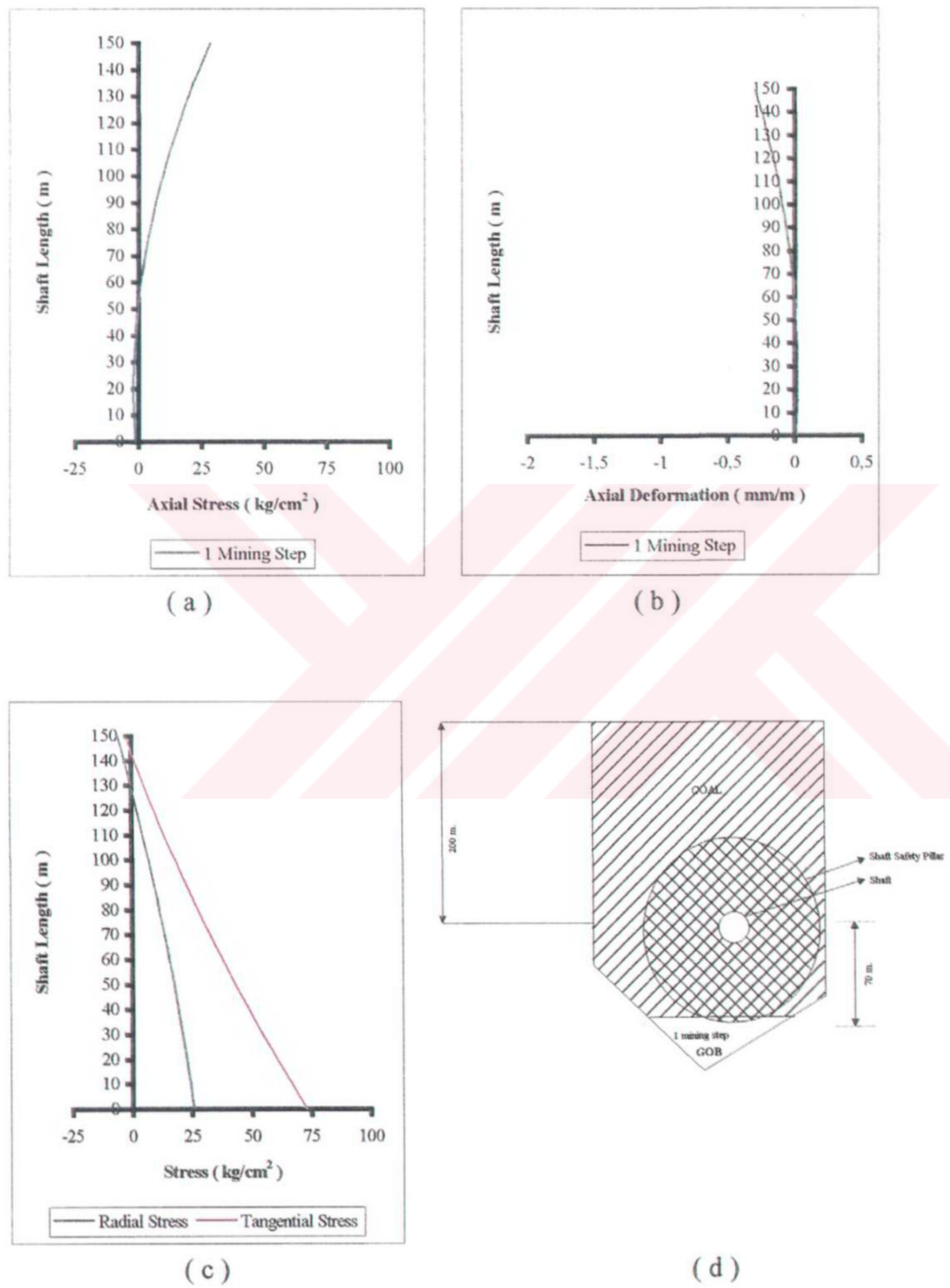

Figure 5.7 Stress and deformation analysis on the boundary of Shaft 1 for mining step 1, a) axial stress, b) axial deformation, c) tangential and radial stress, d) mining step

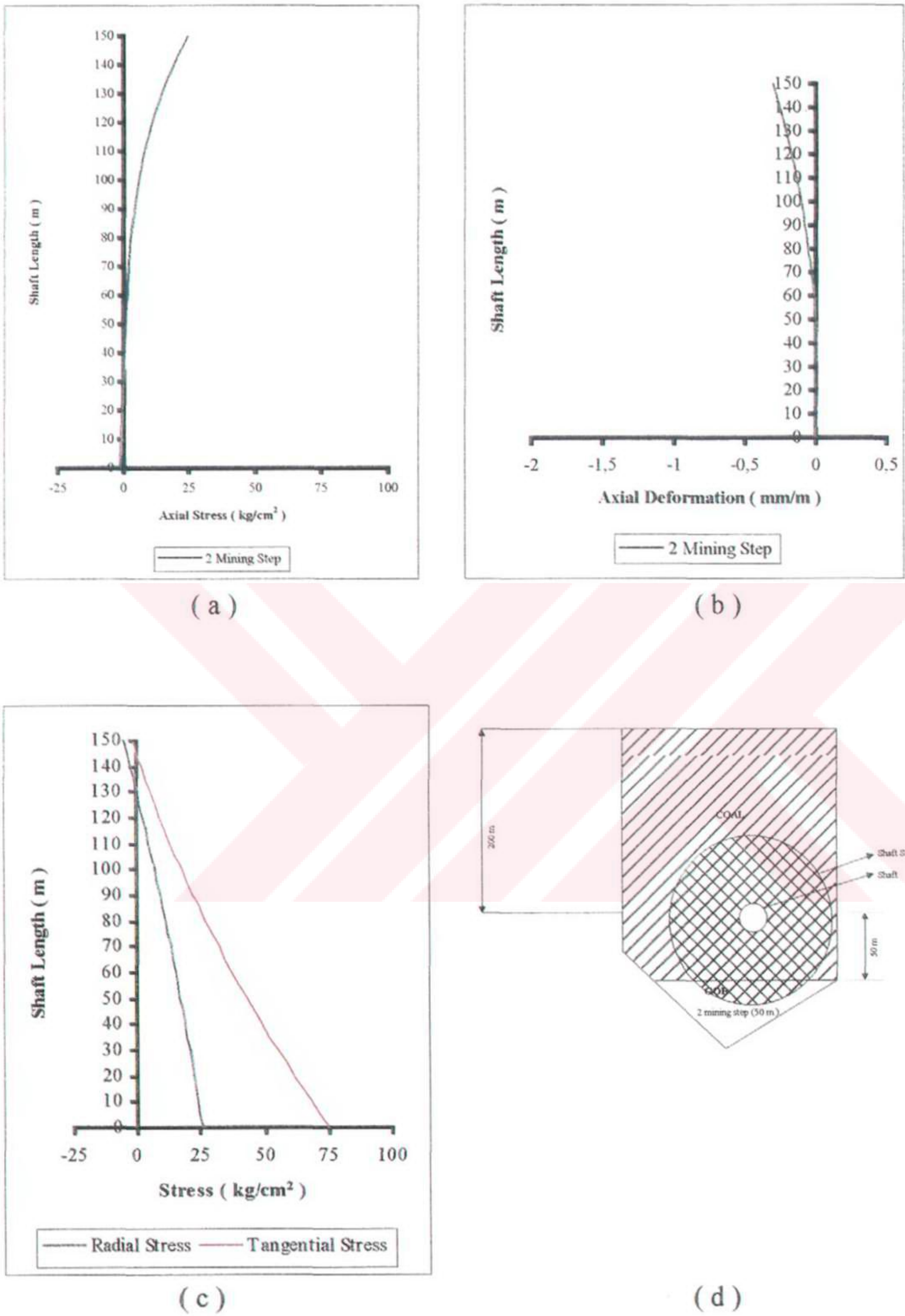

Figure 5.8 Stress and deformation analysis on the boundary of Shaft 1 for mining step 2, a) axial stress, b) axial deformation, c) tangential and radial stress, d) mining step

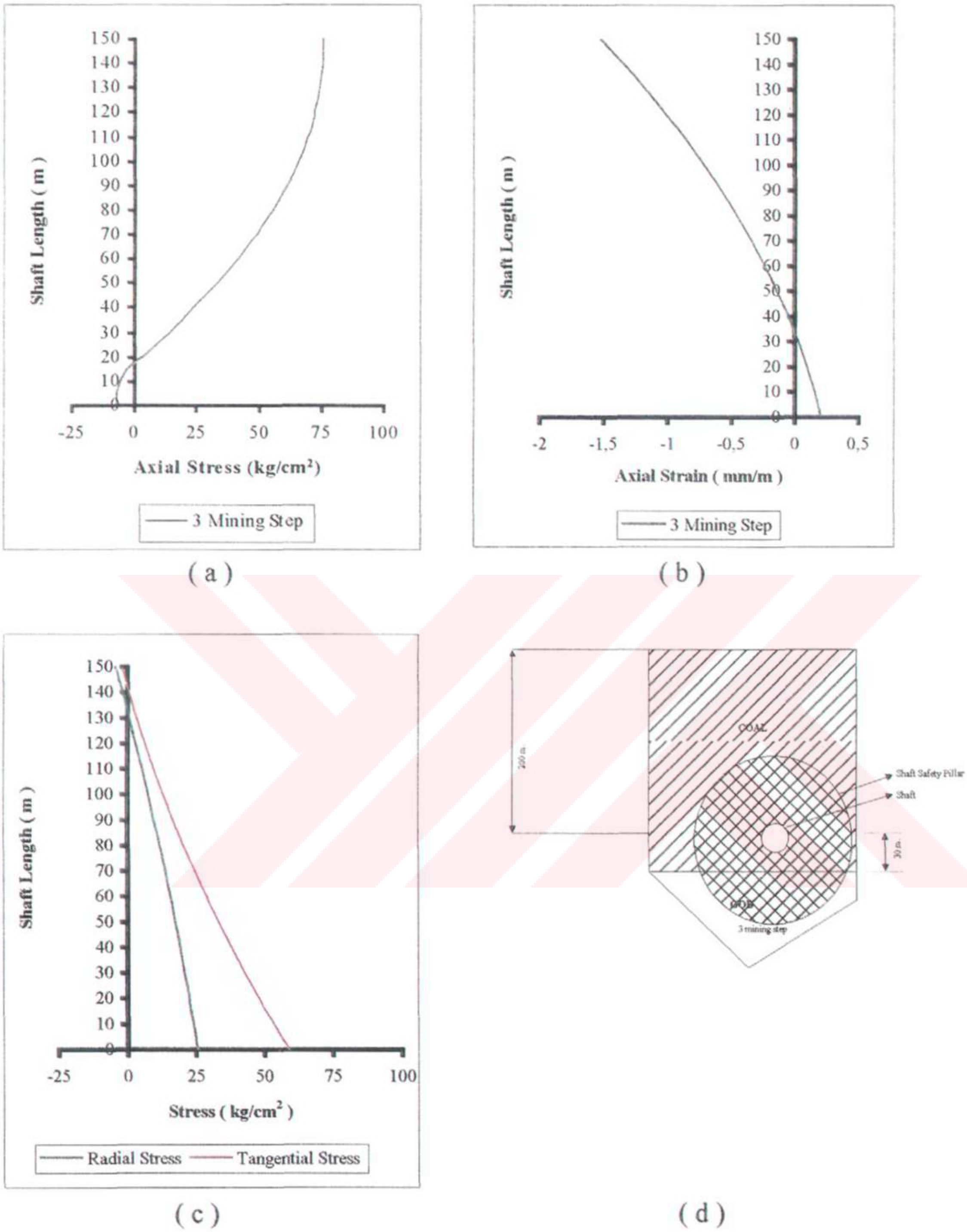

Figure 5.9 Stress and deformation analysis on the boundary of Shaft 1 for mining step 3, a) axial stress, b) axial deformation, c) tangential and radial stress, d) mining step

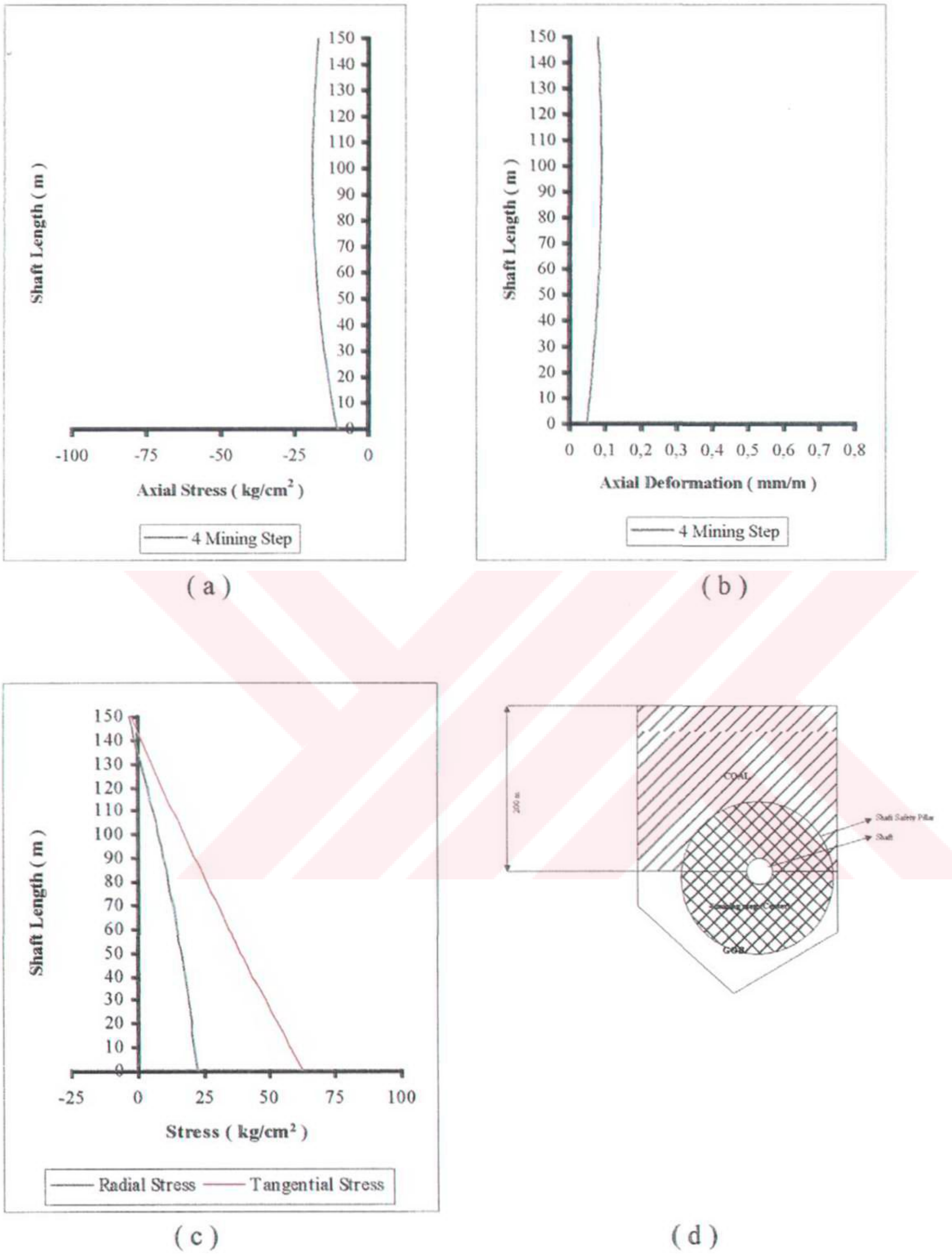

Figure 5.10 Stress and deformation analysis on the boundary of Shaft 1 for mining step 4, a) axial stress, b) axial deformation, c) tangential and radial stress, d) mining step

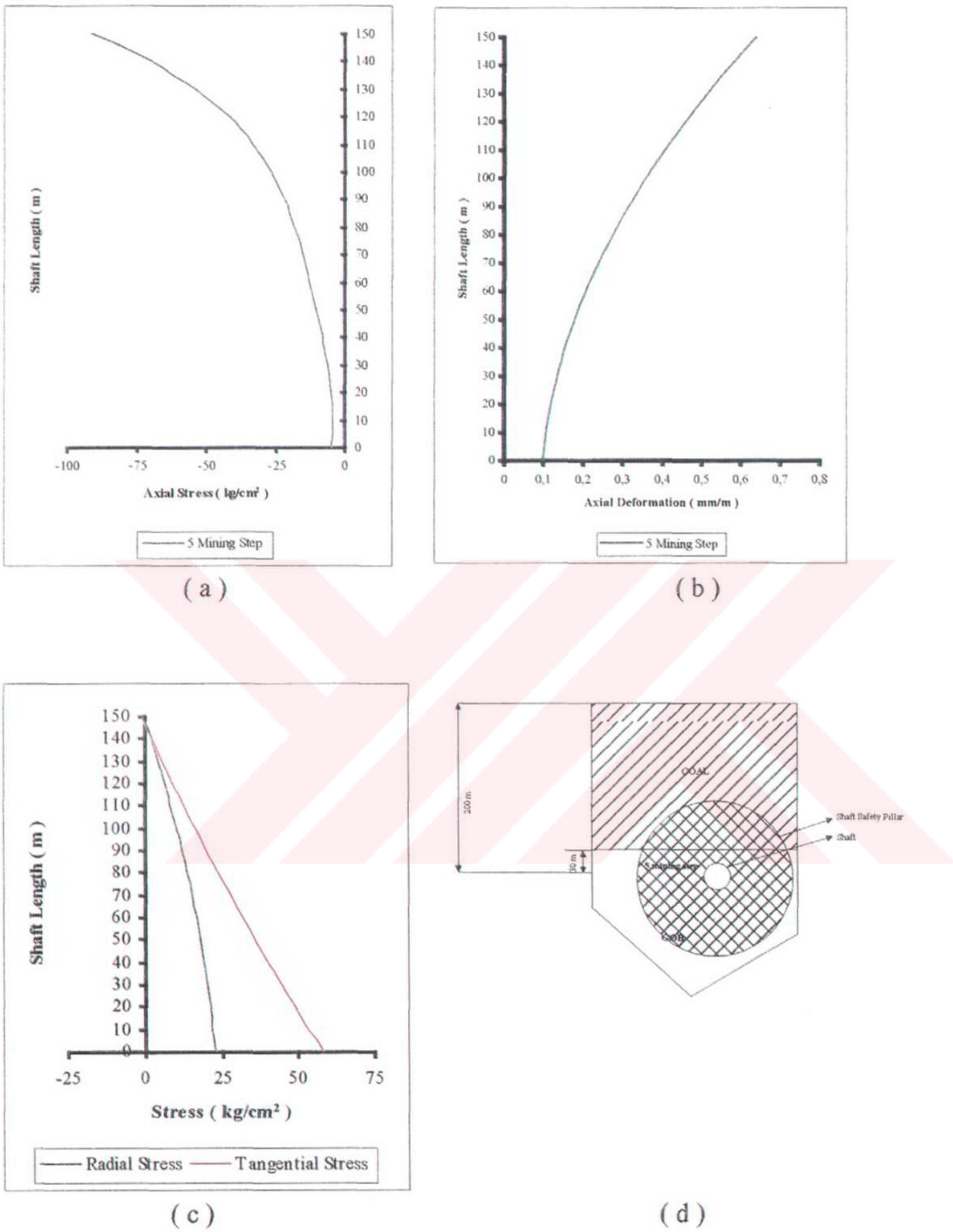

Figure 5.11 Stress and deformation analysis on the boundary of Shaft 1 for mining step 5, a) axial stress, b) axial deformation, c) tangential and radial stress, d) mining step

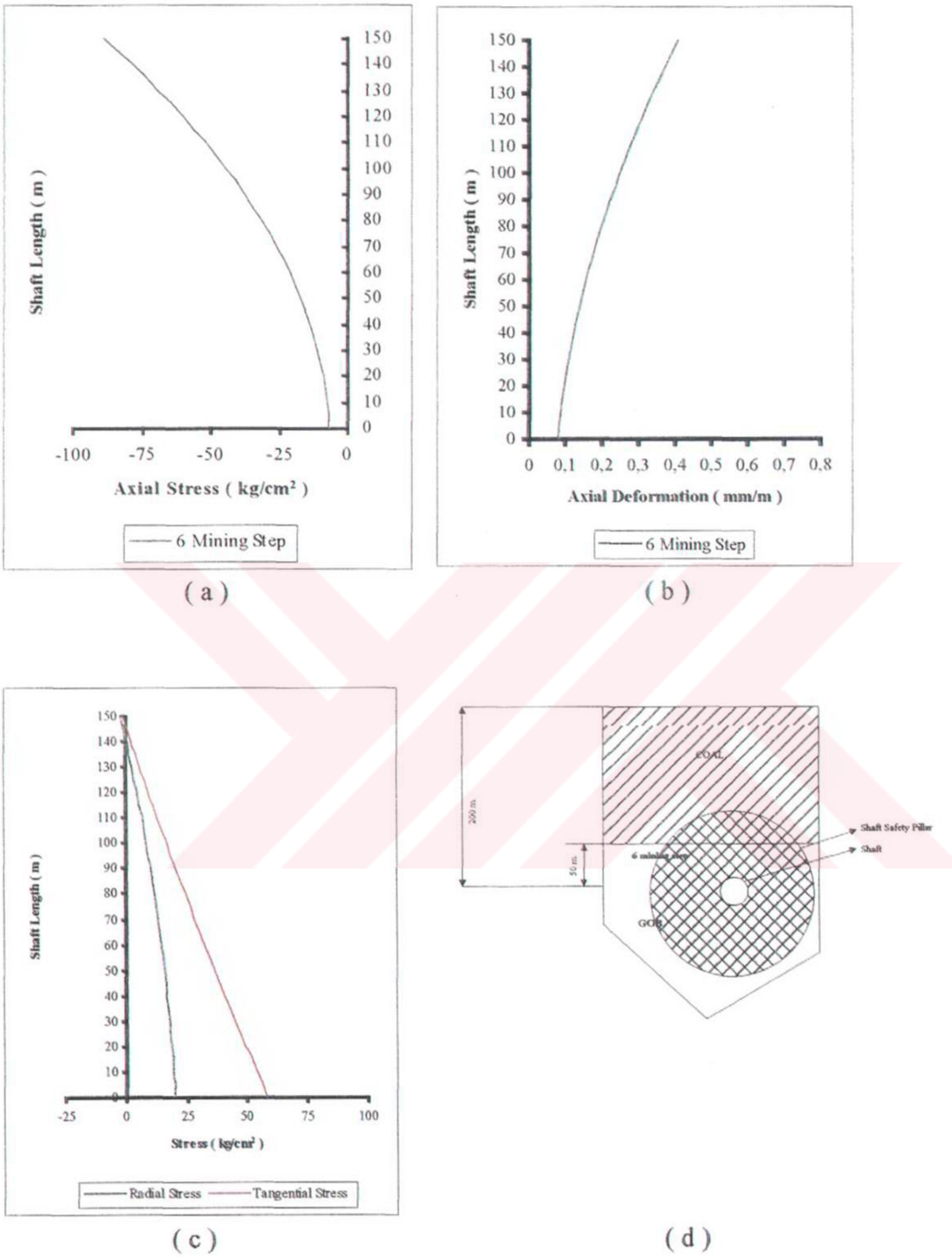

Figure 5.12 Stress and deformation analysis on the boundary of Shaft 1 for mining step 6, a) axial stress, b) axial deformation, c) tangential and radial stress, d) mining step

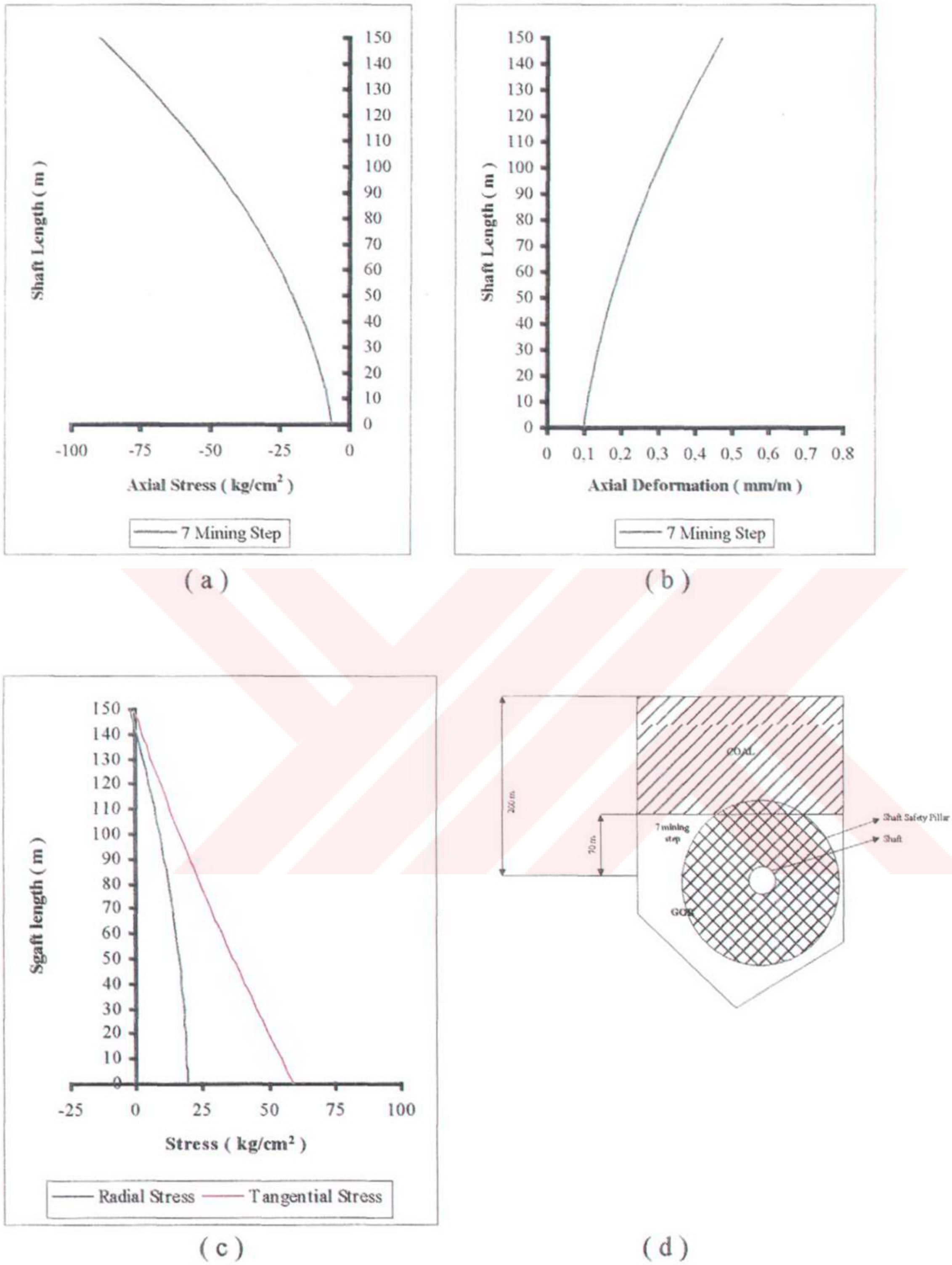

Figure 5.13 Stress and deformation analysis on the boundary of Shaft 1 for mining step 7, a) axial stress, b) axial deformation, c) tangential and radial stress, d) mining step

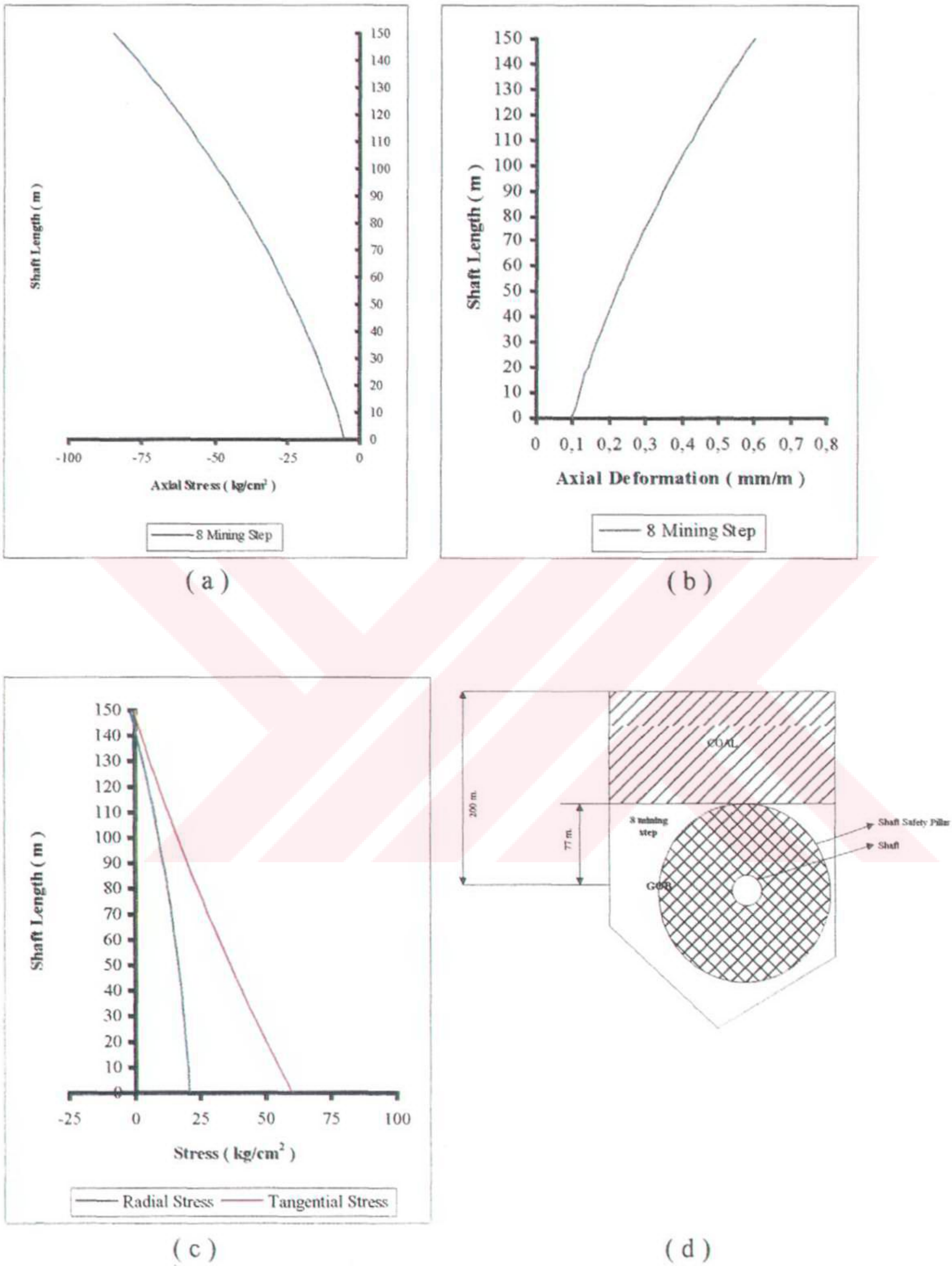

Figure 5.14 Stress and deformation analysis on the boundary of Shaft 1 for mining step 8 a) axial stress, b) axial deformation, c) tangential and radial stress, d) mining step

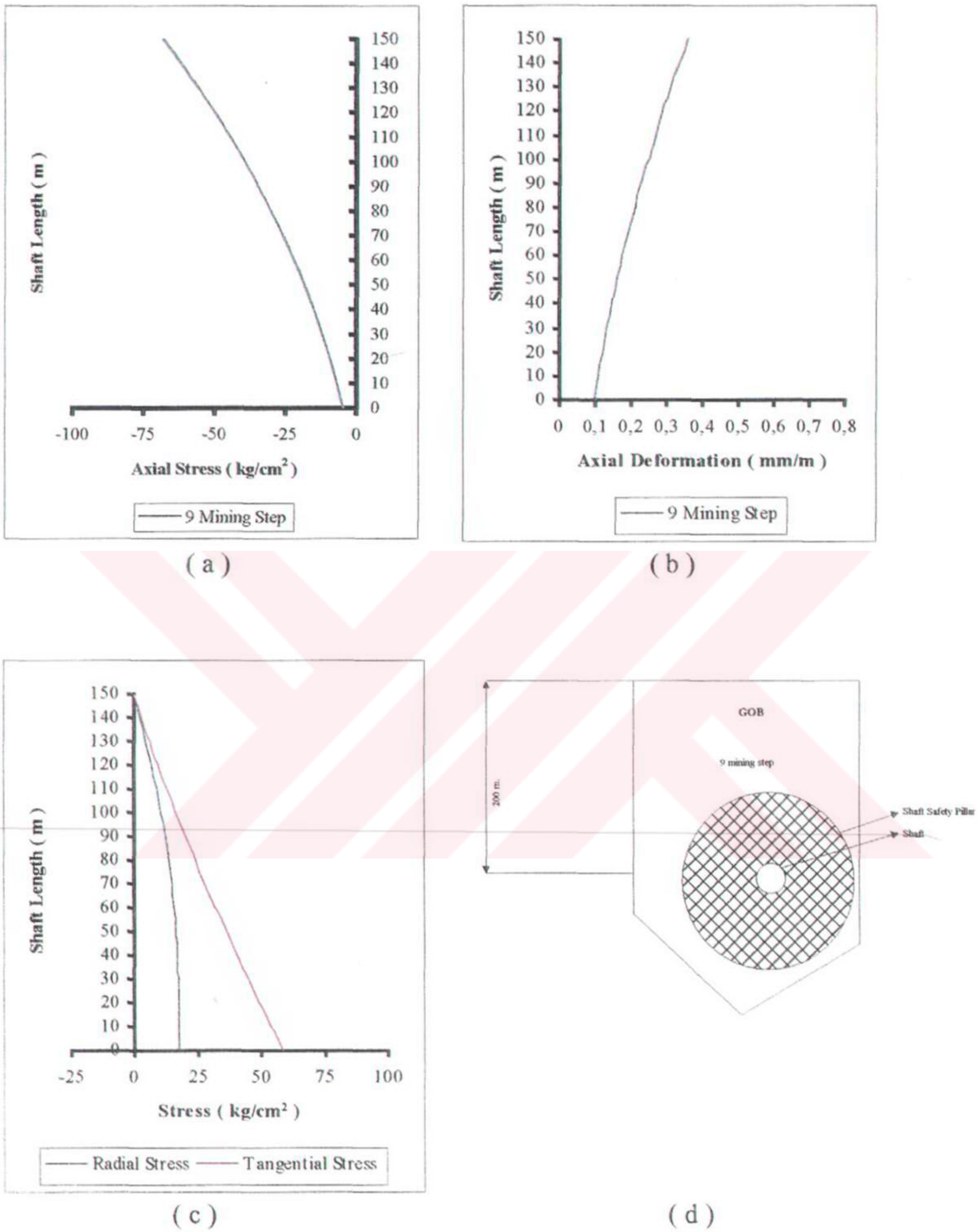

Figure 5.15 Stress and deformation analysis on the boundary of Shaft 1 for mining step 9, a) axial stress, b) axial deformation, c) tangential and radial stress, d) mining step

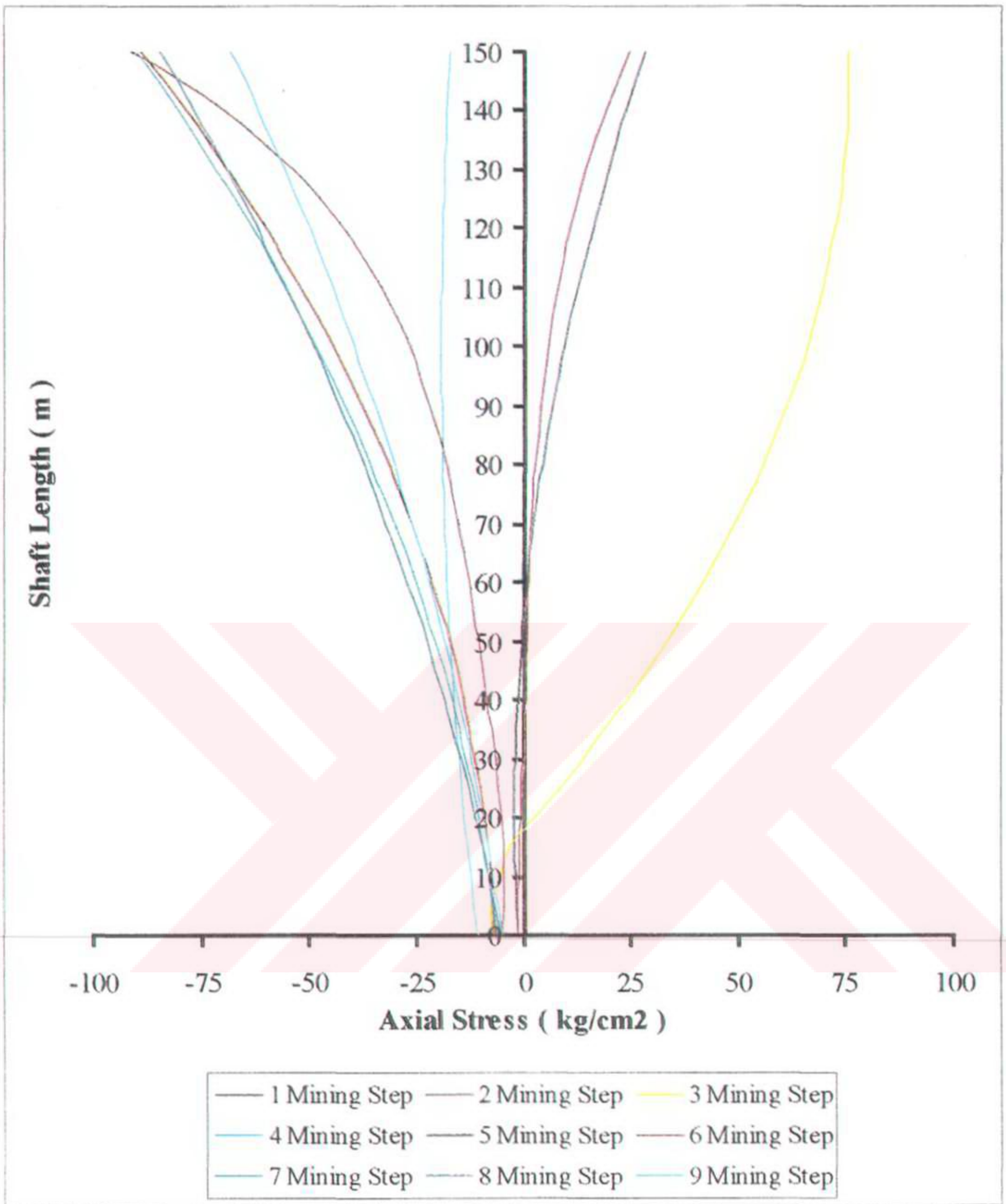

Figure 5.16 Axial stresses for all steps

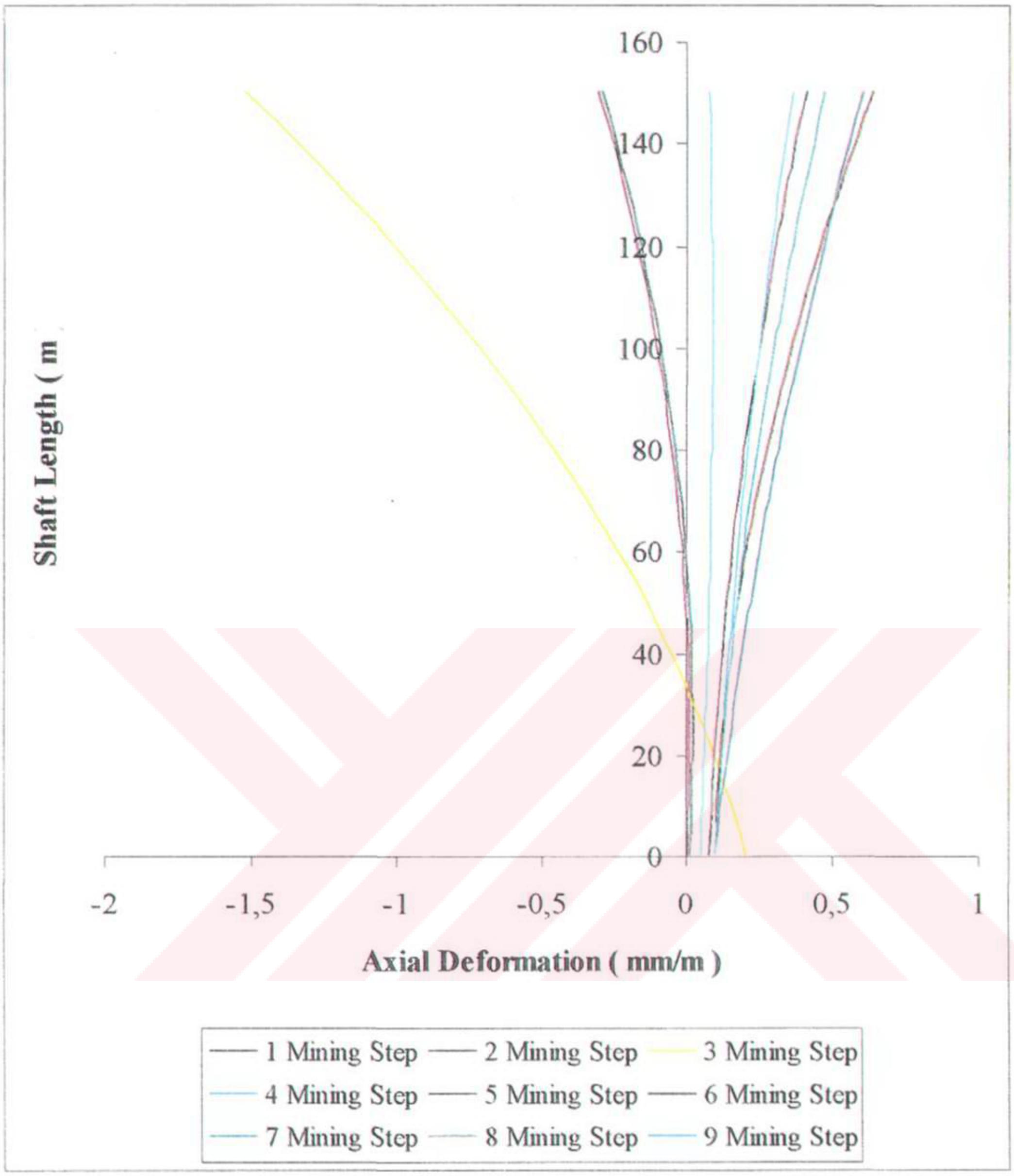

Figure 5.17 Axial deformations for all steps

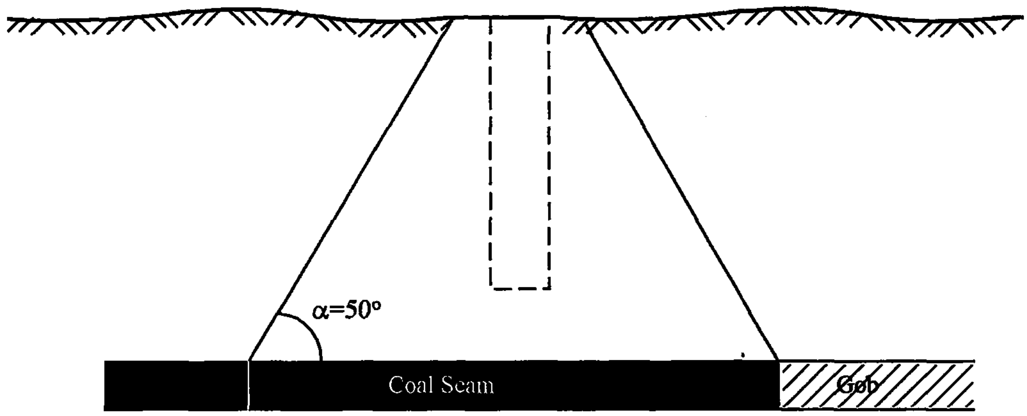

Figure 5.18 First situation for non-excavating safety pillar

During the period, when there is no production within the shaft safety pillar (Figure 5.18), which was left depending on the internal parameters of overburden, no additional deformation and stress on the shaft boundary have been found. These results have conformed with the finite element analyses and field observation.

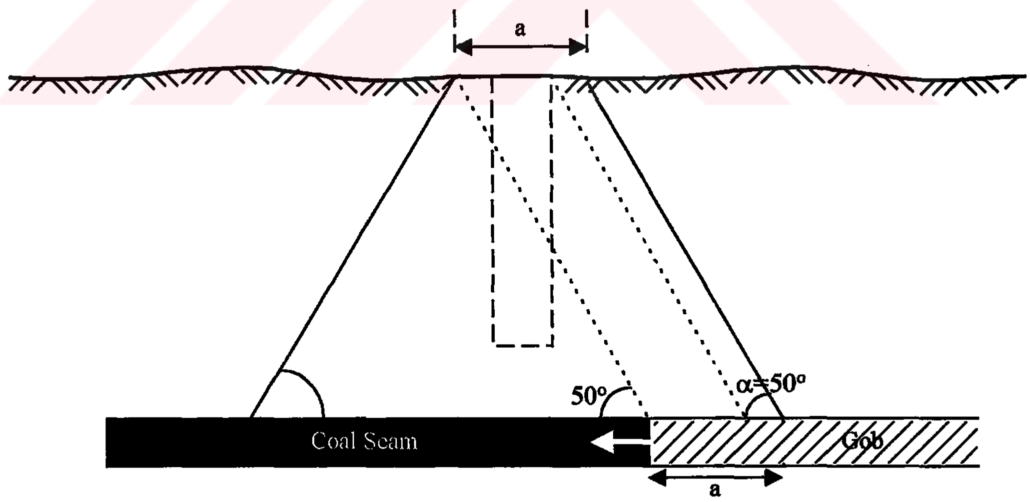

Figure 5.19 First excavation from edge of the safety pillar

During the face advancement, which starts from the edge of the safety pillar and extends to the center of the shaft, top part of the shaft is affected with strata convergence. This is quite natural and expected result. When the top of the shaft is affected, face advance is at point b (Figure 5.19). This event has been observed on field. With face advance, convergence, at point b, and subsidence, at the top of the shaft, will increase. As the bottom of the shaft is rigid, compressive stresses and shortenings of the shaft boundary occur starting from the top of the shaft and continues downwards in a decreasing trend. When the convergence reaches the maximum value at point b, shortenings and compressive stress will reach maximum value at the top of the shaft boundary. At this point, if compressive stress exceeds over compressive strength of the shaft support, shaft boundary will fail. According to the results of finite element analyses, compressive stresses have not exceeded shaft support strength and no damage has occurred on shaft boundary. These results have confirmed with the field observation.

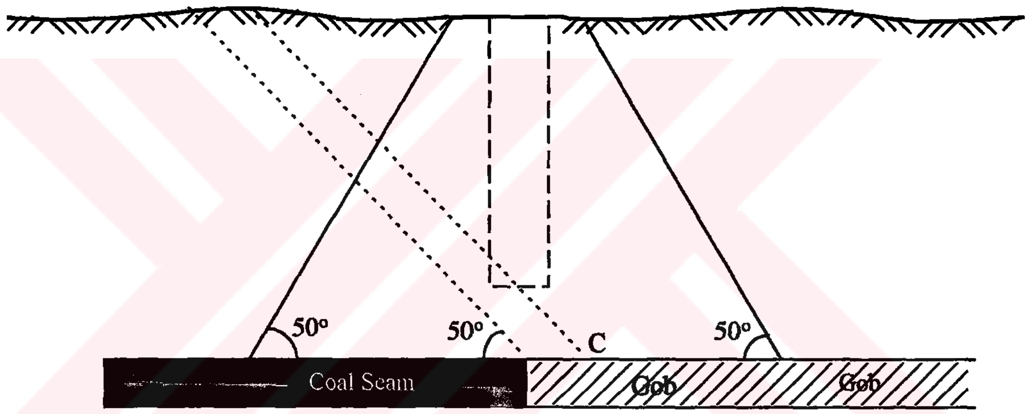

Figure 5.20 Excavation has reached the center of the safety pillar

When the face reaches to the center of the shaft pillar, convergence has occurred at point c (Figure 5.20) and shaft boundary has started move through downwards with rockmass, covering the bottom of the shaft. Therefore, lengthening and tensile stresses occur at the top of the shaft boundary and move downwards.

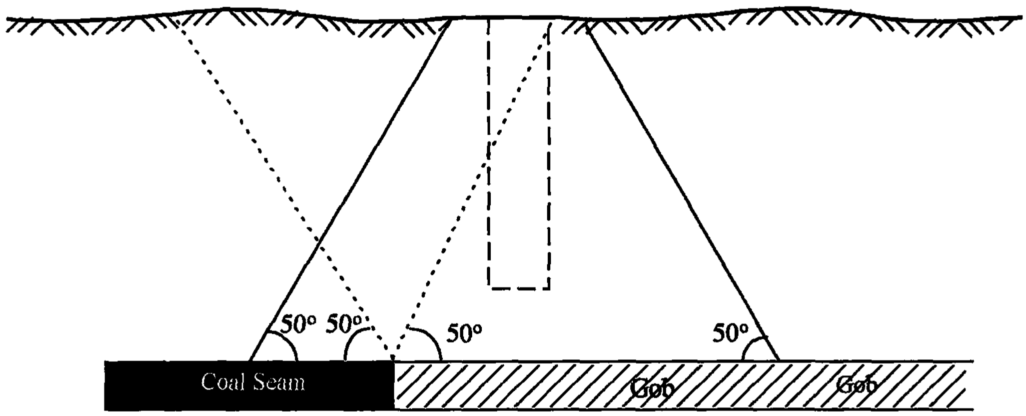

Figure 5.21 After excavation has passed to the center of the safety pillar

After passing the center of the shaft pillar (Figure 5.21), lengthening and tensile stresses increase at the top of the shaft. At this point, if shaft support is made of brick, crack will occur on the shaft boundary. In the case of concrete support, if tensile stress, occurring at shaft boundary, exceeds tensile strength of shaft support, shaft boundary will fail or tensile stress will give damage to shaft boundary. If shaft boundary goes through the seam, damage can be prevented by cutting the shaft boundary. But, if the shaft does not reach the level of the coal seam, in the case of this study, shaft boundary may fall down when the face passes the center of the shaft pillar. In the field application of this study, falling down of the shaft has occurred with rockmass when the coal face has passed about 20m. over the center of the pillar. To prevent this failure, some coal can be left as a pillar under the shaft boundary. At this point, important parameter is coal thickness.

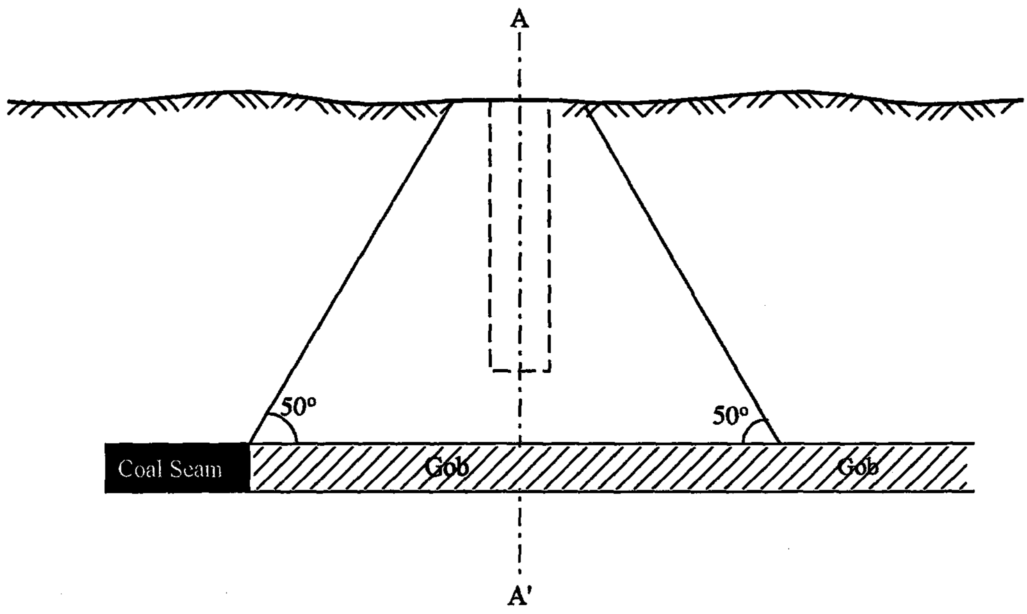

Figure 5.22 After shaft safety pillar has been excavated completely

When the shaft safety pillar has been excavated completely, stresses, on the shaft boundary, will be reduced. Because, convergence and subsidence will have finished at A-A' cross-section (Figure 5.22). According to finite element analyses, after excavation all the shaft safety pillar, there is tensile stress on the shaft boundary due to the different movements between top and bottom of the overburden. At this point, it can be said that bottom of the shaft move with the strata more than top of the shaft boundary.

5.6 Conclusions

- To prevent the occurrence of any damage and for the stability during the process, shaft safety pillar must be designed to account the internal parameters of rockmass and pillar theory.

- Internal parameters of rockmass, like limit angle, breaking angle, cohesion, must be determined carefully. At this study, no damage has occurred on shaft boundary for a long time with aid the of safety pillar. By utilizing boundary element analyses, finite element analyses and field observations, limit angle and breaking angle were found to be 50^0 and 56^0 respectively.

- Shortenings and compressive stress, occurring on the top of the shaft, was started with face advancing in the safety pillar until approximately 15 m. to the front of the center of the safety pillar. These values eventually increased to its maximum value by convergence and subsidence and remained at this level.

- When the face advancement exceeds the pillar center, lengthening and tensile stresses decrease starting from the top of the shaft to the bottom. Further advancement of the face, cause in increase in these values eventually to maximum, where subsidence and convergence are completed.

- After the safety pillar has been fully excavated, some tensile stress and lengthening still remain on the shaft boundary due to the difference in movement the top and bottom of overburden. The reason of these stresses and lengthening can be explained that there is adhesive shear bond between exterior wall and rock and shaft deformation equals to rock deformation at the top and bottom of the shaft. It can be deduced from this study that there is no adhesive shear bond at the bottom of the shaft due to roof caving method and therefore the adhesive shear bond at the top of the shaft causes tensile stresses and lengthenings on the shaft boundary.

- In the case when the shaft has not reached the coal seam, it can be said that the shaft deformation at the bottom part is different then the deformation of rock mass.

Chapter Six
CONCLUSION

Power production dates back to prehistoric times. A great deal of effort has been made for the exploration, evaluation and proper exploitation of energy resources. Rapid development of technology, nowadays, accelerated the need for alternative energy resources. Economic considerations take the first step in energy production as in the other branches of engineering such as raw material production, beneficiation and refining. Nuclear, hydraulic and fossil fuel resources are the main assets of energy production together with recycling materials. Coal has always been an important material within these items.

Coal can be produced by open-pit and underground mining methods. Various parameters should be born in mind during the underground production of coal according to the mining methods utilized.

To realize the underground production and transportation of coal to the surface construction of various facilities such as shafts, drifts and galleries is necessary. Stability and maintenance of these utilities during the life of mine is one of the main concerns of the mining engineer. One of the long practiced methods of maintaining stability is to leave pillars underneath so-called constructions. Coal within the safety pillars is not produced for the duration of operation. As coal production requires deeper mining activities, nowadays, larger pillars are needed. The coal in these pillars can easily be recovered due to its close position to the shaft or main drift and its economics is justified.

In this research work, production of safety pillars in the underground coal mine, which belonging to Hüstaş Co. at Manisa-Soma district of TURKEY, was studied.

Finite element and boundary element methods have been utilized for the determination of stresses and deformations occurring during the recovery of coal. Their resulting effects have been compared with actual observations.

Stress and deformations were studied in the first place to determine the stability of safety pillar during the course of excavations. For this part of the research, LAMODEL computer program of the National Institute for Occupational Safety and Health, City of Pittsburgh, Pennsylvania State of the U. S. A., which was designed to run by boundary element technique, had been utilized. Field data were calculated by using empirical equations of various investigators. Shaft safety pillar strength were found to be between 22,52 MPa and 51,76 MPa and main drift safety pillar strength were calculated to be between 19,49 MPa and 40,56 MPa respectively. Boundary element analyses results indicated that maximum vertical stress occurring during the production of safety pillars were 31,5 MPa for the shaft safety pillar and 28,5 MPa for the main drift safety pillar. These values can be stated as critical for the size of pillars under study. However, these stresses will be reduced 30 % in view of double slice mining production method involved. It is also deduced from the analyses that a yield of 1-1,5 m. at the coal face is found which can be accepted as a reasonable value considering a coal thickness of 18 m. and the material properties of the yield zone. The peak value of stress obtained on the coal is 31,5 MPa and this is 15 m. in front of the coal face. Besides, the maximum vertical stress on the gob is about 4 MPa about 150 m. behind the face and remains still. This stress value is quite comparable with covered stress due to gravitation and no other additional stress takes place on the gob. The models are therefore conforms the theory given by Jacobi known as the plastic overburden layer. The maximum seam convergence is 13,190 m., which coincides 73 % of the 18 m. coal thickness produced. Maximum subsidence obtained on the surface is about 5,95 m., which is approximately one third of the coal thickness. Data obtained from the analyses shows that limit angle and break angle of the field are 50^0 and 56^0 respectively. These results also conform with the field observations and previous studies.

Based on analyses carried out step by step, it can be deduced that the failure of main drift, which is 30 m. above the coal seam and within the immediate roof, may take place 15-20 m. behind the coal face due to huge stress and deformations occurring as a result of caving. This deduction also agrees with field observations.

Considering the line crossing the shaft and perpendicular to the production, the maximum surface subsidence is 5,9 m. and the seam convergence is 11,998 m. These values are 4,896 m. and 9,987 m. respectively on the surface, vertical to the shaft axis. Lengthenings within the shaft support are determined as a result of the above data. These values are also in agreement with field observations. Horizontal strain obtained, due to the subsidence where the shaft localizes, is determined as 0,0031mm/mm.

For the investigation of axial stress and strain within the shaft support due to the surface subsidence, the models are calibrated according to the previous study, have been subjected to finite element method. ANSYS 5.7 version of ANSYS Co.'s program has been utilized for this investigation. According to the results of the original field model before the production commences in the safety pillar, it is confirmed that the limit angle and break angles are 50^0 and 56^0. In the subsequent analyses carried out towards the center of the shaft, it is determined that axial stress and strain increase as the face advances and they reach a maximum value of 7,7 MPa and 1,59 mm/m before a distance of 30 m. to the shaft center. These values are not in damaging level for the shaft support as it is made of concrete. Tensile stress and lengthenings start taking place before the production reaches the shaft center. Because the shaft ends 30 m. above the coal seam level. Tensile stress and lengthenings tend to increase with the face advancement and they reach the maximum value of 9,09 MPa and 0,64 mm/m after passing the shaft center about 30 m.

There are no marked changes on the top part of the shaft with face advancement whereas a considerable increase regarding to tensile stress and lengthenings has been seen at the middle part, again not in a damaging level for the shaft due to high strength of the wire mesh and reinforced concrete material. Stresses at the lower part of the shaft are quite vague. This is due to caving method utilized and the surrounding rock being much fractured. No fracture or cracks have been noticed in the shaft support during the field observations. However, the collapse of shaft with the host rock occurred after the production advanced about 20 m. from the shaft center. The amount of this subsidence is about 5m.

In the case where shaft does not reach the coal seam high stresses occur in the top part of the shaft due to well adhesive shear bond between the shaft support and rock mass. However, this bonding is quite low in the bottom part of shaft because the rock contains lots of fracture and cracks as a result of caving method. With the advancement of the face, shaft will subside with rock mass depending on the internal parameters of rock.

No considerable changes are noticed on horizontal plane in tangential and radial stresses in the shaft support during the excavation. Maximum tangential and radial stresses are 7,49 MPa and 2,56 MPa respectively. These values were obtained in the case where shaft center is 50 m. ahead of the production and they are not at a damaging magnitude as being compressive stresses.

Similar to previous studies in related literature, in thick coal seams, excavation of safety pillars by means of slice mining method, there seems to be no problem in view of stresses occurring on the coal face, due to a reduction of stresses by 30 percent on the top slice.

In the previous studies, which investigated stress and deformations in the shaft support during the recovery of safety pillar, shafts usually go through the coal seam. In this case compressive stresses and shortenings start with the begining of excavation in the safety pillars and move downwards as the production proceed. When the production exceeds the shaft center, tensile stress and lengthenings take place in the upper side whereas compressive stress and shortenings occur in the bottom part of the shaft. The latter reach below the coal seam. Shaft support is usually cut in the production level in order stress and deformations not to harm it.

In this research work, shaft ends about 30 m. above the coal seam. On the contrary to the other research studies, compressive stresses and shortenings within the safety pillar during production, transform to tensile stress and lengthenings depending on the break angle before the excavations reach the shaft center. There are no considerable compressive stress and shortenings occurring in the lower part of the shaft. Therefore, there is no need to cut the shaft support. Besides, there is no clear emphasize regarding the relationship between shaft movement and break angle. Under the operational conditions that the present investigation was carried out, the shaft will subside together with rock mass after the production exceeds the shaft center when bottom part of the shaft enters the area of effect of break angle.

In the foregoing investigations, it was stated that deformations on the upper and lower part of the shaft were more or less the same as of rock. It was also emphasize that the shaft moved with rock mass as there was a proper adhesive shear bond between shaft support and rock. In the case of this investigation where shaft does not reach the coal seam, the top part of the shaft moves with the rock mass due to strong adhesive shear bond. The bottom part, on the other hand, moves in a different manner than the rock as a result of its cracked and fractured nature originating from its immediate roof zone.

REFERENCES

Adler, L. & Sun, M., (1968), Ground Control in Bedded Formation, Bulletin 20, VPI&SU, pp. 94-103

ANSYS Inc., (1994), ANSYS Workbook, Release 5.4

Bals, R., (1939), Abbau von Schachtsicherheitspfeilern, Glückauf, 75, pp. 253-259

Bals, R., (1956), Einwirkungen auf Schachte, Sammelwerk, Glückauf, 2, pp. 709-757

Barron, K., (1984), An Analytical Approach to Design of Coal Pillars, CIM Bulletin, 77, 37-44

Barton, T. M., (1989), Field Evaluation of Three Longwall Pillar System in a Kentucky Coal Mine, BuMines, RI 9283, pp. 1-13

Brauner, G., (1973), Subsidence Due to Underground Mining (in Two Parts), BuMines Circular, IC 8571 and IC 8572, U. S. Department of Interior

Briton, S., (1986), Designing Deep Seam Ground Control, Coal Mining & Processing, May, pp. 60-62

Carr, F. Martin, E., & Gardner, B., (1985), How to Eliminate Roof and Floor Failures with Yield Pillars, Coal Age, January, pp. 44-51

Corp, E. L., (1975), A Finite Element Model for StabilityAnalysis of Mine Waste Enbankments Subjected to Seepage, PhD. Thesis, University of Idaho, Moscow, p. 203

Corp, E. L., Schuster, L. R. & McDonald, M. M., (1975), Elastic-Plastic Stability Analysis of Waste Embankments, BuMines, RI 8069, pp. 18-23

Crane, W. R., (1929), Subsidence and Ground Movement in the Copper and Iron Mines Upper Peninsula, BuMines, Bulletin 295, U. S. Department of Interior

Çetmeli, E., (1974), Çubuk Sistemler, Plaklar ve Kabukların Hesabı İçin Tablolar, Matbaa Teknisyenleri Koll. Şti., İstanbul

Dahl, H. D. & Parsons, P. C., (1972), Ground Control Studies in the Hanpherey No: 7 Mine, Transaction Society Mining Engineering, AIME, 252, pp. 211-222

DeMarca, M. S. & Koehler, J. K., (1988), Characterization of Chain Pillar Stability in a Deep Western Coal Mine – A Case Study, SME-AIME Annual Meeting, January, Phoenix, pp. 25-28

Erçelebi, S. G. & Nasuf, E., (2000), Mine Planning and Equipment, Room and Pillar Design of Istanbul-Yeniköy Coal Field Using Finite Element Method, Balkema, Roterdam, ISBN 90 5809 178 3, pp. 217-274

Gauna, M. Price, K. R. & Martin, E., (1985), Proceedings of the 30th U. S. Symposium on Rock Mechanics, Yield Pillar Usage in Longwall Panel Entry System, pp. 125-132

Golder Associates Consulting Geotechnical and Mining Engineers, (1982), Türkiye Kömür İşletmeleri Kurumu, Feasibility Report on the Soma Işıklar Lignite Deposit, Geotecnnology and Hydrogeology, Vol. 3, Manisa

Haramy, K. Y., (1989), Proceedings of the 30th U. S. Symposium on Rock Mechanics, Comparative Study of Western U. S. Longwall Panel Entry System, pp. 125-132

Heasley, K. A., (1998), Numerical Modeling of Coal Mines With a Laminated Displacement-Discontinuity Code, Ph.D. Thesis, Colorado School of Mines

Holland, C. T., (1963), Pressure Arch Techniques, Mechanization, 27, pp. 45-48

Karabin, G. J. & M. A. Evanto, (1994), Proceedings of the 13th International Conference on Ground Control in Mining, West Virginia University, Experience with the Boundary Element Method of Numerical Modeling as a Tool to Resolve Complex Ground Control Problems, pp. 201-213

Knothe, S., (1969), Bestimmung der Voraussichtlichen Abbaueinflüsse in Schachtsicherheitspfeilern, Przegl. Gorn., pp. 377-381

Kochmanski, T. & Magdziorz, J., (1972), Neue Methcden der Berechnung von Bewegungen und Vermessungen der Tagesoberflache und des Gebirges als Falge untertagigen Abbaus, Freib, p. 527

Köse, H., (1985), 9. Madencilik Kongresi Kitabı, Uzunayak Etrafinda Oluşan Basınçların Kuramsal Modeller Üzerinde İncelenmesi, pp. 297-315

Köse, H. & Çebi, Y., (1988), Türkiye 6. Kömür Kongresi Kitabı, Kalın Kömür Damarlarının Üretilmesi Sırasında Oluşan Gerilmelerin İncelenmesi, pp. 371-382

Kose, H. & Onargan, T., (1991), Yeraltı Madenciliğinde Zemin Çökmeleri va Kontrolu, D. E. U. Muh.-Mim. Fak. Basım Unitesi, Izmir

Kose, H. & Kahraman, B., (1999), Kaya Mekanigi Ders Kitabi, D. E. U. Muh. Fak. Basım Unitesi, Izmir, pp.6.12-6.16

Kose, H. & Onargan, T., (1993), Madencilik Kongresi Bildiri Kitabi, Modern Subsidans Hesaplama Yontemleri ve Erzurum-Oltu-Balkaya Ocaginda Uygulanmasi, pp.343-357

Köse, H., (1978), Programmierte Berechnung ger Abbaueinwirkung auf Schachte nabh dem Modell der Finiten Elemente, Glückauf, 39, pp. 141-145

Kowalczyk, Z., Martin, F., & Lawrence, K., (1976), Abbau von Schactsicherheitspfeilern mit Anwendung Hydraulischen Grubenausbaus, Freiberg-Forsch-H. A, 578, pp. 89-101

Kratzsch, H., (1983), Mining Subsidence Engineering, (Fleming, R. F. S., Trans.), Springer-Verlag Berlin, Heidelberg, New York, pp. 93-116

Kripakov, N. P., (1981), Analysis of Pillar Stability on Steeply Pitching Seam Using Finite Element Method, BuMines RI 8579, p. 33

Kuscu, S., (1985), Proceedings 6th International Congress International Society for Mine Surveying Harrogate, Mining Damage and Settlement Problems Due to Coal Mining in the Zonguldak Coal Field of Turkey, September, pp. 1018-1027

Lehman, K., (1938), PlanmaBige Abbauführung, Glückauf, 74, 321-332

Madden, B. J. & Hardman, D. R., (1992), Proceedings Symposium on Construction Over Mined Areas, Long Term Stability of Board and Pillar Workings, pp. 37-51

Mark, C. & F. E. Chase, (1997), Proceedings: New Technology for Ground Control in Retreat Mining, Analysis of Retreat Mining Pillar Stability (ARMPS), NIOSH IC9446, pp. 17-34

Mark, C. & Barton, T. M., (1997), Proceedings: New Technology for Ground Control in Retreat Mining, Pillar Design and Coal Strength, NIOSH: IC 9446, pp.49-59

Mark, C., & Iannacchione, A. T., (1992), Proceedings Workshop on Coal Pillar Mechanics and Design, Coal Pillar Mechanics: Theoretical Models and Field Measurements Compared, IC 9315, pp. 78-93

National Coal Board, (1975), Subsidence Engineering Handbook, London

Onargan, T, Koca, Y. & Köse, H. (2000), 7th National Mine Surveying Conference with International Participation, Determination of "Break Angle" from Subsidence Cracks in Soma-Eynez Coal Field of Turkey, June, pp. 189-201

Pappas, D. M. & C. Mark, (1993), Behavior of Simulated Longwall Gob Material, BuMines RI 9458, p. 39

Peng, S. S., (1986), Coal Mine Ground Control, John Willey& Sons Inc. New York

Pielok, J. & Sroka,A., (1979), Verringerung der Deformationen im Schachtausbau Durch Entsprechende Zeitlich-Raumliche Gestaltung des Abbaus, International Symposium on Mine Surveying (ISM), Aachen, Vol. 4, pp. 97-114

Riplay, E., Redmann, R. & Crowder, A., (1996), Environmental Effect of Mining, Queen's University, CANADA, pp. 311-336

Sauer, A., (1975), Die Einflüsse von Durchbauungsgrad, Abbaukonzentration und Abbaugeschwindiykeit auf die Vorausberechnung von Bodenbewegungen, Glückauf, 36, pp.16-26

Serata, S. (1976), Stress Control Technique- An Alternative to Roof Bolting, Mining Engineering, May, pp. 51-56

Serata, S. (1982), Proceedings of 1st International Conference on Stability in Underground Mining, Stress Control Methods: Quantative Approach to Stabilizing Mine Openings in Weak Ground, August, pp. 52-93

Sitz, P., (1968), Haftfestigkeitsuntersuchungen Zwischen Beton bzw. Mörtel und Verschiedenen Gesteinsarten und ihre Bedeutung für den Untertagigen Bergbau, Diss. Freiberg

Skuta, E., (1979), Die Wirkung von Abbau und Grundwasserentzug auf dieTübbingschaacte des Steinkohlenbergwerkes, Emin Mayrisch, Markschedewesen, 86, pp. 130-140

Sljacheckij, V. K., (1974), Verringerung der Abbauverluste an Kohle durc Schubsicherheitspfeiler, Bezopasnot Truda Promyslenosti, pp. 21-23

Tsang, P. & Peng, S. S., (1989), Proceedings of the 30th U. S. Symposium on Rock Mechanics, Yield Pillar Application under Strong Roof and Strong Floor Condition- A Case Study, pp. 411-418

Voigth, B. & Pariseau, W., (1970), State of the Predictive Art in Subsidence Engineering, Journal of the Soil Mechanics and Foundation Division, Proceedings of the American society of Civil Engineers, 96, pp. 721-750

Wagner, H., (1974), Proceedings 3rd International Congress on Rock Mechanics, Determination of the Complete Load-Deformation Characteristics of Coal Pillar, Denver, pp. 1076-1081

Wilson, A. H., (1973), An Hypothesis Concerning Pillar Stability, Mining Engineering, 131, 409-417

Zienkiewicz, B., (1971), The Finite Element Method in Engineering Science, McGraw-Hill, London

Appendix A

SOME PHOTOS TAKEN FROM FIELD

Figure 1 A view of transfer raise

Figure 2 A view of G4 drift

Figure 3 A view of K5 drift, west limit of mine

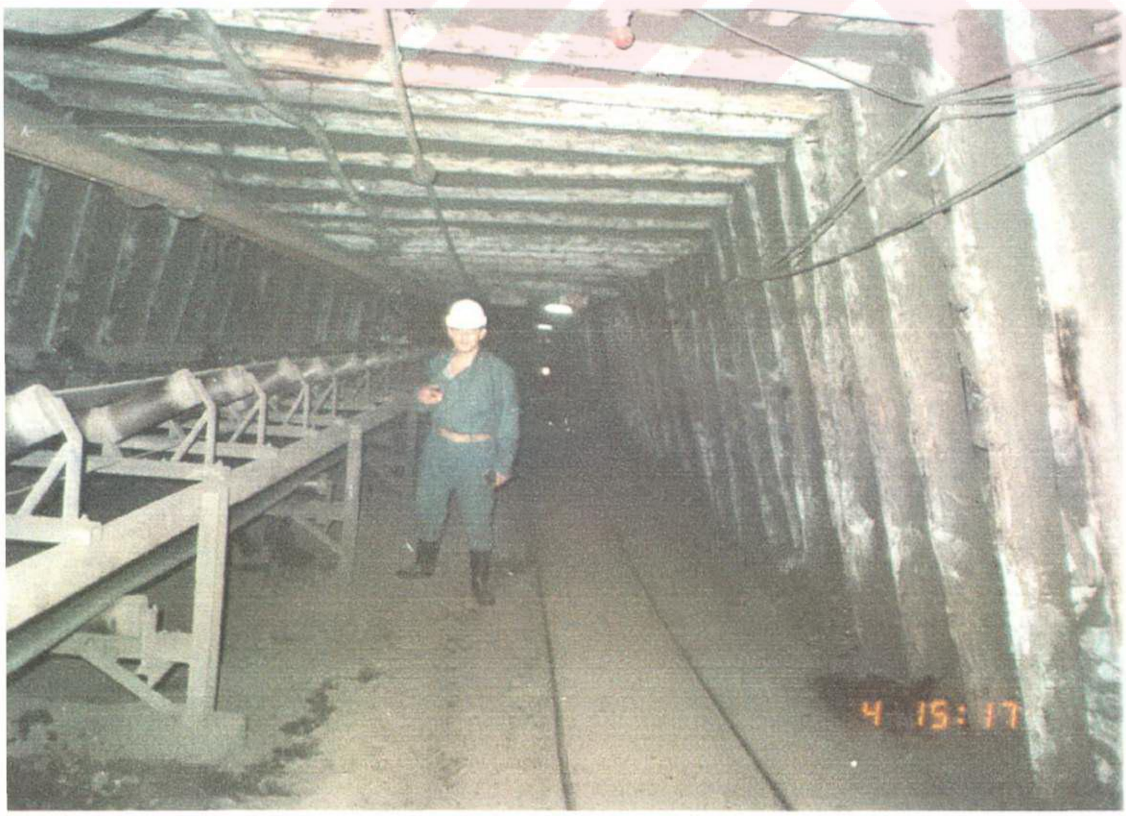

Figure 4 A view of main drift

Figure 5 A view of subsidence cracks, west of mine

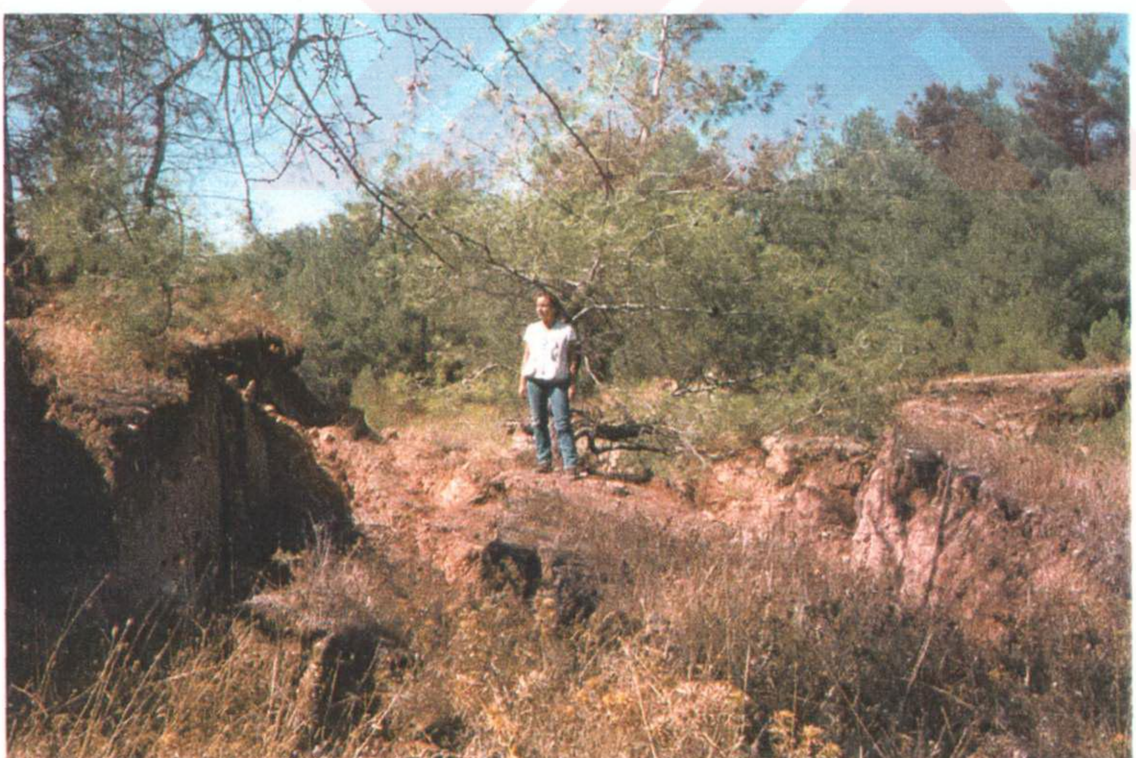

Figure 6 A view of subsidence cracks, west of mine

Figure 7 A view of subsidence cracks, southwest of mine

Appendix B

THE GRAPHS OF VERTICAL STRESS

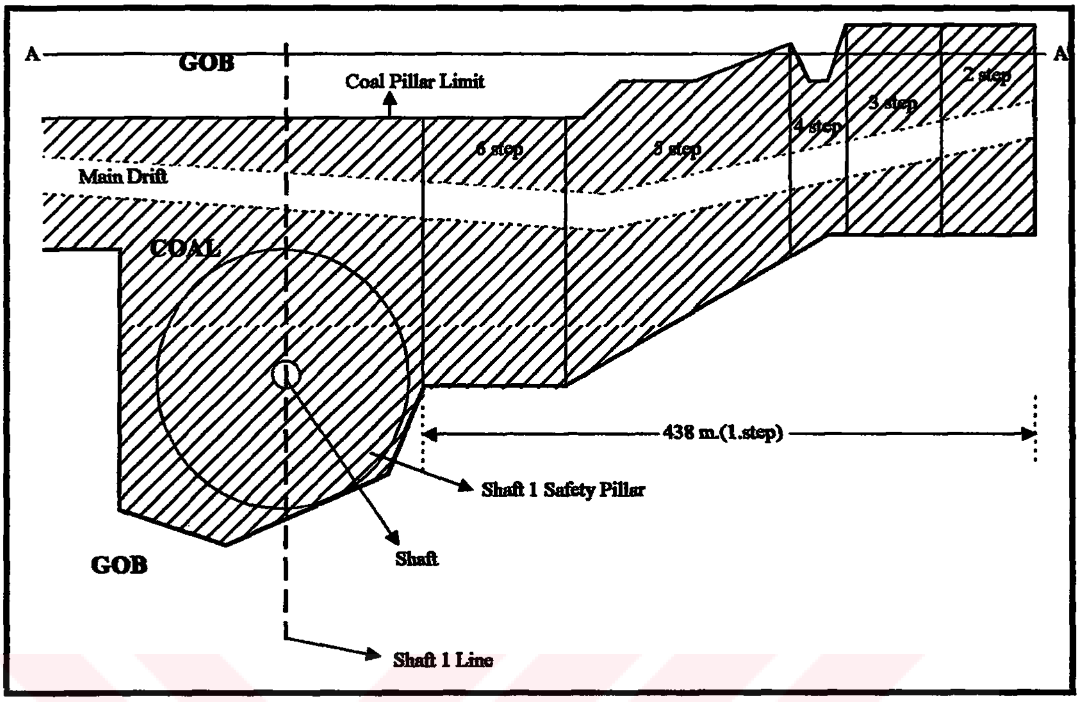

(a)

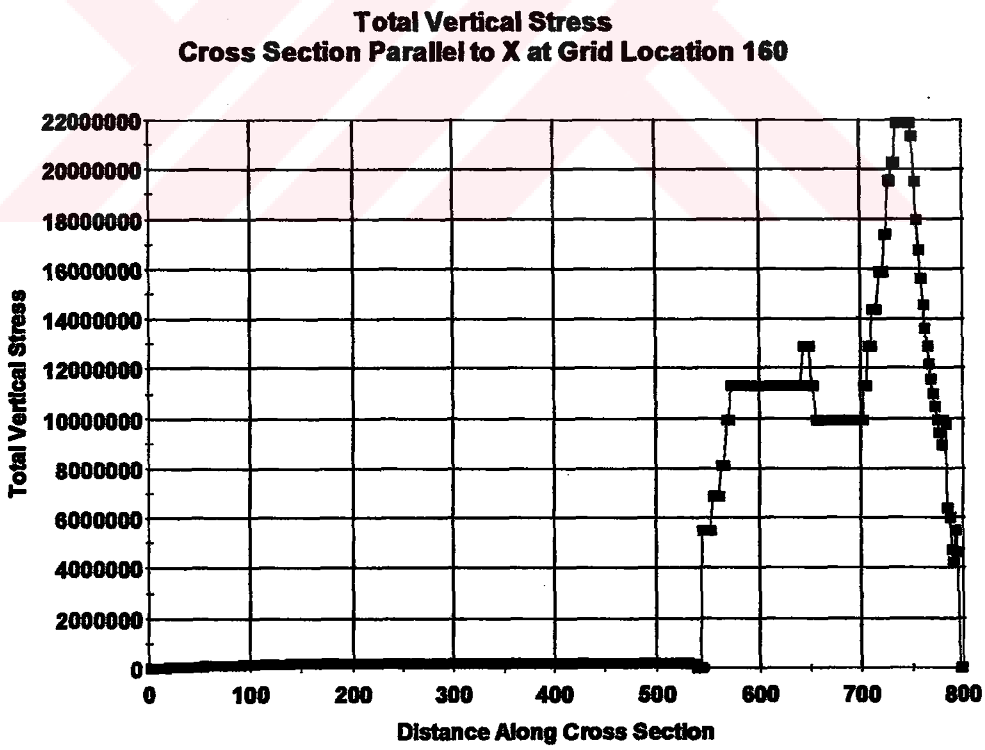

(b)

Figure 1 Vertical stress for 1 mining step on A-A' cross-section for main drift safety pillar mining, a, pillar limit; b, vertical stress in Pascal

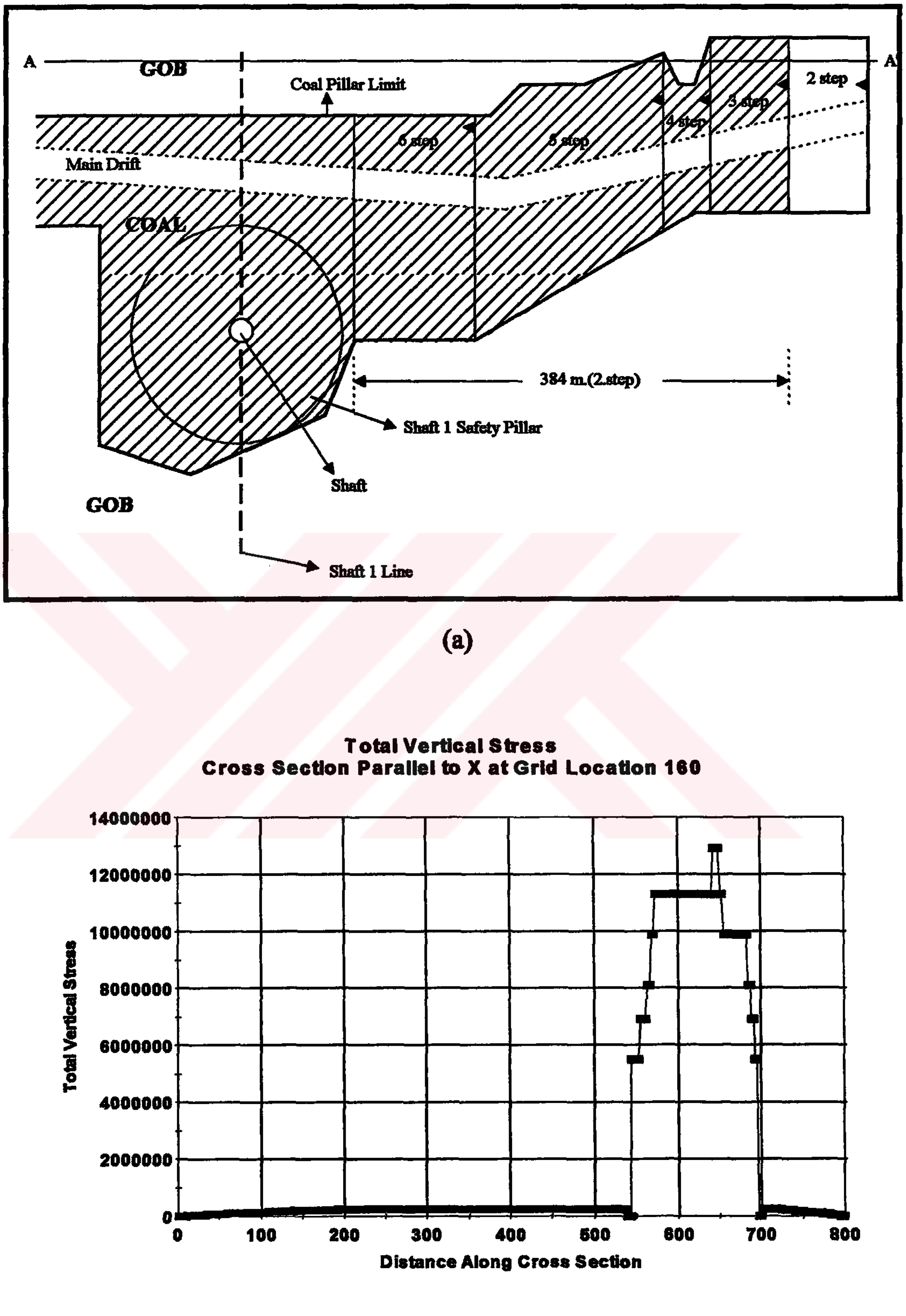

Figure 2 Vertical stress for 2 mining step on A-A' cross-section for main drift safety pillar mining, a, pillar limit; b, vertical stress in Pascal

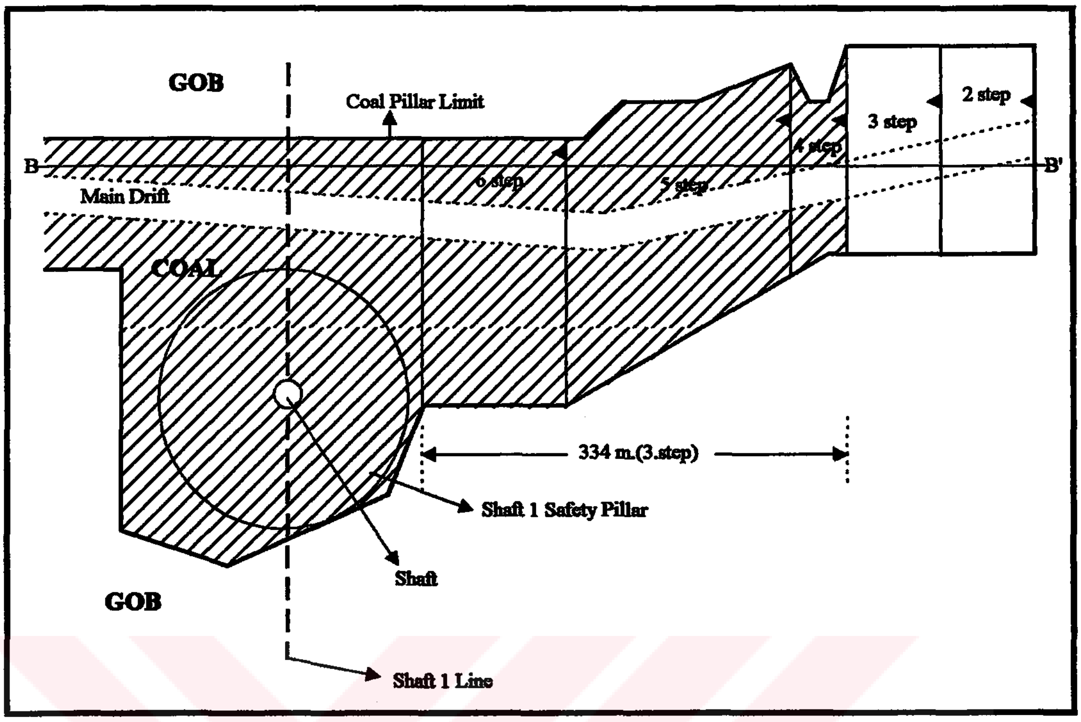

(a)

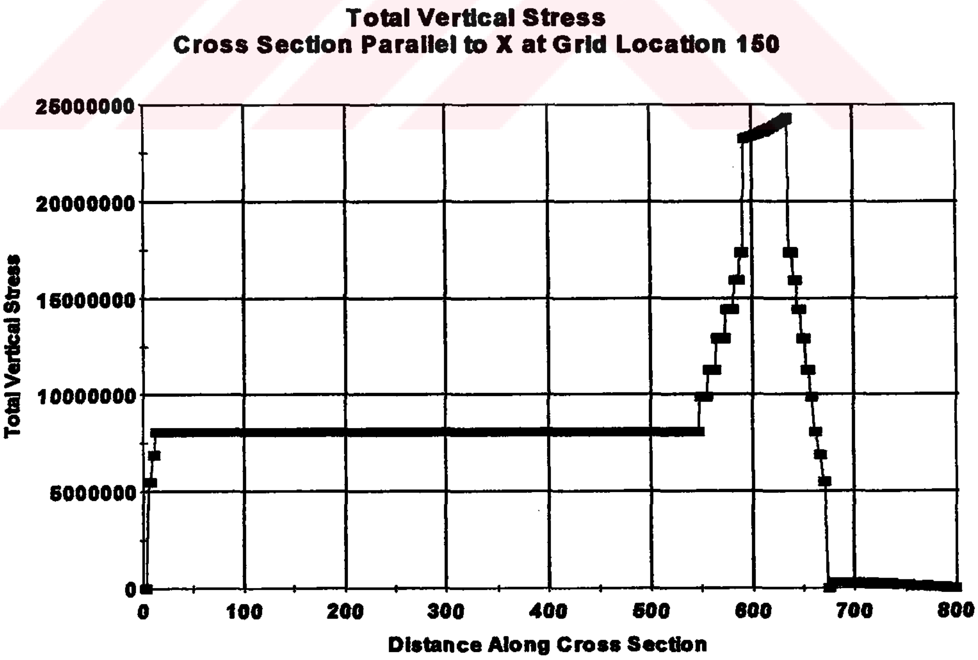

(b)

Figure 3 Vertical stress for 3 mining step on B-B' cross-section for main drift safety pillar mining, a, pillar limit; b, vertical stress in Pascal

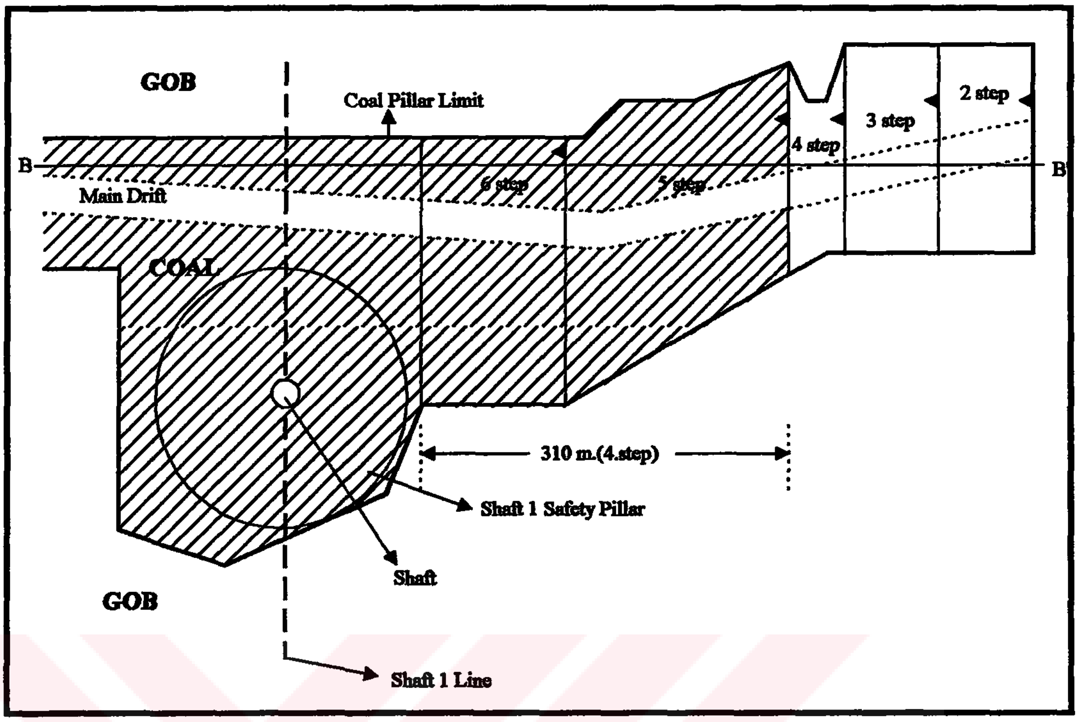

(a)

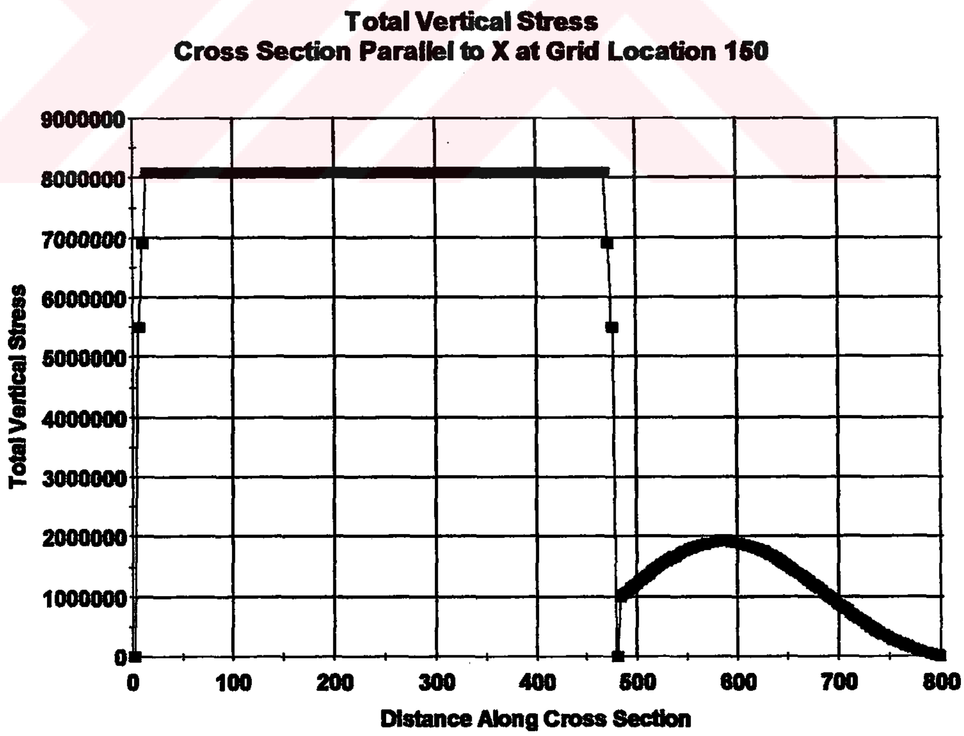

(b)

Figure 4 Vertical stress for 4 mining step on B-B' cross-section for main drift safety pillar mining, a, pillar limit; b, vertical stress in Pascal

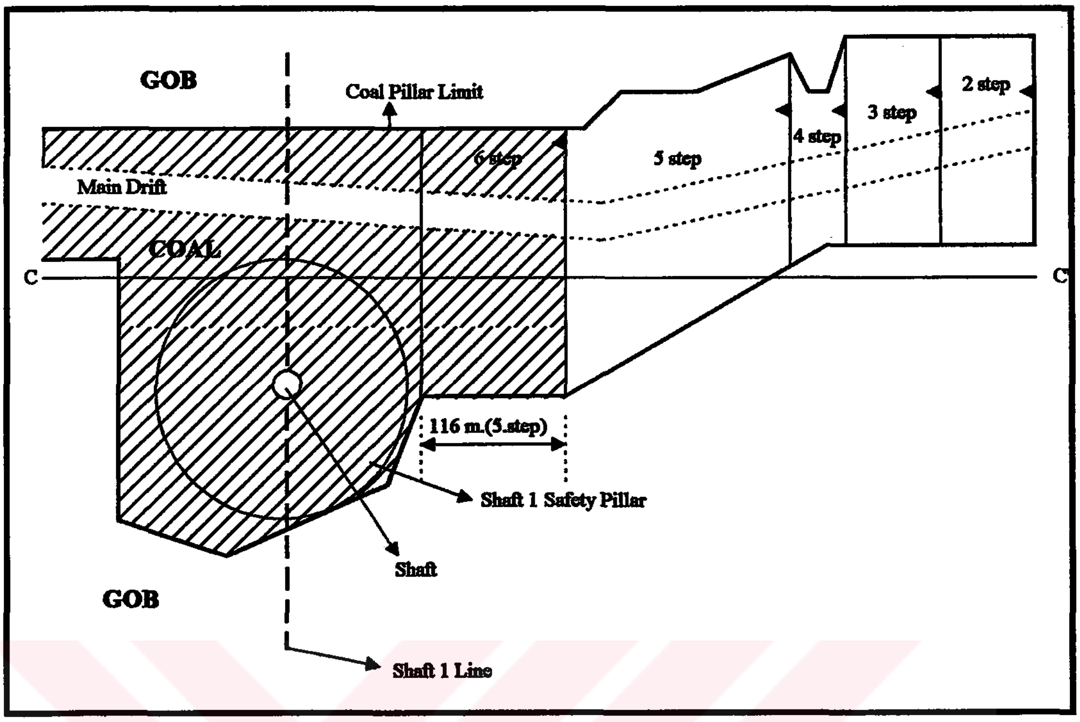

(a)

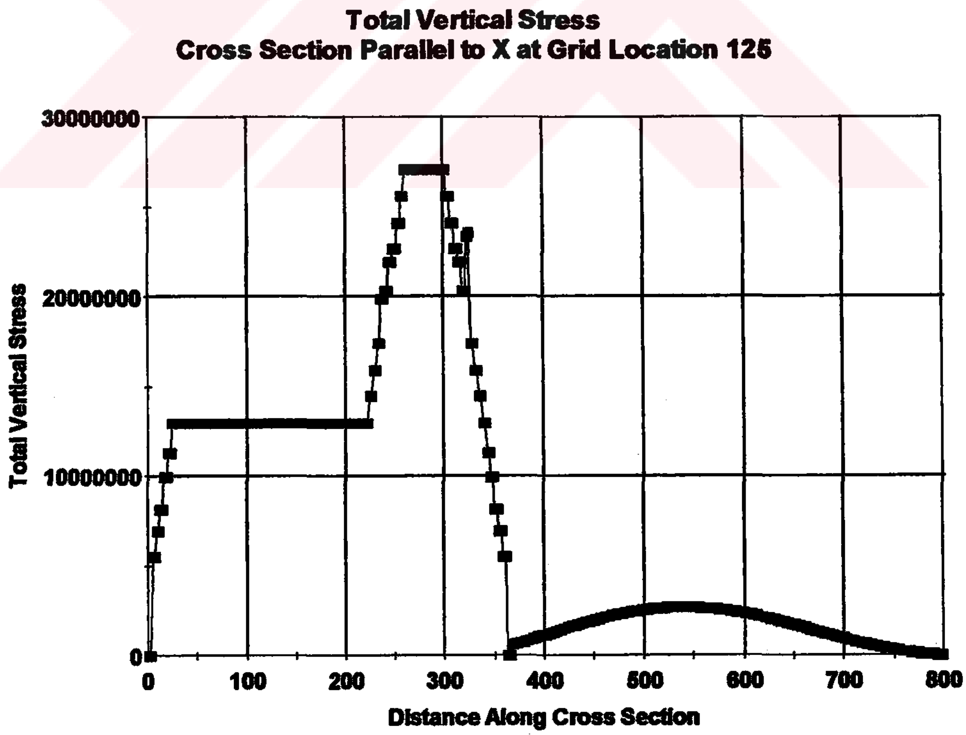

(b)

Figure 5 Vertical stress for 5 mining step on C-C' cross-section for main drift safety pillar mining, a, pillar limit; b, vertical stress in Pascal

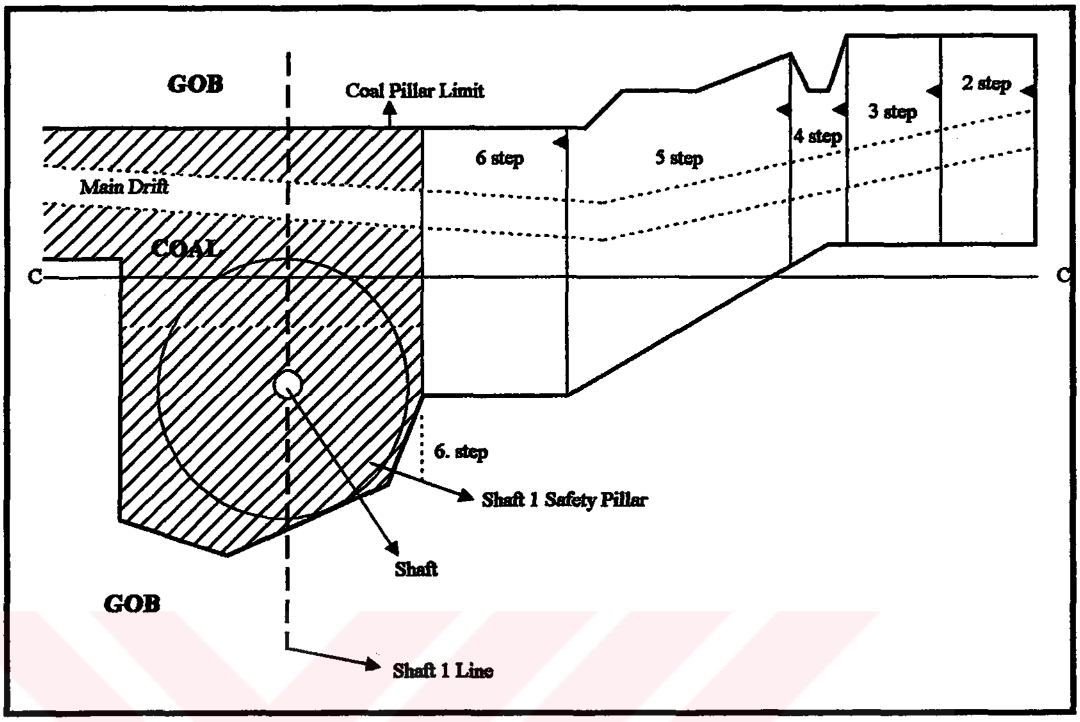

(a)

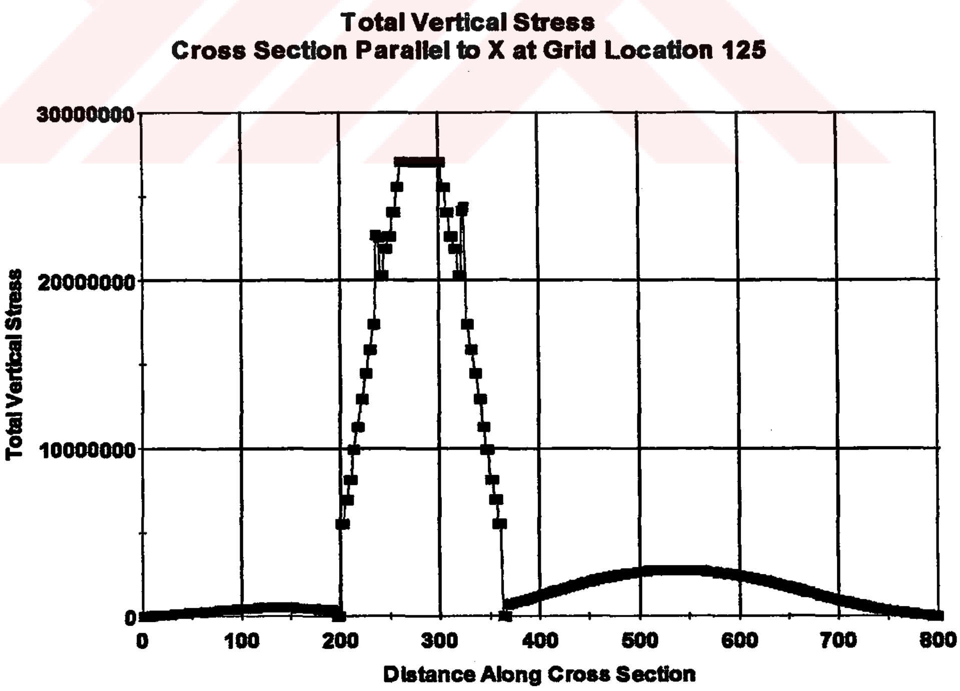

(b)

Figure 6 Vertical stress for 6 mining step on C-C' cross-section for main drift safety pillar mining, a, pillar limit; b, vertical stress in Pascal

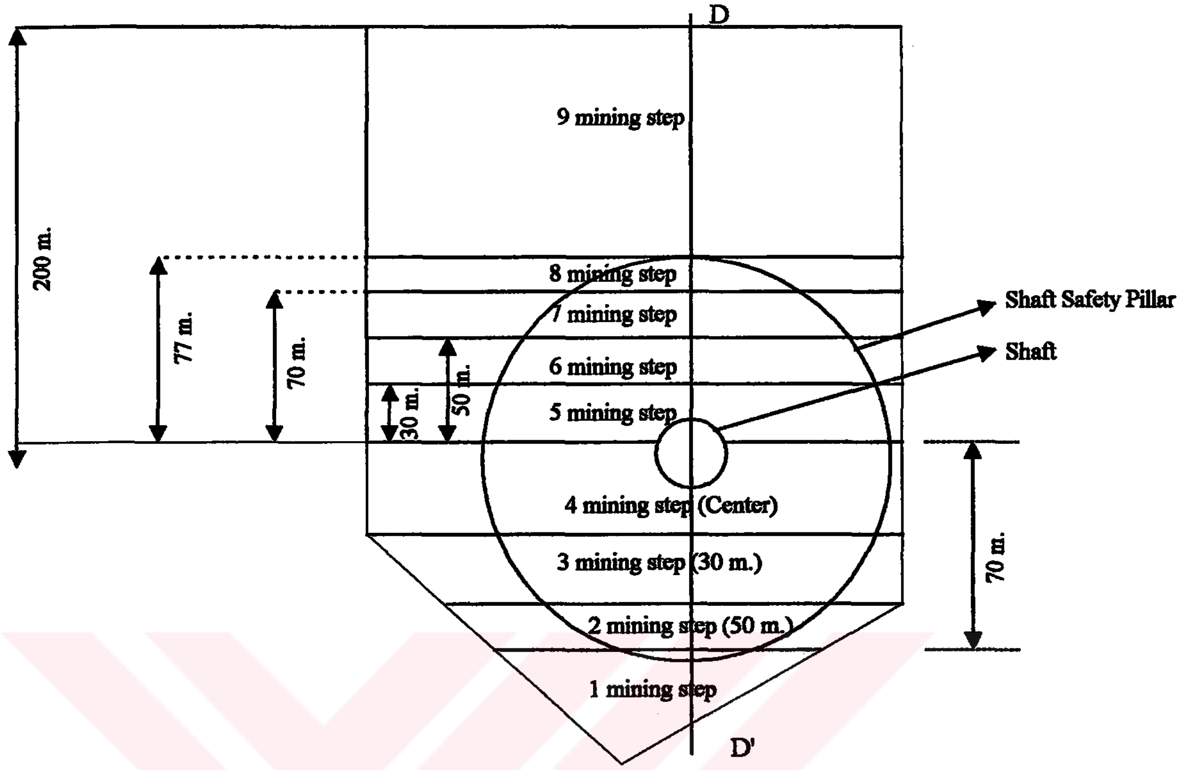

Figure 7 D-D' cross-section for shaft safety pillar mining steps

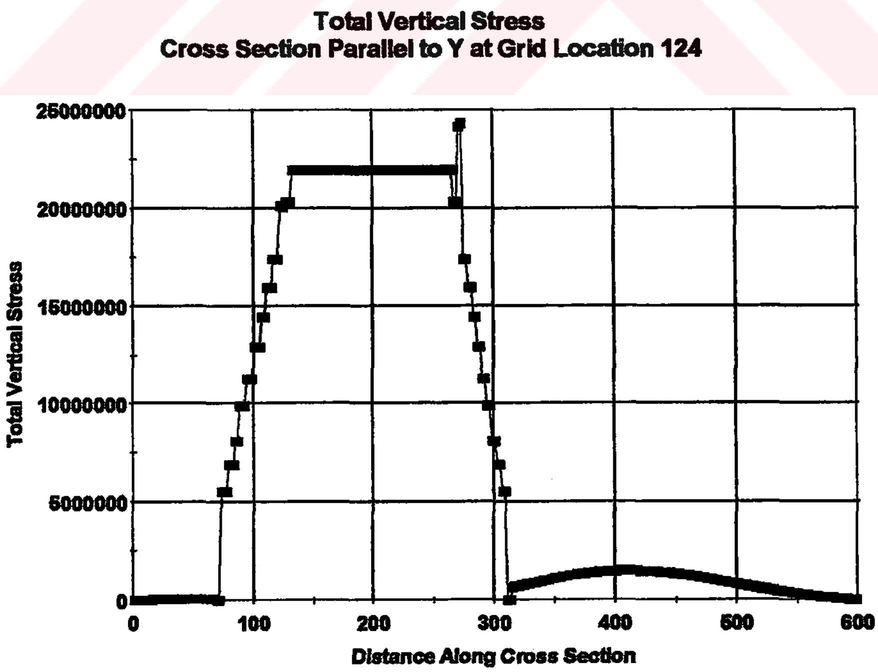

Figure 8 Vertical stress for 1 mining step on D-D' cross-section for shaft safety pillar mining

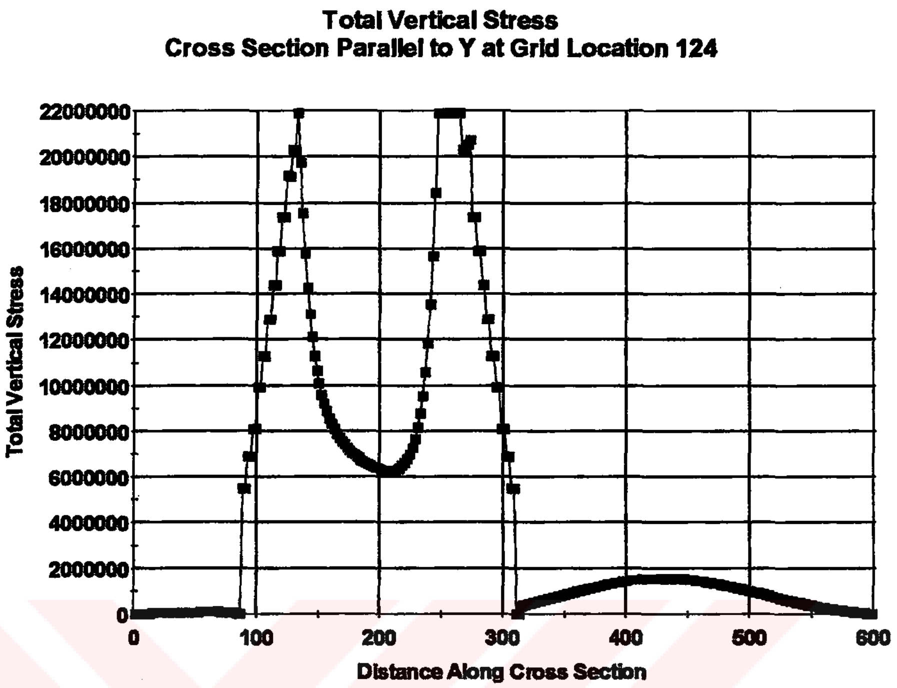

Figure 9 Vertical stress for 2 mining step on D-D' cross-section for shaft safety pillar mining

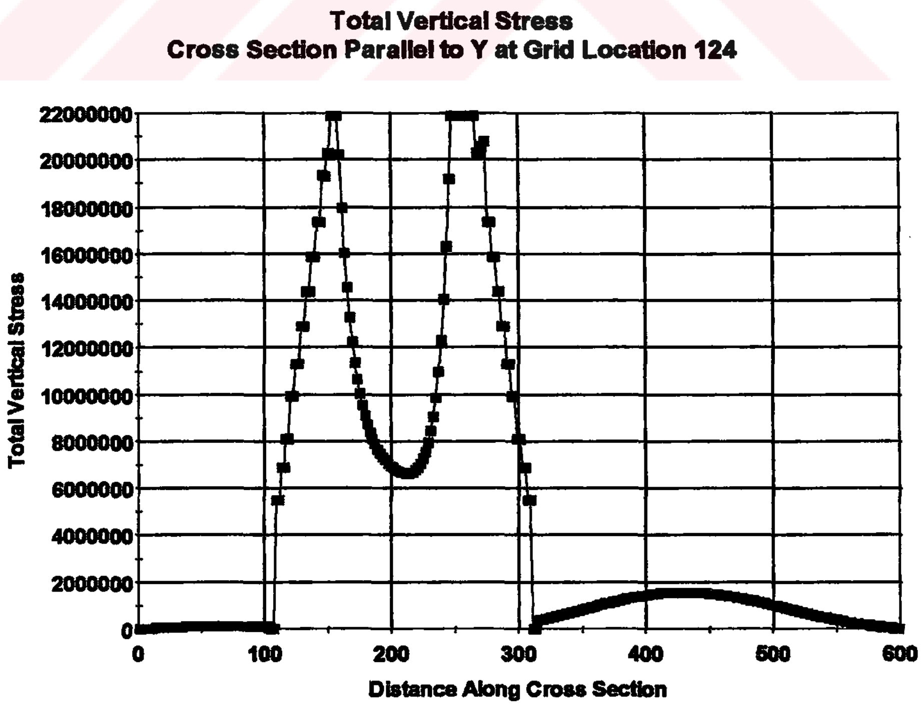

Figure 10 Vertical stress for 3 mining step on D-D' cross-section for shaft safety pillar mining

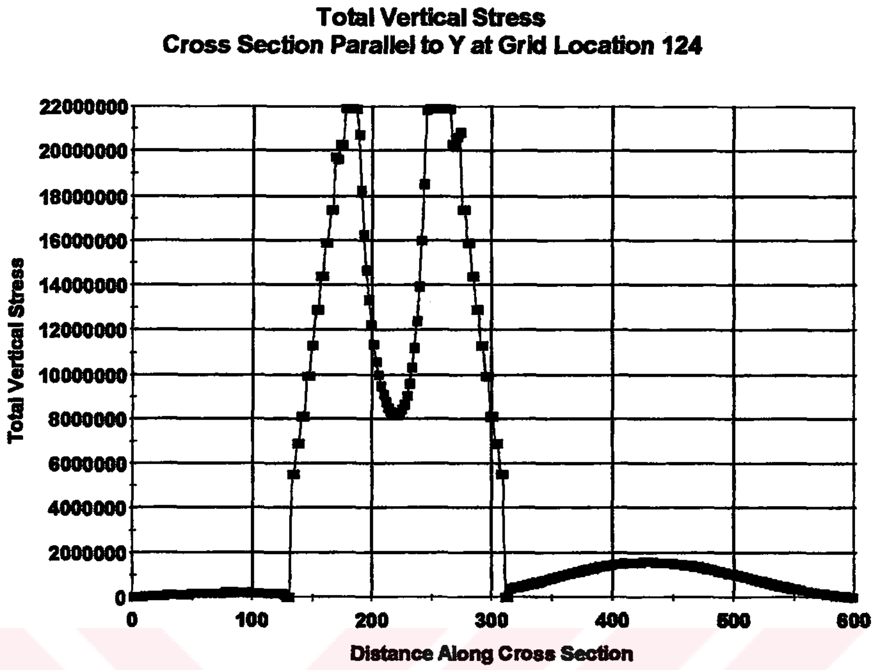

Figure 11 Vertical stress for 4 mining step on D-D' cross-section for shaft safety pillar mining

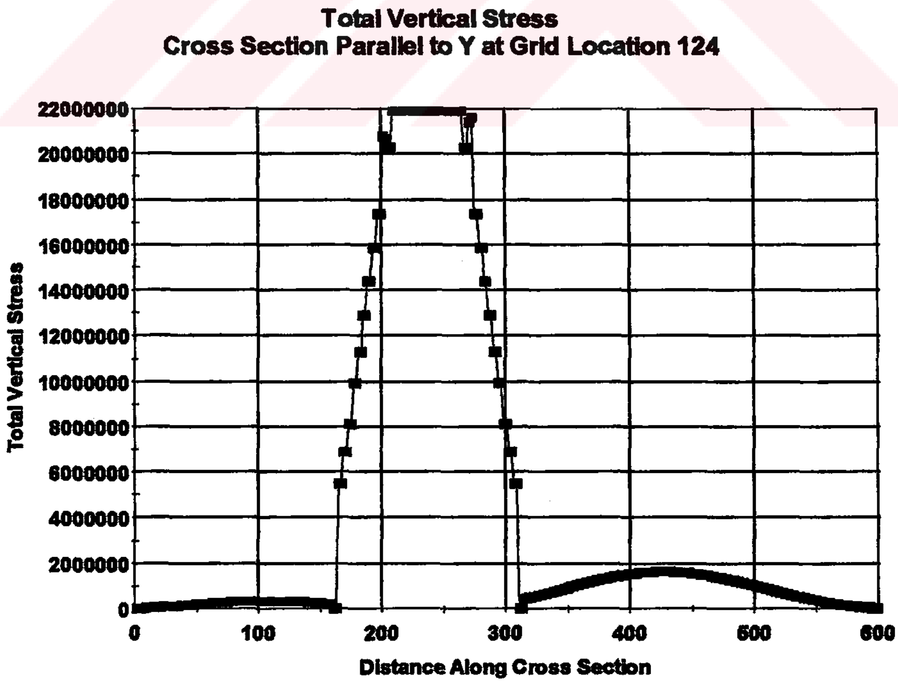

Figure 12 Vertical stress for 5 mining step on D-D' cross-section for shaft safety pillar mining

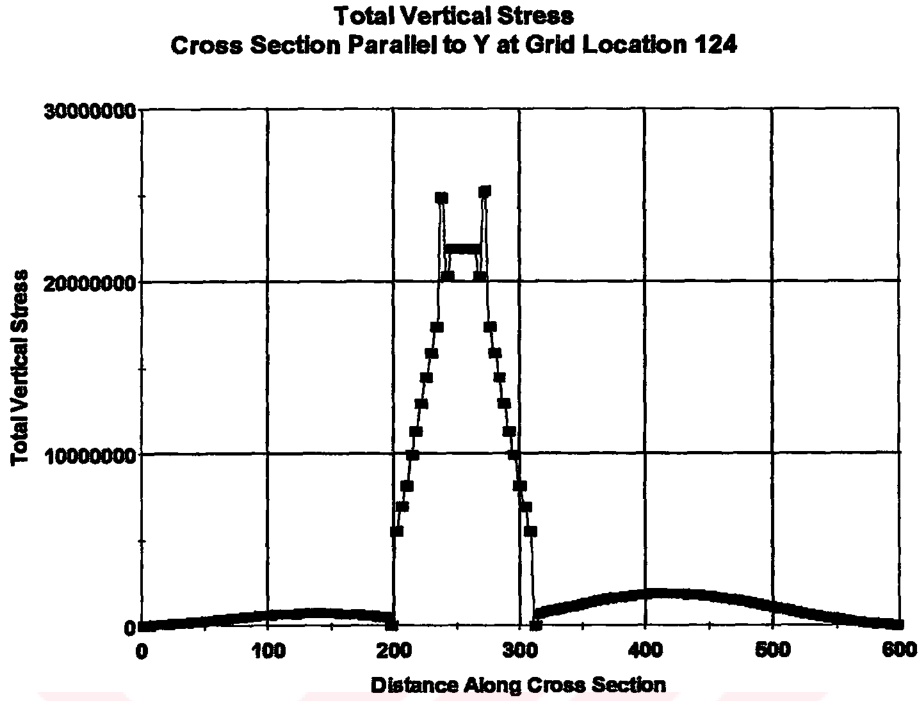

Figure 13 Vertical stress for 6 mining step on D-D' cross-section for shaft safety pillar mining

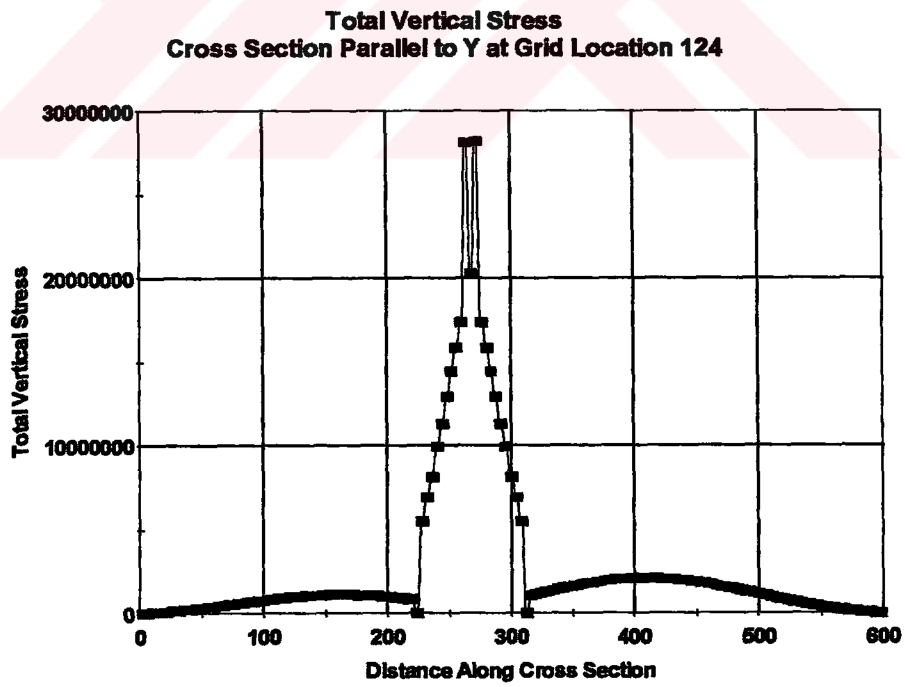

Figure 14 Vertical stress for 7 mining step on D-D' cross-section for shaft safety pillar mining

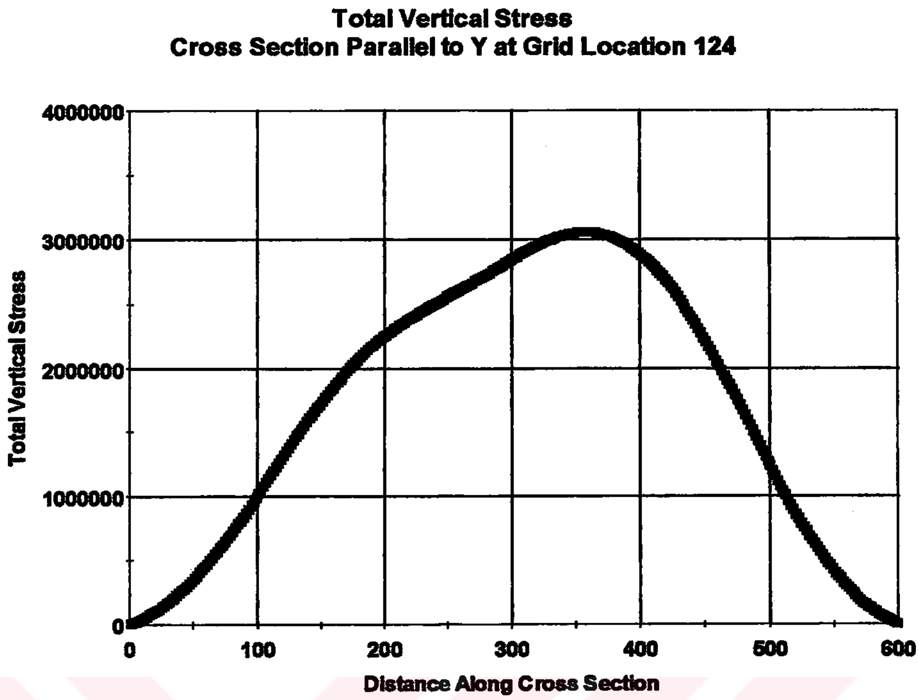

Figure 14 Vertical stress for 8 mining step on D-D' cross-section for shaft safety pillar mining

Appendix C

FINITE ELEMENT MODDELING RESULTS

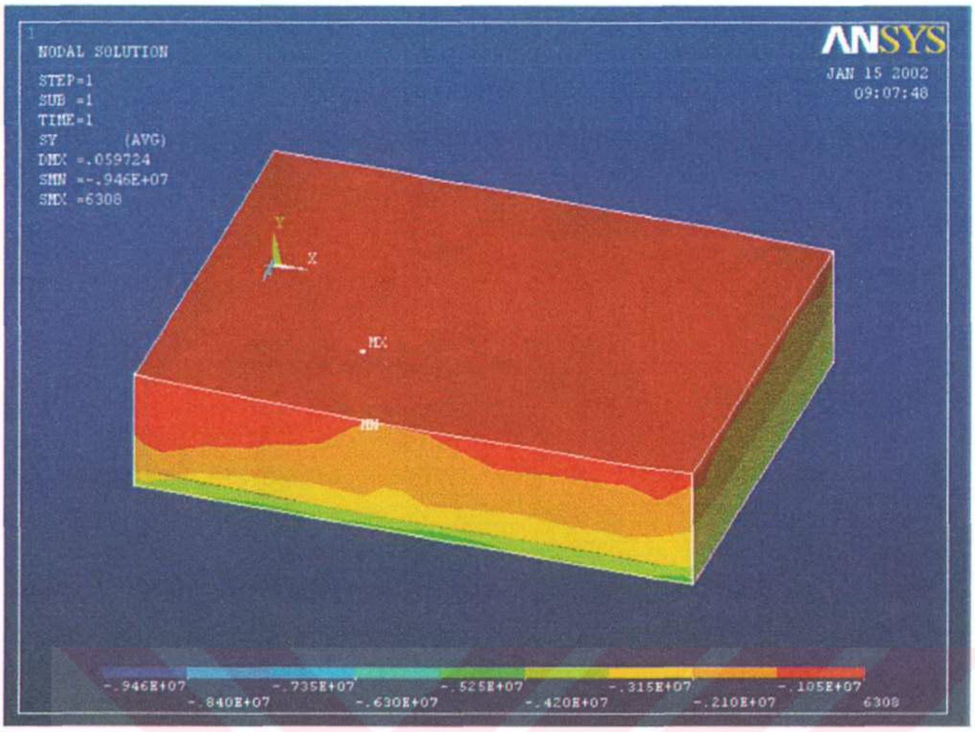

Figure 1 Finite element modeling result for original field (stresses are in Pascal)

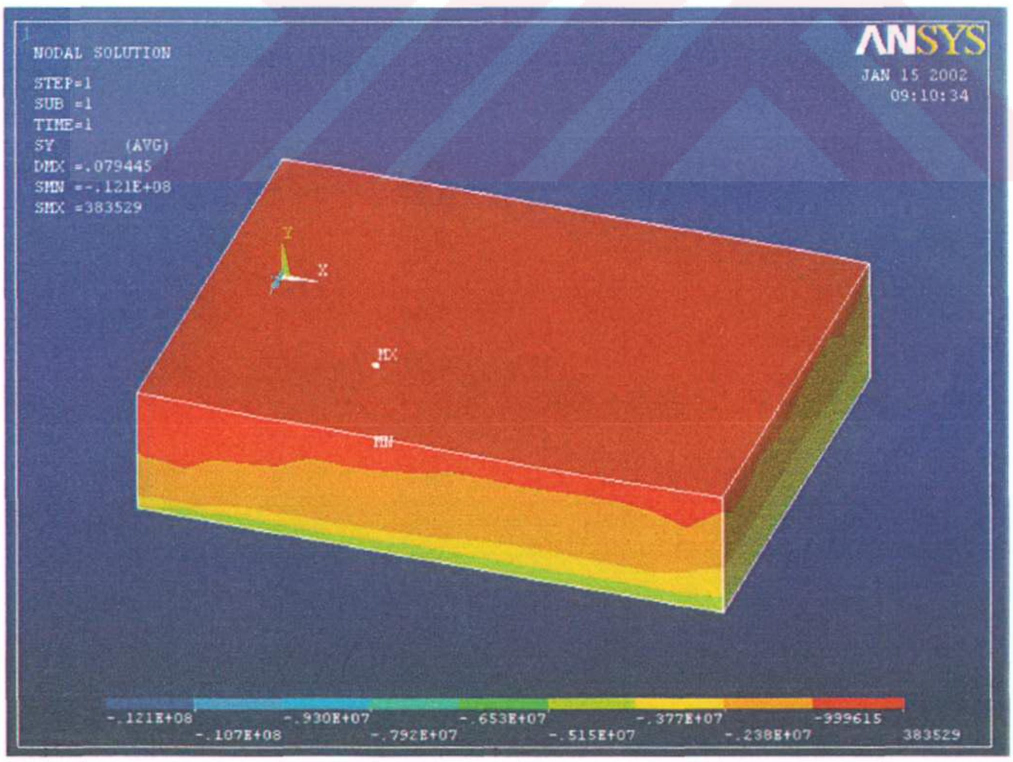

Figure 2 Finite element modeling result for 1 mining step (stresses are in Pascal)

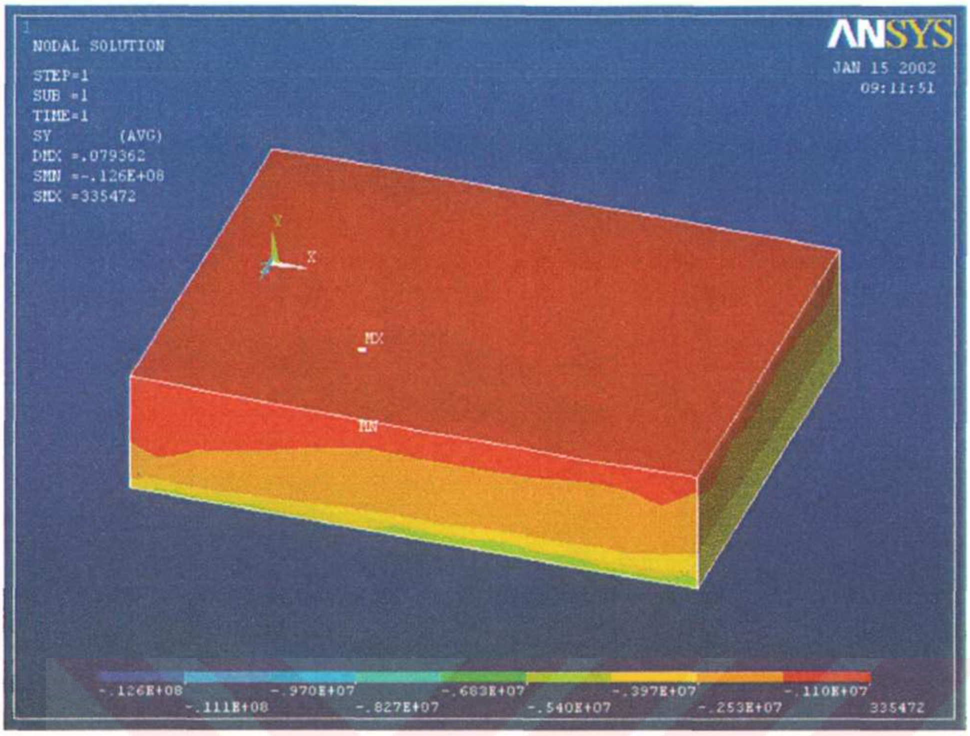

Figure 3 Finite element modeling result for 2 mining step (stresses are in Pascal)

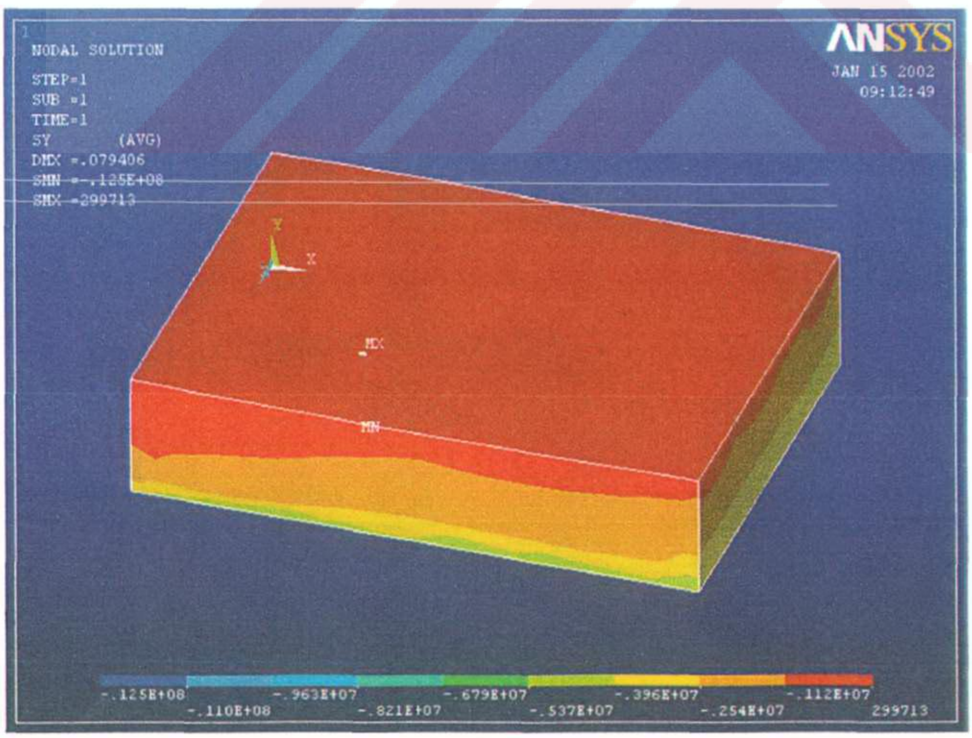

Figure 4 Finite element modeling result for 3 mining step (stresses are in Pascal)

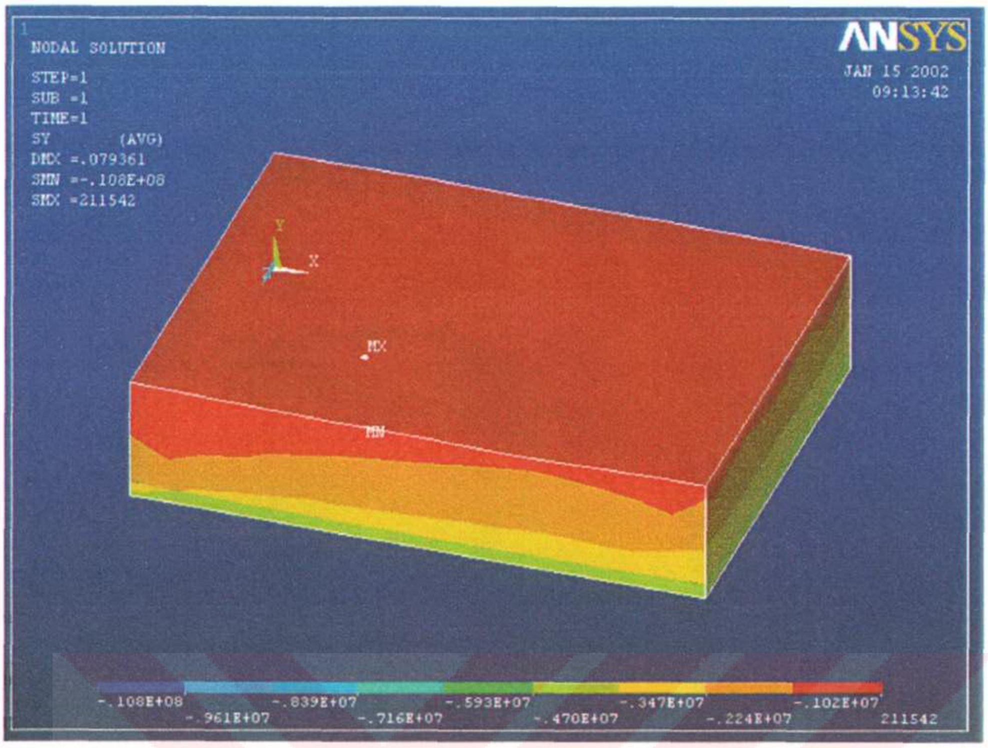

Figure 5 Finite element modeling result for 4 mining step (stresses are in Pascal)

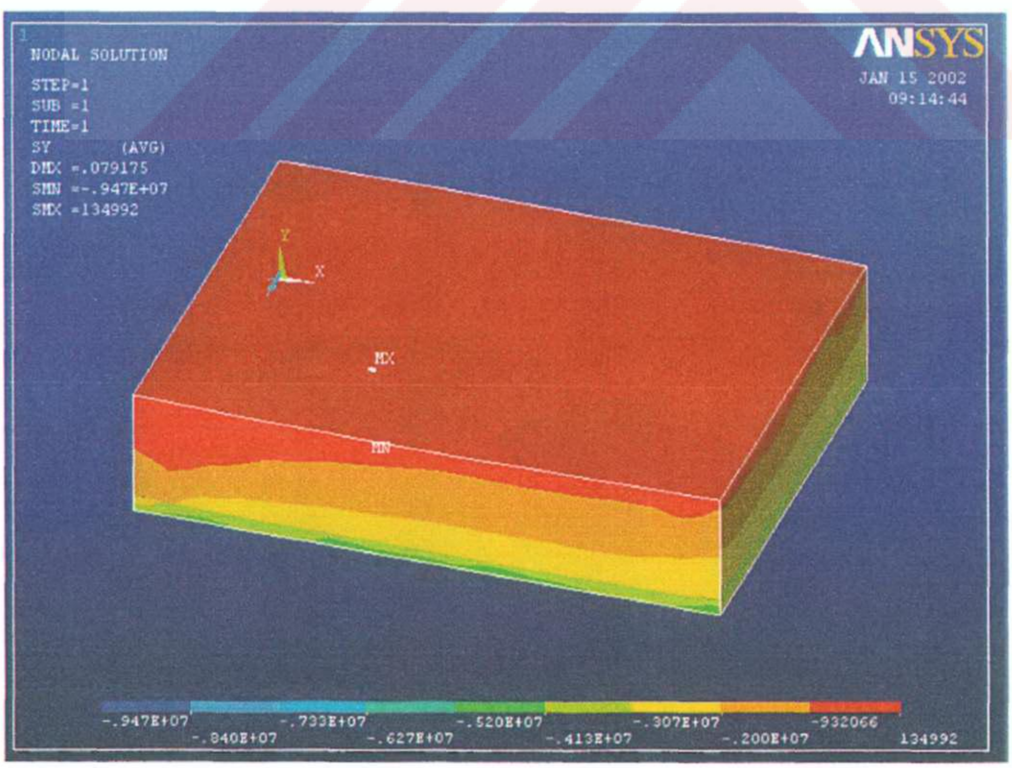

Figure 6 Finite element modeling result for 5 mining step (stresses are in Pascal)

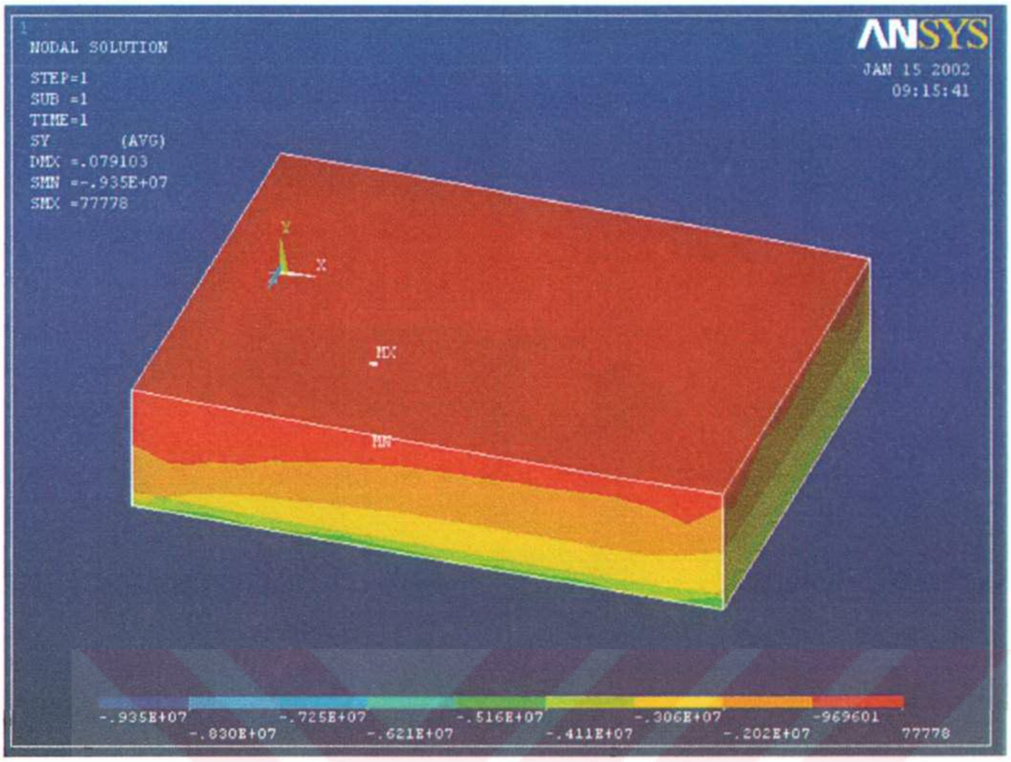

Figure 7 Finite element modeling result for 6 mining step (stresses are in Pascal)

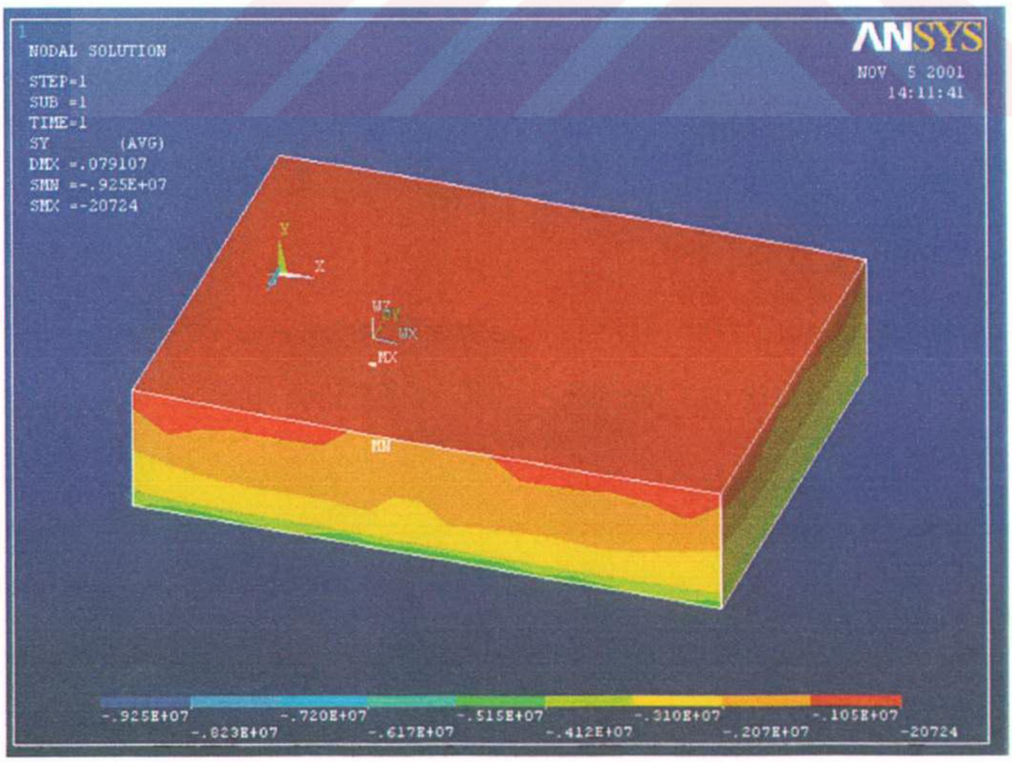

Figure 8 Finite element modeling result for 7 mining step (stresses are in Pascal)

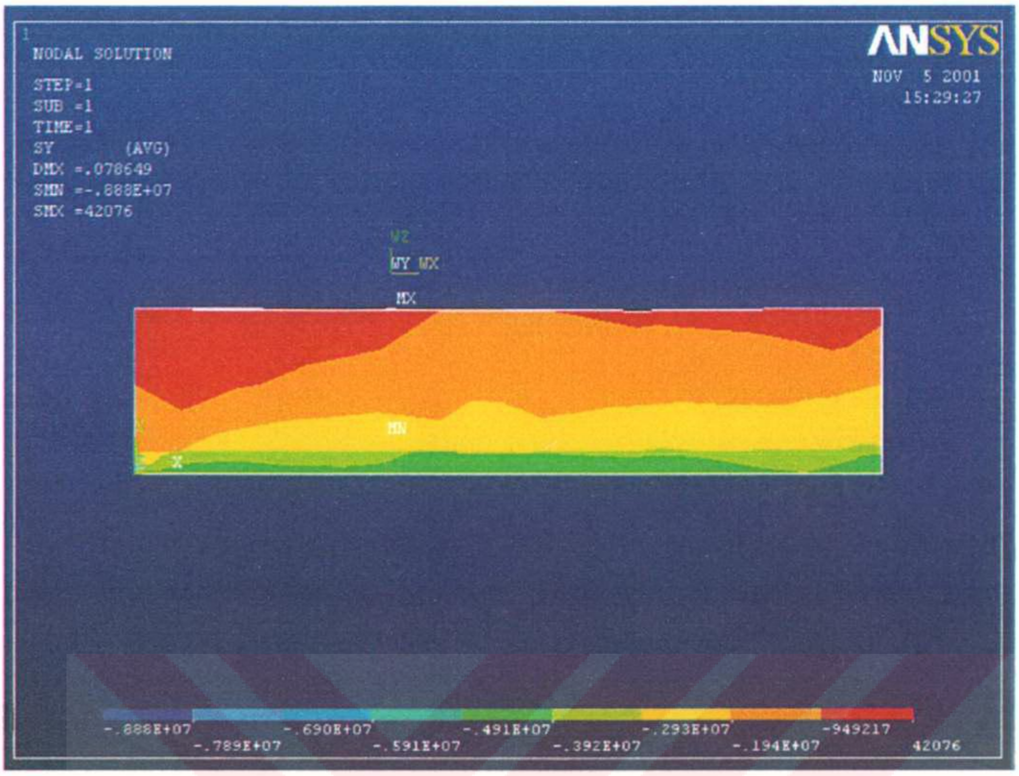

Figure 9 Finite element modeling result for 8 mining step (stresses are in Pascal)

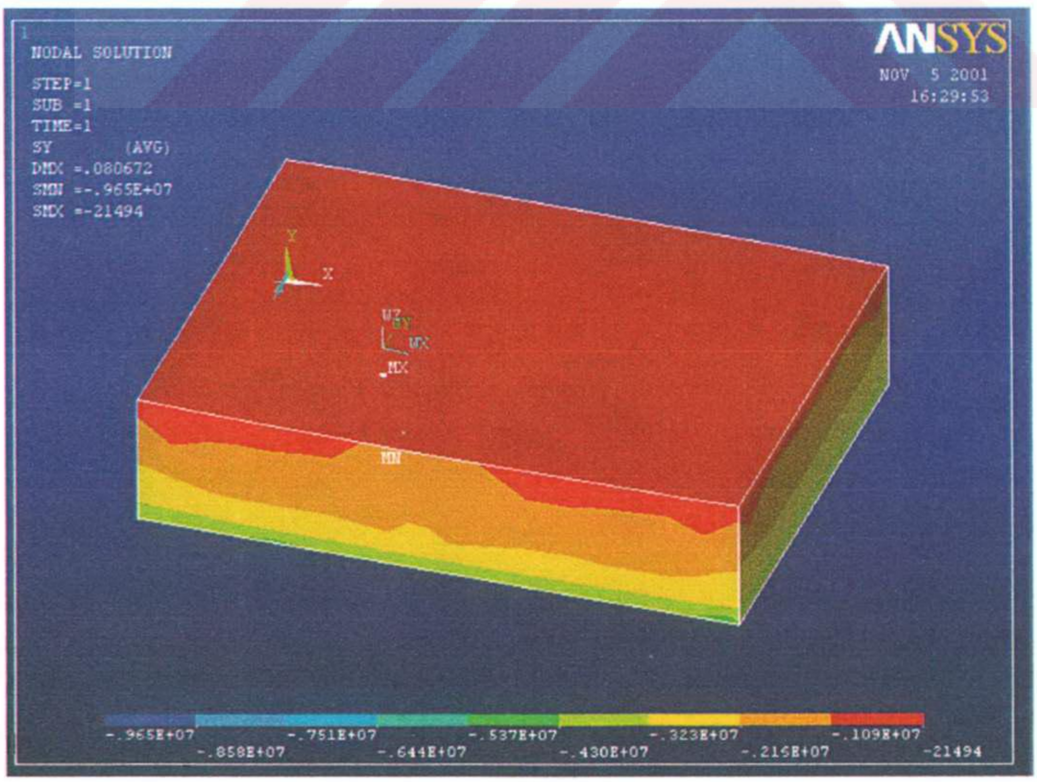

Figure 10 Finite element modeling result for 9 mining step (stresses are in Pascal)